

California State University, San Bernardino

**CSUSB ScholarWorks**

---

Theses Digitization Project

John M. Pfau Library

---

2009

## Digital reconstruction of a ceratopsid pes

Ken Conrad Noriega

Follow this and additional works at: <https://scholarworks.lib.csusb.edu/etd-project>



Part of the [Paleontology Commons](#)

---

### Recommended Citation

Noriega, Ken Conrad, "Digital reconstruction of a ceratopsid pes" (2009). *Theses Digitization Project*. 3792.

<https://scholarworks.lib.csusb.edu/etd-project/3792>

This Thesis is brought to you for free and open access by the John M. Pfau Library at CSUSB ScholarWorks. It has been accepted for inclusion in Theses Digitization Project by an authorized administrator of CSUSB ScholarWorks. For more information, please contact [scholarworks@csusb.edu](mailto:scholarworks@csusb.edu).

DIGITAL RECONSTRUCTION OF A CERATOPSID PES

---

A Thesis  
Presented to the  
Faculty of  
California State University,  
San Bernardino

---

In Partial Fulfillment  
of the Requirements for the Degree  
Master of Science  
in  
Biology

---

by  
Ken Conrad Noriega  
March 2009

DIGITAL RECONSTRUCTION OF A CERATOPSID PES


---

A Thesis  
Presented to the  
Faculty of  
California State University,  
San Bernardino

---

by  
Ken Conrad Noriega  
March 2009

Approved by:

  
Stuart Sumida, Chair, Biology

  
David Polcyn

  
Anthony Metcalf

*19 March 2009*  
Date

## ABSTRACT

A complete and fully articulated right pes of a centrosaurine ceratopsid from the Sage Creek Locality of Late Cretaceous (Campanian) Dinosaur Park Formation of southern Alberta, Canada provides important information regarding the structure and function of the pelvic limb in this group. This specimen has the potential to add important information to our understanding of the morphology of the centrosaurine pes, hind limb posture, and realistic ranges of locomotor behavior. Each of the completely prepared elements was subjected to three-dimensional digital scanning and then digitally reconstructed using three-dimensional sculpting software. The Sage Creek specimen was used as the base model from which relative size and positional information was determined. This base model was compared to other isolated, unaltered pedal elements in the collections of the Royal Tyrrell Museum, the Yale Peabody Museum, The United States National Museum, and the American Museum of Natural History to guide the reconstruction. In this manner a reconstructed centrosaurine foot, with all data coming directly from actual specimens, could be accurately

modeled in three-dimensional morphospace and provide the basis of a digital atlas of the elements.

## ACKNOWLEDGMENTS

My most sincere gratitude must be extended to the entire Biology Department of California State University, San Bernardino. You have all been very patient with me and I know that you are glad and relieved to see me graduate. Specifically, I must thank Drs. Stuart Sumida, David Polcyn and Anthony Metcalf for agreeing to serve on my committee. Thank you Debbie Reynolds for always cheering me on and helping me whenever I missed my deadlines.

To my colleagues, Natalia Kennedy, Kim and Eric Scott, Gavan Albright and Beth Rega many thanks for your support and illuminating discussions. Also thanks to you and Stuart for leading the way and showing me what real paleontologists do and what real paleontology is like.

Thank you to the Royal Tyrrell Museum of Palaeontology and specifically Dave Eberth, Jim Gardner, Don Brinkman and Jackie Wilke for allowing me the opportunity to study and make use of their magnificent collections. Thanks also go to Dan Brinkman, Lyndon Murray, Michael Anderson and Marilyn Fox at the Yale Peabody Museum; Carl Mehling and Rick Edwards at the American Museum; Matt Carrano, Jann Thompson and Michael Brett-Surman at the Smithsonian for

their invaluable assistance and incredible hospitality when I visited their collections.

Many thanks and eternal gratitude to Azam Khan of Autodesk who supplied me with free copies of Maya and Motion Builder to use for this study. None of this would have been possible without the generosity of Autodesk and Mr. Khan.

Thanks to Johnny Fisk and Bear Williams of Atomic Monkey for their excellent 3-D laser scans of not only my original specimen, but also the reference specimens necessary for the reconstruction.

Finally, my thanks to my family who stood by me and cheered me on throughout this long process.

To my family and to my friends. Without your support I could never have finished this thesis.

Mom and Dad, I owe all my successes to you and I will always appreciate you allowing me to stand upon your shoulders to reach my goals.

Mia, Mika and Chris thank you for always believing in me and encouraging me to finish.

Stuart and Beth, thank you for opening my eyes to the world of science, specifically comparative anatomy and paleontology. I wouldn't be here without you.

Finally, thank you to my good friend, colleague and mentor, Pep. Your not so subtle reminders and frank talk was exactly what was necessary for me to finally get off my butt and finish this. Thanks Pep.



TABLE OF CONTENTS

ABSTRACT ..... iii

ACKNOWLEDGMENTS ..... v

LIST OF FIGURES ..... ix

CHAPTER ONE: INTRODUCTION ..... 1

    Materials and Methods ..... 5

        Geological Context ..... 6

        Materials ..... 8

        Methodology ..... 12

            Scanning ..... 15

            Software ..... 16

            Separation of Fused Elements ..... 22

            Correcting Deformation ..... 23

            Mesh Combination ..... 27

CHAPTER TWO: RESULTS I: ANATOMICAL DESCRIPTION

    Tarsus ..... 31

    Metatarsals ..... 32

    Phalanges ..... 38

        Proximal Phalanges ..... 38

        Intermediate Phalanges ..... 43

        Unguals ..... 45

CHAPTER THREE: RESULTS II: FUNCTIONAL HYPOTHESES AND INTERPRETATIONS

A Biological Problem .....	50
A Multidisciplinary Approach and Solution .....	57
Postural Interpretations and Implications of the Reconstructed Pes .....	60
Revisiting the Ceratopsian Pes .....	62
Life Reconstructions .....	64
APPENDIX A: SPECIMENS UTILIZED IN THIS STUDY .....	68
APPENDIX B: MEASUREMENTS OF TMP 89.97.01, BEFORE RECONSTRUCTION .....	71
APPENDIX C: QUARRY MAP OF SITE FROM WHICH TMP 89.97.01 WAS RECOVERED .....	76
APPENDIX D: ILLUSTRATIONS OF TMP 89.97.01 INDIVIDUAL ELEMENTS, BEFORE RECONSTRUCTION .....	78
APPENDIX E: ILLUSTRATIONS OF TMP 89.97.01 INDIVIDUAL ELEMENTS, AFTER RECONSTRUCTION .....	102
APPENDIX F: DVD OF QUICKTIME FILES AND IMAGES OF TMP 89.97.01 .....	125
LITERATURE CITED .....	127

## LIST OF FIGURES

Figure 1.	Diagrammatic Stratigraphic Column in Which the Position of Bonebed 43 in Dinosaur Park Formation, Late Cretaceous, Alberta, Canada is Indicated by the Black Arrow. This Illustrates the Stratigraphic Level From Which Materials Utilized in This Study Were Obtained. After Eberth (2005). . . . .	7
Figure 2.	Dorsal View of TMP 89.97.01 <i>in situ</i> . This Demonstrates the Fact That the Specimen Was Found Complete and Intact. Also, Note the Presence of the Tibia Articulating With the Pes in the Lower Right of the Frame. Medial is to the Top of the Frame, Distal is to the Right. Reproduced With Permission of the Royal Tyrrell Museum of Paleontology, Drumheller, Alberta, Canada. . . . .	10
Figure 3.	Dorsal View of the Complete, Articulated Pes of the Centrosaurine Dinosaur <i>Centrosaurus</i> . This is the Only Known Example of a 3-D Accessible, Completely Articulated Foot for the Group. Lateral is to the Top of the Frame, Distal is to the Left. . . . .	11
Figure 4.	Metatarsal II Wiremesh With Holes. This Demonstrates the Holes Created During Separation of the Fused Elements. Dorsal is to the Top, Distal is to the Right. . . . .	23
Figure 5.	Alignment of Original and Reference Specimens. The Illustrated Element is Metatarsal I. Dorsal is to the Top, Distal to the Right. . . . .	26
Figure 6.	Wiremeshes Merged in ZBrush. Note the Different Shades of the Wiremesh. This is an Indicator That the Wiremeshes Are Separate, Not a Single Unified Mesh. . . . .	28
Figure 7.	Metatarsal I, With Visible Seams. . . . .	30

Figure 8.	Metatarsals I to V. Note the Closely Packed Metatarsals With Tightly Fitting Proximal Ends. Dorsal is Facing the Viewer, Distal is Down. ....	33
Figure 9.	Distal Articular Surface of Metatarsal II. This Rugose Surface is Indicative of the Presence of Cartilages Covering the Surface in Life. Dorsal is to the Top. ....	34
Figure 10.	Proximal Articular Surfaces of Metatarsals II and III. The Bases of Metatarsals II and III are Quite Different in Shape, Which Allows Them to Fit Closely Together. ....	36
Figure 11.	Proximo-Medial View of the First Phalanx of the First Digit. Illustrates the Bias of the Base With the Thicker Lateral Aspect and Narrower Medial Aspect Leading to the Formation of a Prominent Flange on the Medial Aspect. ....	39
Figure 12.	Lateral View of the First Phalanx of the First Digit. This View Illustrates the Lateral Pits at the Distal End of the Phalanges With Their "Rams Horn" Like Border. Dorsal is to the Top, Distal to the Right. ....	41
Figure 13.	Chevron Shape of an Intermediate Phalanx. This is the Characteristic Shape of an Intermediate Phalanx. Dorsal is Facing the Viewer, Distal is to the Bottom. ....	46
Figure 14.	Ungual Demonstrating the Proximally Directed Processes. ....	48

## CHAPTER ONE

### INTRODUCTION

Nearly fifteen years ago, Sumida and Lombard (1992) were asked to participate in a review of the most important developments in the previous quarter century of progress in vertebrate paleontology. Somewhat surprisingly, they concluded that although some important localities and taxa had indeed come to light, the most significant developments were outside the realm of biological paleontology. Rather, the landmark geological understanding of plate tectonics and the entomological origin of cladistic methods of phylogenetic analysis appeared to have had the most profound influence on the study of extinct tetrapods. Now, nearly two decades after their review, the animals themselves have returned to the forefront of vertebrate paleontological study. However, a multidisciplinary approach is not only critical to a more thorough understanding of the lives of extinct animals, but much more attainable now that new techniques of analysis have developed. To that end, a powerful new set of tools that did not exist a decade ago now promises to revolutionize paleontological inquiry again—that of high-resolution

digital modeling and animation (Boyd and Motani, 2008; Evans and Fortelius, 2008; Polly and MacLeod, 2008; Rybczynski et al., 2008; Smith and Strait, 2008; Hutchinson and Gatesy, 2006; Gatesy et al. in press). Although animating animals (and even dinosaurs) is not new, very few academic paleontologists currently employ the most powerful tools currently available for such work.

To be sure, there have been previous attempts to characterize the locomotor behavior of ceratopsid dinosaurs (Bakker, 1987; Johnson and Ostrom, 1995; Garstka and Burnham, 1997; Paul and Christiansen, 2000). But they have been limited in their utility. With the advent of computer graphic imaging (CGI) assistance in analyzing fossil materials, the next logical step is to choose a group with the following features: (1) a well resolved phylogenetic context within which functional hypotheses may be generated, (2) well preserved and completely represented materials from all or a particular part of the skeleton, and (3) availability to researchers. For this study, the ideal group presented as ceratopsian dinosaurs.

Ceratopsian dinosaurs are a well known and well studied group of ornithischian dinosaurs. The group in its entirety has been described by Hatcher (1907) and Lull

(1933) as well as many descriptions of individual species subsequently. Neither Hatcher nor Lull had access to the enormous breadth and depth of ceratopsian collections available today; furthermore, a bias toward cranial structures in collection, as well as for characters for phylogenetic analyses, have resulted in the most distal portions of the appendages being less well known than they could or should be.

The suborder Ceratopsia contains two infraorders: Psittacosauria and Neoceratopsia, with Neoceratopsia able to be further subdivided into the families Protoceratopsidae and Ceratopsidae (Dodson, 1996). Ceratopsid dinosaurs are famous for their elaborately frilled and horned heads and it is those heads by which the individual genera and species are differentiated. Ceratopsians in general, and ceratopsids in particular, are restricted in time and location. Neoceratopsians are only known from the Late Cretaceous Period (65-97 mybp) (Eberth, 2005) and the ceratopsids have only been found in North America (Dodson, 1996). Within those groups, the postcranial skeleton is extremely conservative and with the exception of size differences are similar across the family (Dodson and Currie, 1990).

Although the current fossil record for ceratopsids is remarkably complete, it is still a rare occurrence to find a specimen with the most distal elements of the feet fully intact, associated and articulated. The overall skeletal structure is considered well known, but most pedal elements are composites constructed of associated elements. I was fortunate to have access to a specimen which was found completely intact and articulated for comparison with individual elements from other ceratopsian individuals.

Whereas ceratopsids are abundant in the fossil record and have been extensively studied, the majority of studies to date have focused on taxonomic description and differentiation. Descriptive morphological studies are necessary for phylogenetic analyses but description alone cannot provide functional or and biomechanical hypotheses. Thus ceratopsids presented a group well represented enough to allow the development of biomechanical hypotheses. Fortuitously, adequate representative components of the skeleton were made available to the vertebrate paleontology laboratory at CSUSB by Dr. David Eberth of the Royal Tyrrell Museum of Paleontology, Drumheller, Alberta, Canada. (See materials section for details.)



It is important to note that a major limitation of previous studies of ceratopsid locomotion has been the reliance on two-dimensional (2-D) data from traditional illustrations and photographs. The only study which used three-dimensional (3-D) models was that of Johnson and Ostrom (1995) and that was limited to a single model consisting of casts of specimens. The evolution of computer technology, both hardware and software, allows greater access to the infinite variations and possibilities of the digital world.

Recently, computer modeling and animation has been used to great effect by paleontologists such as Gatesy et al. (1999). However, these uses of animation were essentially three-dimensional illustrations of hypothesis that were tested by more traditional two-dimensional methods.

#### Materials and Methods

A survey of all centrosaurine specimens in the collections of the Royal Tyrrell Museum of Palaeontology lead to a focus on the neoceratopsid genus *Centrosaurus*, specifically those from a single locality. The specimens that provided the central focus of this study come from a

geologically and temporally constrained bonebed that has been demonstrated to be a large, monospecific mass kill site that preserves skeletal elements from thousands of excellently preserved individuals (Ryan, et al., 2001). The site (Figure 1) is in the Late Cretaceous (65-97 mybp) (Eberth, 2005) Dinosaur Park Formation in Alberta Canada. The enormous number of specimens from this mass kill bonebed guarantees that skeletal components utilized in this study were available for coeval individuals of equivalent ontogenetic stage. All of the necessary elements were available in the vertebrate paleontology collections of the Royal Tyrrell Museum of Palaeontology, Drumheller, Alberta, Canada (Appendix A).

#### Geological Context

The specimens utilized in this study were recovered from from two bone beds in the Late Cretaceous (Upper Campanian) (73-83 mybp) (Eberth, 2005), Dinosaur Park Formation, have been excavated in Dinosaur Provincial Park, Alberta, Canada. This locality (referred to as either bonebed 43 or "the *Centrosaurus* bonebed" (Ryan et al., 2001)) is located approximately sixteen meters above the base of the Late Campanian (73-83 mybp) (Eberth, 2005) Dinosaur Park Formation (Figure 1).

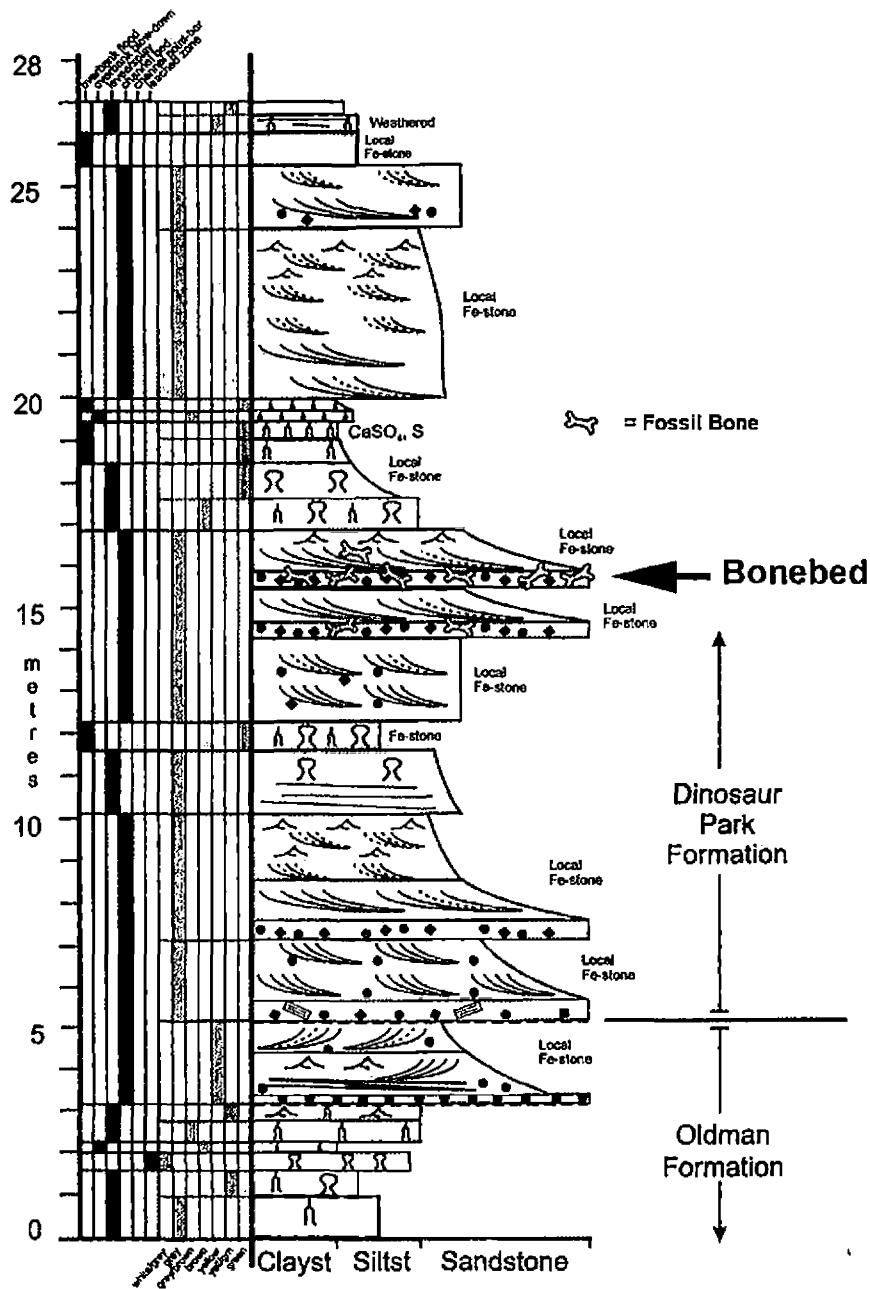


Figure 1. Diagrammatic Stratigraphic Column in Which the Position of Bonebed 43 in Dinosaur Park Formation, Late Cretaceous, Alberta, Canada is Indicated by the Black Arrow. This Illustrates the Stratigraphic Level From Which Materials Utilized in This Study Were Obtained. After Eberth (2005).

The locality is one of a string of mass kill sites that preserve some of the largest accumulations of individual neoceratopsian dinosaurs anywhere in the world. All of the materials are held in the collections of the Royal Tyrrell Museum of Paleontology, Drumheller, Alberta, Canada.

The elements have been confidently identified as the centrosaurine ceratopsid *Centrosaurus* (Ryan, 1992; Ryan et al., 2001). The taphonomic context of the mass kill sites that generate the specimens suggests that although individuals of all ontogenetic stages are present, the upper size range of the specimens confidently represents adult individuals of comparable size and maturity (Ryan, 1992; Ryan et al., 2001).

### Materials

A focus on the pes was made for several reasons: (1) The pes and the manus are simultaneously the least well represented in the overall history of descriptive morphology of the Ceratopsia - and (2) they are the most critical part of the substrate-to-organism interface when considering biomechanical or locomotor hypotheses; (3) it provided some of the best preserved materials represented by both complete and articulated as well as well preserved individual elements; (4) of all the known complete or

articulated ceratopsian appendicular elements, the specimen which was selected as the focus of this study is the only known complete and articulated manus or pes to be completely removed from the surrounding matrix, the rock surrounding the fossil, thus allowing 3 dimensional access for laser scanning; (5) the particular specimen selected has been meticulously documented as being both complete and articulated with photographs and quarry maps, thus ensuring that positional and relational information can be assumed to be accurately rendered for the purposes of developing an articulated digital model (Figure 2; Appendix C). These factors led to the pes as presenting the best initial opportunity to develop a complete digital model of a non cranial component of a dinosaurian skeleton.

Standard paleontological nomenclature for referring to specimens in the literature is to use an abbreviation of the name of the museum in which the specimen is housed followed by the accession number of the specimen. This convention will be used in this paper. Institutional abbreviations include the following standard abbreviations: American Museum of Natural History—AMNH xxxx; Royal Tyrrell Museum of Paleontology—TMP xx.xx.xx; United States National Museum—USNM xxxx; Yale Peabody Museum—YPM xxxx.

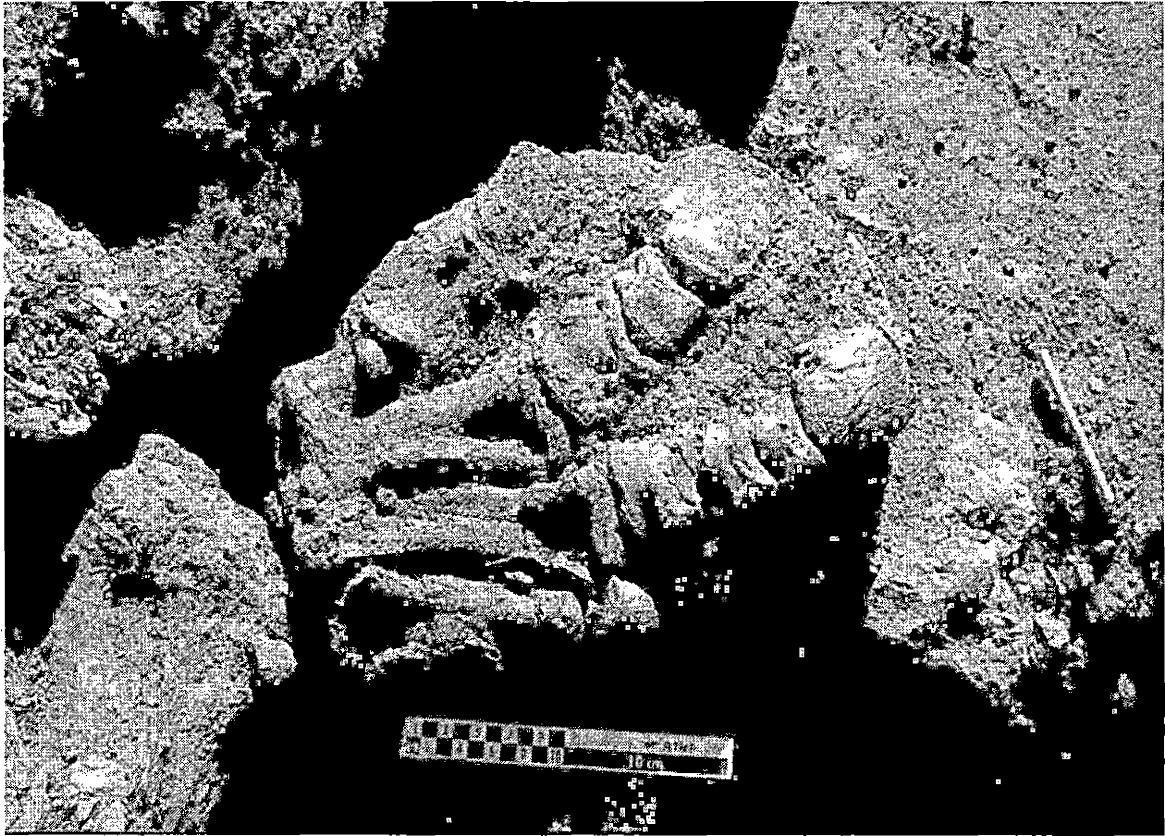


Figure 2. Dorsal view of TMP 89.97.01 *in situ*. This Demonstrates the Fact That the Specimen Was Found Complete and Intact. Also, Note the Presence of the Tibia Articulating With the Pes in the Lower Right of the Frame. Medial is to the Top of the Frame, Distal is to the Right. Reproduced With Permission of the Royal Tyrrell Museum of Paleontology, Drumheller, Alberta, Canada.

Unaccessioned specimens are abbreviated with locality information as in: Bonebed-BB xx-xxx. References to specific museums, institutions or locales follow similar conventions, without including the accession numbers of specimens as in: California State University, San

Bernardino-CSUSB; Dinosaur Provincial Park-DPP. The articulated basis of the digital model is TMP 89.97.01 a specimen in the collections of the Royal Tyrrell Museum of Paleontology (RTMP) (Figure 3).

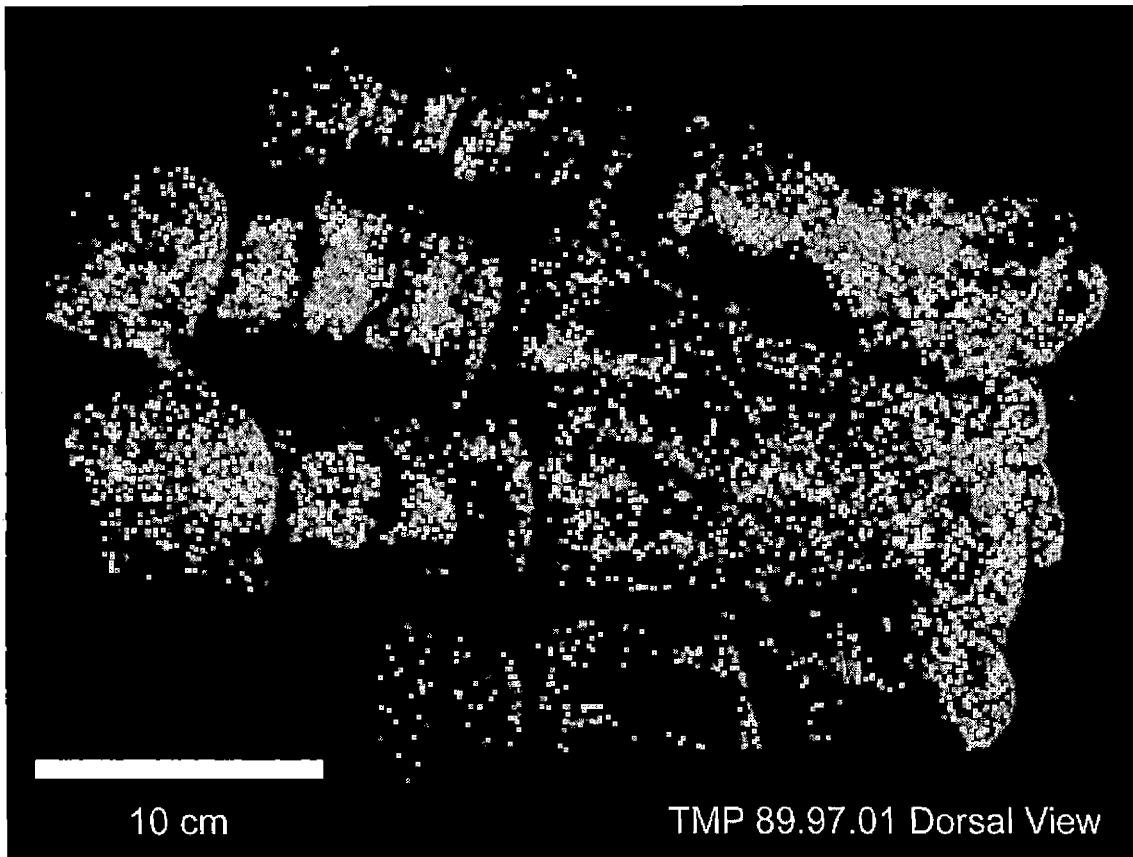


Figure 3. Dorsal View of the Complete, Articulated Pes of the Centrosaurine Dinosaur *Centrosaurus*. This is the Only Known Example of a 3-D Accessible, Completely Articulated Foot for the Group. Lateral is to the Top of the Frame, Distal is to the Left.

Additionally over 150 disarticulated, unassociated individual elements, representative of the various metapodial and phalangeal elements of the pes were included in the study to provide three-dimensional information and views of as many components of the pes as possible (Appendix A). Unfortunately, no reference specimens were available for the tarsal bones or for Metatarsal V owing to the exceptional rarity of these particular elements.

#### Methodology

Several trips were made to the RTMP to select from all available specimens; TMP 89.97.01 as well as reference specimens. On these trips, visits were made to both the museum proper and the field station within Dinosaur Provincial Park (DPP). Both accessioned specimens from the museum proper and unaccessioned specimens from the DPP field station were evaluated. All specimens were carefully examined and only those deemed to have acceptable size, maturity, quality of preservation and lack of deformation were chosen to serve as reference specimens. Once selected and approved for loan to the CSUSB Vertebrate Paleontology laboratory, specimens were hand-carried from Drumheller to CSUSB.



All selected specimens studied were cleaned through standard vertebrate paleontological mechanical preparation techniques. Individual methods may have varied between museums and across specimens but the techniques all share the use of mechanical methods to remove matrix, the rock material surrounding the fossil, from the specimen. In essence, all mechanical preparation involves the use of a tool to apply an external force to the matrix in order to separate it from the underlying fossil. Mechanical methods utilized here included the use of dental picks and jeweler's pin vises to separate the fossil from the matrix by hand and the use of, a miniature pneumatic jackhammer, known as an aircscribe, to vibrate the matrix off the specimen. The specific model aircscribes used in the CSUSB Vertebrate Paleontology Laboratory are the PaleoTools Micro-Jack models 3, 4 and 5. Fossil preparation also includes the extremely important techniques of using consolidants and adhesives. Often, fossils are found in fragmentary form or they may be intact, but too fragile to be handled or moved. In these instances, consolidants are used to strengthen the specimen, and adhesives are used to reunite pieces that have been separated but are determined to be fragments of a single element. Specimens are assumed

to have been prepared by the staff of the museum in which they are housed unless otherwise noted.

In addition to the collections of the RTMP, specimens from the Yale Peabody Museum (YPM), the United States National Museum (USNM) and the American Museum of Natural History (AMNH) were also studied and measured for comparison. Published descriptions of the specimens on display at each of these institutions were invaluable references as well (Lull, 1933; Brown, 1917). Detailed measurements of the unreconstructed dimensions of TMP 89.97.01 were made with calipers and the specimen was also photographed alongside a standard 10 cm scale bar (Appendix B).

TMP 89.97.01 shows some distortion in the form of crushed elements and an overall shift toward the medial aspect. To correct for this deformation during reconstruction, additional specimens from the collections of the RTMP were selected as references. All reference specimens were selected from unassociated, individual elements of the ceratopsid foot with areas of minimal to no distortion. Undamaged portions of the reference specimens were used as a framework to guide the reconstruction of the shapes of the individual elements of TMP 89.97.01. All

components of the pes were digitally scanned for external shape.

Scanning. 3-D laser scans of all specimens, TMP 89.97.01 and reference specimens, were conducted by Mr. John Fisk and Mr. Bear Williams of Atomic Monkey Inc. (Glendale, California). 3-D laser scans were produced using a NextEngine Desktop 3D scanner with SD Scanning Software. Reflective surfaces on the specimens will often produce extraneous information which present themselves as spikes of varying sizes on the digital versions of the specimens (Fisk, pers. comm. 2008). To reduce shine on the specimens, prior to scanning all specimens were lightly dusted with talcum powder with a Kabuki brush. After scanning, the powder was removed with a clean brush. The actual scanning and data capture proceeded as follows: points were first marked with artists tape for reference when data were patched. Although not always necessary, this procedure provides a clear point to reference when piecing scan patches together. Bones were dusted for any shine and placed on an auto-rotating plate for scanning. Two complete 360 degree scans were implemented, one complete horizontal and one complete vertical. Once that was completed the data were "patched" together using

NextEngine Software. When the patches were completed the software sealed any gaps in the data to create a complete surface (Fisk, pers. comm. 2009).

Data produced by the scanner were made available in the form of object files (.OBJ) which are easily read by a number of 3-D software packages. Within the software, the object files are displayed as a polygonal mesh, also referred to as a wireframe (Derakhshani, 2004).

Software. A fully animatable digital reconstruction of the foot of the centrosaurine dinosaur *Centrosaurus* was created using 3-D modeling and sculpting software. By way of manipulation in the 3-D imaging software, individual elements are viewable from anywhere in the 3-D space that surrounds the modeled objects.

All work on the digital files produced by the laser scans was conducted on a Boxx 8300 series workstation. This workstation was equipped with 2 dual-core AMD Opteron processors at 2.4 gigahertz (GHz) and 4 gigabytes (GB) of memory and an NVIDIA Quadro FX 1500 video card with 256 megabytes (MB) of memory. The software utilized on the workstation was Autodesk Maya version 8.0 for Windows XP x64 and Pixologic ZBrush version 3.1. The modeling and sculpting software ZBrush was used primarily to effect

small scale changes in the specimens as well as to separate fused elements. The modeling and animation software Maya was used to correct for large scale shifts and deformations in the elements and to combine separate polygonal meshes into a single mesh.

ZBrush was chosen to make small scale changes because it is primarily a digital sculpting program that is used for modeling. The true strength of ZBrush over Maya for smaller changes lies in the ability of ZBrush to easily select and modify polygons through the use of brushes of varying size and intensity (Pixologic, 2007). Ultimately, Maya is the more powerful software, but it is rendered less useful for reconstruction purposes by the very aspects which make it so powerful: selection of elements in Maya can be extremely complicated because there are so many choices. In Maya, elements can be selected through the use of three selection modes. A subset of the selection modes is selection masks which vary depending on which selection mode is chosen (Derakhshani, 2004; Autodesk Maya Press, 2006). This gives an enormous amount of control over which elements of the polygonal mesh are selected. Unfortunately, this is not an intuitive system and once the selection masks are in place, elements must still be

selected one-by-one. Selecting a large group of adjacent polygons can become a tedious and time-consuming process. Once these elements are selected any number of transformations can be performed. However, in most circumstances the transformations will effect the entire selection in exactly the same manner. When a group of polygons is selected and then moved or rotated, all the polygons will move in exactly the same direction with the exact same transformation applied equally to all the polygons (Derakhshani, 2004; Autodesk Maya Press, 2006). This makes it extremely difficult to effect subtle changes to a model in which adjacent polygons are each moved in different directions with differing degrees of transformation. It is possible, but once again, tedious and time consuming.

Alternatively, selection of polygons in ZBrush is much simpler and more intuitive: the options are limited to selection of polygons, specifically the faces of the polygons. . It is not possible to select points or edges of the polygons, as is possible in Maya (Derakhshani, 2004; Autodesk Maya Press, 2006; Pixologic, 2007). Selection of polygons in ZBrush can be a simple matter of selecting a brush, selecting its attributes and then painting the

selection onto the wiremesh. Any polygons the brush touches are selected (Lutz, 2007; Pixologic, 2007). Once selected, the polygons can easily be manipulated through the use of various brushes and strokes. Unlike Maya, the selected polygons can be affected in different manners and directions simultaneously. This can be accomplished by using different brushes coupled with various strokes and alphas, which act as stencils to alter the effect of the brush (Lutz, 2007; Pixologic, 2007). With a single stroke of the brush a rough or uneven surface on the model can easily be smoothed, even though the polygonal faces are all facing completely different directions.

These differences in the manner in which the software packages work can be attributed to the fact that Maya is a modeling and animation program and ZBrush is a sculpting and modeling program (Derakhshani, 2004; Autodesk Maya Press, 2006; Pixologic, 2007). To these differing ends, Maya is designed to allow the end user significant control over how polygons and their component vertices, edges, and faces are manipulated. This is in order that the wireframe model does not have polygons that inadvertently overlap or create mathematically impossible or incongruent vector equations (Derakhshani, 2004). Creating untenable vector

equations to describe the wireframe will lead to problems with the model during animation in which the results are less than satisfactory. Possible undesirable results include the separation of a model at the seams when it is bent in an animation or the obvious twisting or bending of polygons within the model (Derakhshani, 2004). ZBrush is different from Maya in that the end user does not have anywhere near the same amount of control over how polygons are manipulated. In ZBrush, the user selects a brush, stroke and possibly an alpha and then begins to paint strokes onto the wireframe (Lutz, 2007; Pixologic, 2007). The exact manner in which the polygons react to the brush are not user defined. Rather, the program determines how the polygons are transformed to produce the effect desired by the user. This is because ZBrush is essentially a sculpting program, not an animation program. Although ZBrush does have features and provisions which aid in readying 3-D models for animation, the main purpose of ZBrush is to allow the user to sculpt and manipulate the model without constant concern for the polygons and how the geometry of the wireframe will be affected when animated (Lutz, 2007; Pixologic, 2007). Working with ZBrush has been likened to working with digital clay, rather than with



mathematical equations, as is the case with Maya (Derakhshani, 2004; Pixologic, 2007). The one significant and unfortunate side effect of this ease of use is that the user does not control the geometry of the wireframe as it is changed. The program determines how the geometry is changed and this can lead to the type of mathematically convoluted results that are undesirable in modeling and animation. The ZBrush user can make changes to the form of a model easily and intuitively, but the geometry may become distorted to the point where the model is completely unable to be used for animation or even exported to a different 3-D modeling package.

The end result is that Maya is best suited to making changes to the wireframe which do not alter the geometry in a manner that is mathematically untenable; this is typified in this study by the use of lattice deformers, which alter the overall shape of the wireframe while retaining the relationships between polygons (Derakhshani, 2004, Autodesk Maya Press, 2006). ZBrush is best suited to making small scale changes to the wireframe in localized areas and to rapidly selecting and transforming polygons on the model (Pixologic, 2007).

Separation of Fused Elements. Unfortunately, mechanical preparation methods were not sufficient to separate all elements of TMP 89.97.01. After preparation, metatarsals I through III remained united at the base, metatarsals IV and V were also united at the proximal end, and the tarsal was fused to the proximal end of the metatarsal I-III unit. It was not possible to separate these by traditional mechanical methods as the degree of fusion or distortion was too severe to isolate confidently the outlines of the individual elements at these locations.

These fused elements were digitally separated in ZBrush. This was accomplished by masking off the desired elements. The mask was applied by following the most probable outline of the element; the exact outline of the element was not required as in mechanical preparation because the reference specimens would be used to achieve the proper outline and shape. Once the mask was created, the unmasked area was hidden. The hidden parts of the wireframe were then deleted and only the desired element retained. The original scan consisted of a hollow shell of polygons, not a solid object. As a result, deletion of polygons leads to a specimen with large holes in the geometry (figure 4).



Figure 4. Metatarsal II Wiremesh With Holes.  
This Demonstrates the Holes Created During Separation of  
the Fused Elements. Dorsal is to the Top, Distal is to  
the Right.

These holes do not affect adversely the reconstruction  
process and are eliminated in the final product.

Correcting Deformation. Boyd and Motani (2008)

describe the two basic categories of fossil deformation:

There are two primary categories of fossil  
deformation, brittle and plastic. Brittle is  
structural cracking without shape change of the  
individual broken pieces, whereas plastic  
deformation is described as shape change without  
breakage. Plastic deformation alters the true

shape of a fossil, the shape of the body part during life.

All elements of TMP 89.97.01 showed signs of brittle deformation, but not all showed obvious signs of plastic deformation when compared to individual, disarticulated reference specimens in the collections of the RTMP. Plastic deformation was seen in all metatarsal elements, but not all phalangeal elements.

Correcting deformation in the elements of TMP 89.97.01 began with aligning the original element with a reference specimen in ZBrush, regardless of whether the element showed signs of plastic deformation. The original element was loaded onto the canvas first and then the reference specimen was appended as a subtool. The subtool was positioned and if necessary, scaled to match the original element as closely as possible. If plastic deformation was determined to have occurred, then the original element and its subtool were exported as .OBJ files. The .OBJ files were imported into Maya and a lattice deformer was created around the original element. The lattice deformer is especially useful for correcting large scale deformation, such as a plastic deformation in which the entire element is shifted in a single direction. Lattices are

particularly useful when editing is required for a relatively complex poly mesh or NURBS surface that is otherwise too dense to efficiently edit directly with control vertices. A lattice is assigned and used to create changes without having to move the surface's individual surface points (Derakhshani, 2004).

The lattice was used to manipulate the form of the original element to more closely match the homologous portions of the reference specimen. The original specimen was then exported as a new .OBJ and imported back into ZBrush. This new .OBJ file was then loaded onto the canvas and the reference specimen was appended as a subtool. At this point, only brittle deformation was left to be corrected and the procedure was identical for all specimens.

To correct for brittle deformation the reference specimen was aligned as closely as possible to the original, or target, specimen. The external morphology of the reference specimen was used as a guide and the target was placed within the boundaries of the reference specimen (figure 5). Small cracks, fissures or holes were manually corrected by using a brush to push or pull polygons into a conformation that matched the reference specimen exactly.

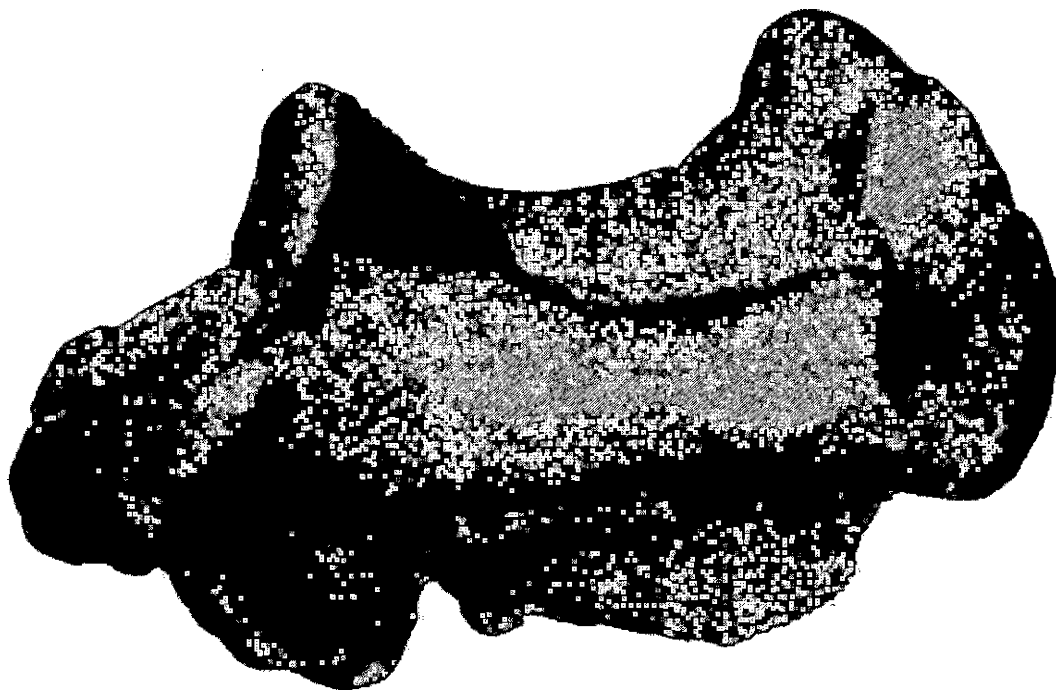


Figure 5. Alignment of Original and Reference Specimens. The Illustrated Element is Metatarsal I. Dorsal is to the Top, Distal to the Right.

Larger cracks or sections that were entirely missing (due to brittle deformation of the original fossil or the digital separation of fused elements) or unable to be properly visualized, as in the bases of the previously fused metatarsals, were aligned with the reference but the polygons of the target were not positioned into an exact match of the reference. Rather, the target was aligned in a manner such that the missing sections could be replaced

by segments of the reference specimen. In some instances, particularly those of the unguals, it was possible to use the original specimen itself as a reference specimen. In these situations a mirror image of the undistorted portion of the element was created and subsequently used as a reference specimen. When the target and reference were aligned as closely as possible, they were exported as .OBJ files.

Mesh Combination. Aligned target and reference .OBJ files were imported into Maya. Although ZBrush is an excellent program for matching the target mesh to the reference mesh, it is unable to combine the two into a single wireframe. The closest approximation to this is merging meshes (Lutz, 2007; Pixologic, 2007). Unfortunately, the merging of meshes in ZBrush results not in a single, unbroken mesh, but rather a hybrid of the two original meshes, which are united and move together, yet remain distinct from each other (figure 6). For this very reason, it was necessary to export the aligned elements to Maya for mesh combination. Once imported into Maya, the meshes were combined into a single unbroken wireframe. This wireframe was exported as a single .OBJ file to be imported into ZBrush.

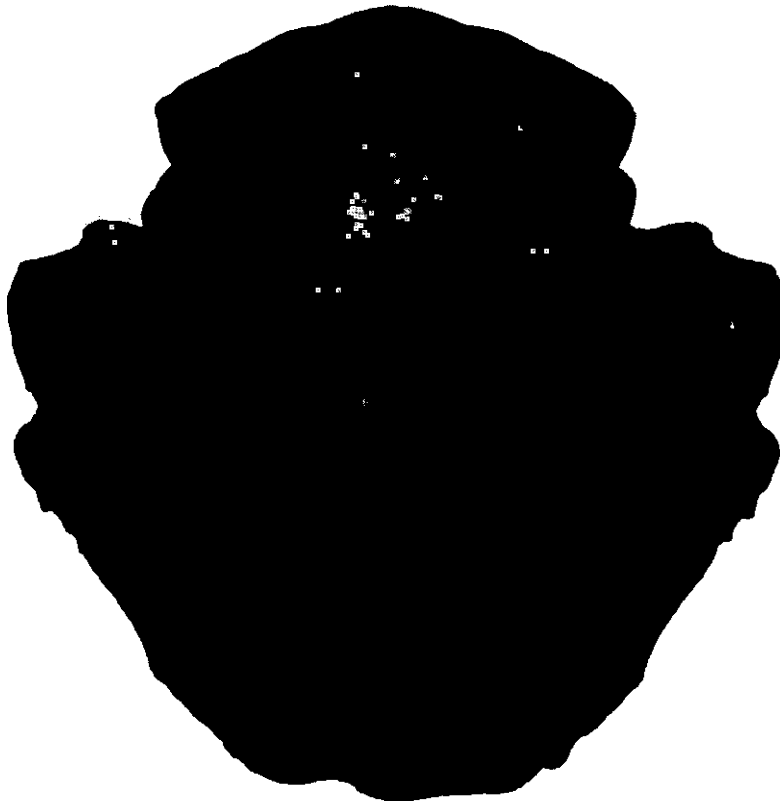


Figure 6. Wiremeshes Merged in ZBrush.  
Note the Different Shades of the Wiremesh.  
This is an Indicator That the Wiremeshes  
Are Separate, Not a Single Unified Mesh.

The .OBJ file resulting from the mesh combination in Maya was imported into ZBrush for the final smoothing of the joints where the two meshes were fused. Even with careful preparation the joints where the two meshes meet are often obvious due to the abrupt change in the geometry



of the wireframe where the joint occurs (figure 7). These joints were smoothed out in ZBrush through the use of brushes which relaxed the geometry along the seams and allowed the intersection of the previously separate meshes to follow a more logical flow.

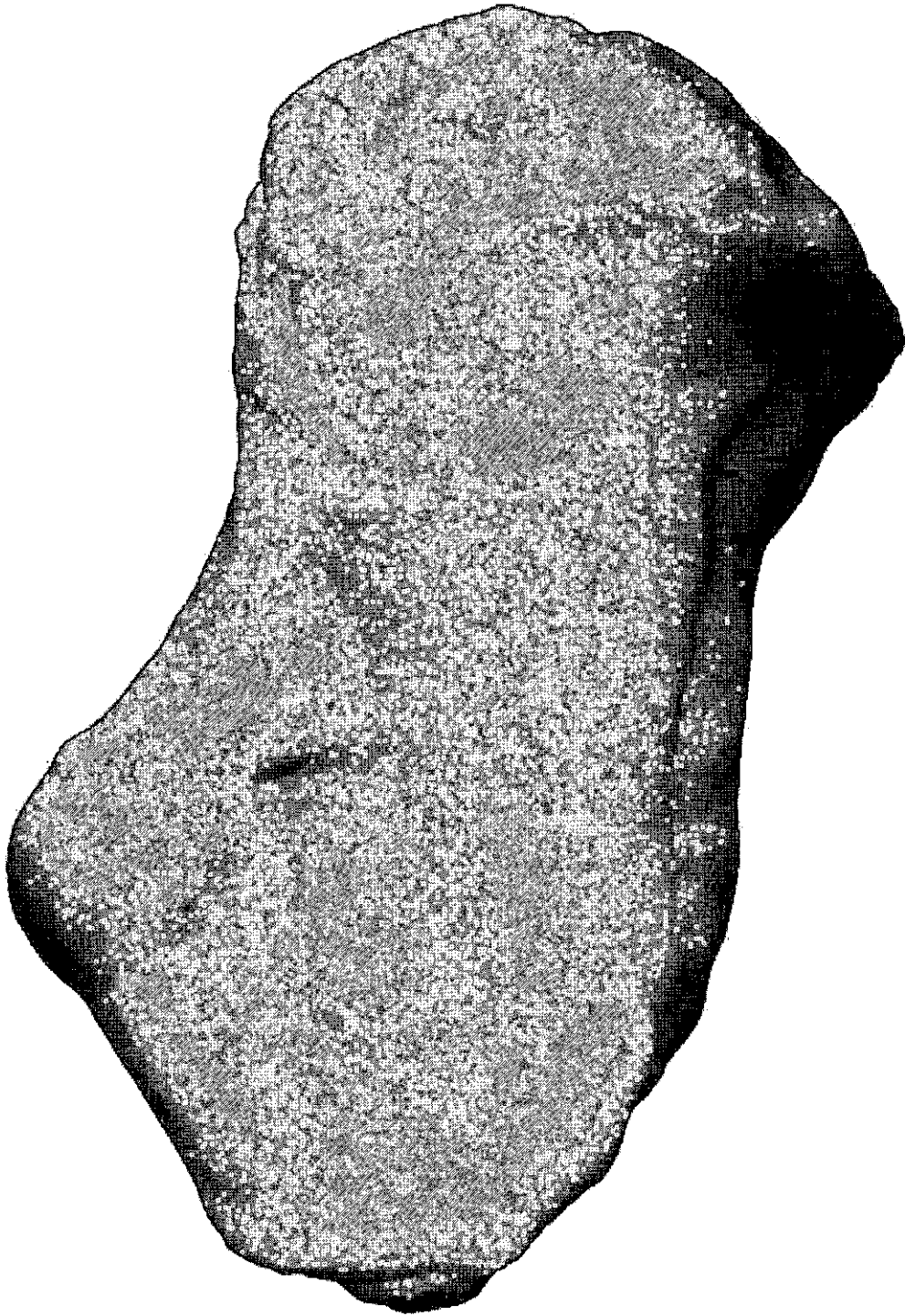


Figure 7. Metatarsal I, With Visible Seams.

## CHAPTER TWO

### RESULTS I: ANATOMICAL DESCRIPTION

#### Tarsus

Only one tarsal is present in this specimen. Other tarsals are known from other specimens. Most descriptions list four tarsals; two in the proximal row, astragalus and calcaneus, and two in the distal row. Gilmore's (1917) description of *Brachyceratops* describes five tarsals; two in the proximal row and three in the distal row. Of the described tarsals, this specimen is most likely the first and largest tarsal of the distal row. The confusion as to which tarsal this is arises from the possible shift in the position of this tarsal as well as the lack of other definite tarsals of the distal row for relational comparison. Conflicting descriptions make it difficult to determine exactly which tarsal this is. Based on Brown's (1917) previous description, Brown (1917) and Lull (1933) list the largest tarsal of the distal row as articulating with the fourth metatarsal. Gilmore (1917) describes the largest as articulating with the second metatarsal, the smallest with the third and the last tarsal exclusively associated with the fourth metatarsal.

The unreconstructed tarsal of TMP 89.97.01 was fixed firmly to the base of the third metatarsal by matrix. The element is discoid in shape with flattened proximal and distal surfaces and expansion toward the dorsal, plantar, medial and lateral surfaces. The circumference along those dorsal, plantar, medial and lateral surfaces is rugose. The proximal articular surface is slightly concave and smooth with the distal articular surface generally convex, with a cranio-caudally oriented groove creating a shallow depression in the center. The body of the disc is the thickest portion with a gentle tapering toward the circumference giving the tarsal the shape of a saucer with blunted edges.

#### Metatarsals

The proximal ends of each metatarsal fit together and are closely applied to each other. The third is the largest, followed closely in size by the second. The fifth is the smallest and the first is the next smallest (figure 8). The second through fourth articulate closely along their entire proximo-distal length to form a single functional unit with the third metatarsal as the axis.

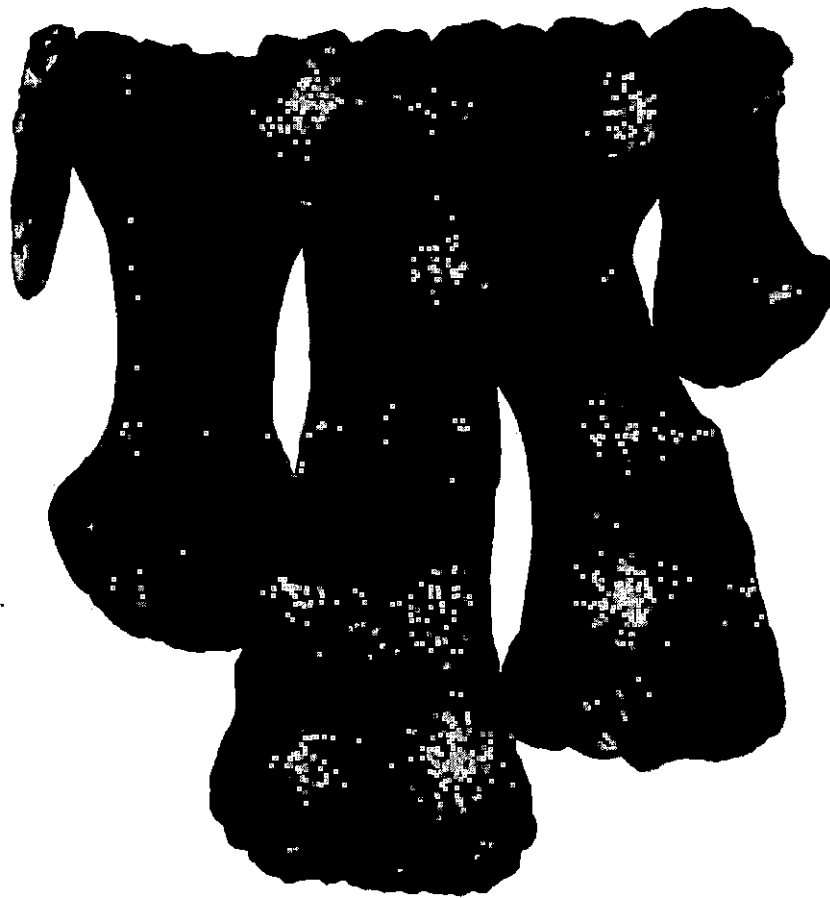


Figure 8. Metatarsals I to V.  
Note the Closely Packed Metatarsals With  
Tightly Fitting Proximal Ends. Dorsal is  
Facing the Viewer, Distal is Down.

All except the fifth show constriction or compression along the shaft and are expanded at the proximal and distal articular surfaces. The expansion is medio-laterally directed at the distal end whereas it is cranio-caudally directed at the proximal end.

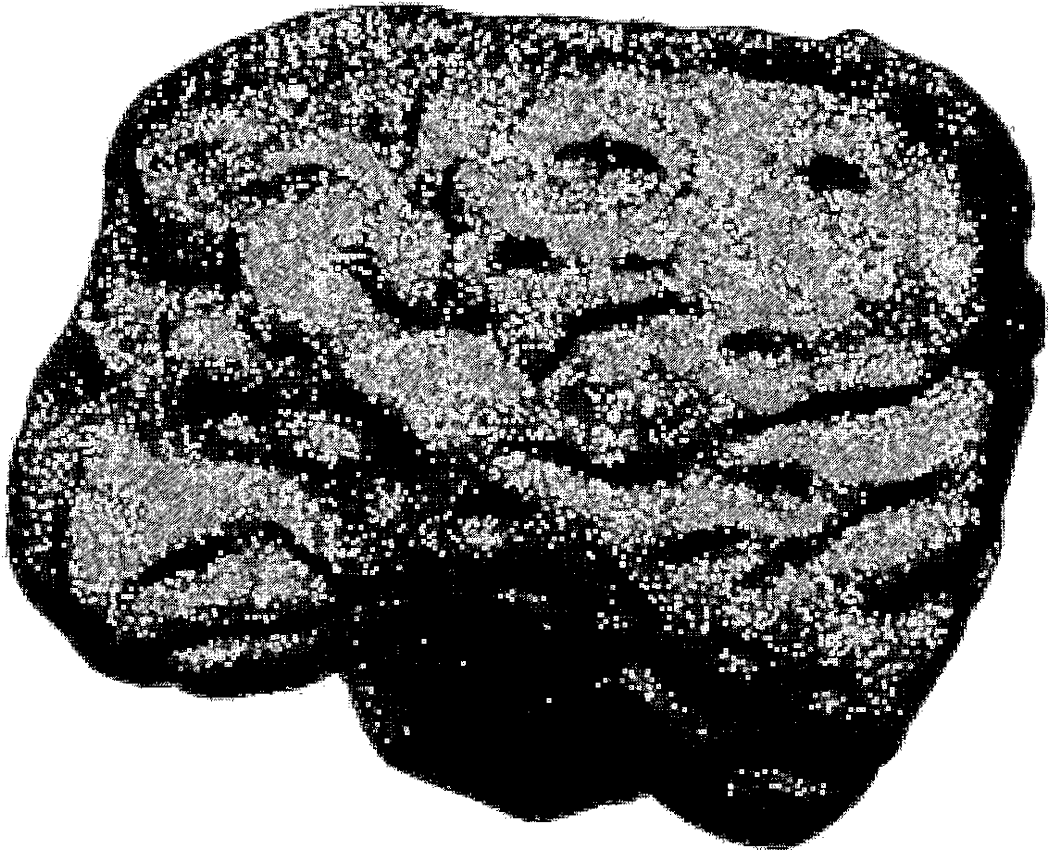


Figure 9. Distal Articular Surface of Metatarsal II. This Rugose Surface is Indicative of the Presence of Cartilages Covering the Surface in Life. Dorsal is to the Top.

Both proximal and distal articular surfaces are rugose, presumably due to the presence of articular cartilages in life (figure 9).

Metatarsal I (see figure 8) is short and stout with an irregular shape. The first metatarsal is approximately

half the length of the second. The proximal surface is roughly triangular with a small indentation on the dorsal surface lending a heart shape to the surface. The distal surface is quadrangular with the lateral aspect being larger than the medial aspect. The distal end of the metatarsal turns medially away from the second metatarsal.

Metatarsal II and metatarsal III are nearly identical in shape, though there is some slight difference in relative size, as well as in the shape of the base (figure 10). The third metatarsal is slightly longer than the second and is the longest of all metatarsals. Both elements possess a quadrangular cross section throughout. The medial aspects of their proximal ends are concave to allow a close articulation with the metatarsal that is immediately adjacent on their medial aspect. The lateral aspect of the proximal end of metatarsal II is shallowly convex to articulate with metatarsal III. The lateral aspect of the base of metatarsal III is also convex, with a relatively more pronounced curvature leading to a more triangular shaped base than that of the quadrangular second metatarsal (figure 10). The distal ends of both metatarsal II and III are notched on the plantar aspect giving rise to distinct medial and lateral condyles.



Figure 10. Proximal Articular Surfaces of Metatarsals II and III. The Bases of Metatarsals II and III are Quite Different in Shape, Which Allows Them to Fit Closely Together.

Metatarsal IV is nearly equal in length to the second metatarsal but has a dramatically different shape (see figure 8). The base is roughly triangular in a manner similar to that of the third metatarsal with the narrow apex of the triangle located on the lateral aspect. The apex of the triangle at the base of the metatarsal projects laterally giving the base of this element an especially



flared outline when viewed dorsally. The triangular cross section continues through the shaft of the element changing gradually into the quadrangular distal articular surface. The distal articular surface is the most truly quadrangular of all the metatarsals. Of all the elements' articular surfaces, this comes closest to being truly square. That square shape is interrupted only by the presence of a concavity on the medial aspect to allow for a close articulation with the shaft of the third metatarsal. The distal articular surface is rugose and concave similar to the other metatarsals but, like the first metatarsal, lacks distinct condyles. Rather, the distal articular surface forms a true head.

Metatarsal V is only partially preserved in this specimen. The fifth metatarsal of TMP 89.97.01 is represented only by the proximal portion, which was firmly united to the base of the fourth metatarsal. In accordance with Brown (1917), Gilmore (1917), and Lull (1933) this element is interpreted here to be vestigial and remains only in the form of a narrow splint which is applied to the plantar and lateral aspects of the base of the fourth metatarsal.

## Phalanges

The phalanges of this ceratopsid pes follow the standard ceratopsian phalangeal formula of 2-3-4-5-0. The proximal and intermediate phalanges of all digits are fairly conservative and consistent in shape, with only the unguals being markedly different. The basic shapes of the proximal and intermediate phalanges are quadrangular with a concave base at the proximal articular surface and a saddle shaped head at the distal articular surface. The heads of these phalanges all show lateral depressions with very pitted surfaces. The proximal articular surfaces of the proximal phalanges and unguals are rugose, whereas all other articular surfaces are smooth.

### Proximal Phalanges

The proximal phalanx of the first digit is the longest and is approximately the same length as the first metatarsal. The base is concave with a rugose articular surface. The phalanx of the first digit is not only longer than it is wide, it also has a distinct bias to the orientation of the base. The base of the proximal phalanx of the first digit is slanted from proximo-medial to disto-lateral (figure 11). This angulation results in a prominent flange on the dorso-medial aspect of the phalanx.



Figure 11. Proximo-Medial View of the First Phalanx of the First Digit. Illustrates the Bias of the Base With the Thicker Lateral Aspect and Narrower Medial Aspect Leading to the Formation of a Prominent Flange on the Medial Aspect.

The shaft of the phalanx is constricted slightly with the base and head being slightly wider. The lateral side of the phalanx is very nearly perpendicular to the cranio-caudal plane in sharp contrast to the medial side which gradually slopes down from the long axis of the phalanx. This results in a proximo-distally oriented ridge on the dorsal aspect of the lateral side with the ridge falling off sharply on the lateral edge and sloping gradually toward the medial edge. With the exception of the

aforementioned sloping ridge, the shaft of this phalanx, although narrower than the base and head, follows a relatively smooth straight line from the base to the head with no distinct concavity along any of the sides. The head of the phalanx is slightly wider than the shaft yet retains the sharp lateral edge and sloping medial edge all the way to the articular surfaces. There are two lateral depressions in the head of the phalanx with extremely pitted surfaces. These lateral pits have thick, curved borders reminiscent of rams' horns which extend from the dorsal aspect down to the plantar aspect and define the limits of the distal articular surface (figure 12). The distal articular surface of this phalanx does not show the saddle shape typical of the other phalanges, but is instead smoothly cylindrical as it curves from the narrower dorsal edge to the broader plantar edge.

The bases of the proximal phalanges of the second and third digits are straight and perpendicular to the axis of the digit, unlike the slanted bases of the first and fourth digits.



Figure 12. Lateral View of the First Phalanx of the First Digit.  
This View Illustrates the Lateral Pits at the Distal End of the Phalanges With Their "Rams Horn" Like Border. Dorsal is to the Top, Distal to the Right.

The proximal phalanges of the second and third digits are shorter than those of the first digit and more squared off with a length that more closely matches the width of the element. The proximal phalanx of the second digit is nearly square in outline, whereas the proximal phalanx of the third digit is wider than it is long. The base and head of the phalanx is wider than the shaft, with the shaft being constricted equally along both sides in the medio-lateral plane. When viewed from the side however, there is

an obvious arch resulting from a convex bump or raised surface on the dorsal aspect and a concavity or bend in the plantar aspect. This arch is a feature which is characteristic of, and peculiar to, the proximal and intermediate phalanges of the second, third and fourth digits, which are most likely the weight bearing digits of the foot. The bump or arch is present on all proximal and intermediate phalanges of the second and third digits, but is limited to the first two phalanges of the fourth digit. The distal articular surfaces at the heads of the proximal phalanges of the second and third digits show a characteristic saddle shape with medial and lateral edges extending distally and the dorsal and plantar surfaces falling off in the proximal direction. The saddles are approximately symmetrical, but it isn't clear if the head of the proximal phalanx of the second digit is completely symmetrical. It has not been possible to determine whether this element is symmetrical in the manner of the third digit, or if it has a naturally occurring bias toward the lateral side. It is possible that the slant is due to distortion during preservation. However, if the slant is natural, then it is due to the lateral edge of the head of the phalanx extending further distally than the medial

edge. The heads of the proximal phalanges of the second and third digits both exhibit the same lateral pits seen on all proximal and intermediate phalanges. These elements retain the "rams' horn" shape of the proximal phalanx of the first digit, although in a relatively more gracile form.

In a manner similar to the proximal phalanx of the first digit, the base of the proximal phalanx of the fourth digit is also slanted, but in the opposite direction. The slant of the phalanx of the fourth digit results in a flange or lip on the lateral aspect of this phalanx. The proximal phalanx of the fourth digit continues the trend of becoming shorter and similar to the third digit, this element is broad and short. With the singular exception of the slanted base the proximal phalanx of the fourth digit is similar in all other respects to its counterpart in the third digit. There are no known phalanges of the fifth digit.

#### Intermediate Phalanges

The first and fifth digits do not possess intermediate phalanges. The intermediate phalanges of the second and third digits are similar in shape and differ only in size. The shape is reminiscent of the proximal phalanges with

only minor differences. The bases of these elements are not squared off and perpendicular to the axis of the digit. Rather, the base is a saddle-shaped articular surface which complements the saddle of the distal articular surface of the more proximal phalangeal element. The saddle-shaped base of the intermediate phalanges is a result of the articular surface extending proximally along the dorsal and plantar edges and receding distally along the medial and lateral edges. The short shafts of the intermediate phalanges retain the dorsal ridge and the medio-lateral constriction of the proximal phalanges. The lateral depressions are present as well in a shallow, reduced form. They are readily distinguished by their pitted surfaces. The "ram's horn" effect associated with the depressions is reduced as well owing to the less robust borders of the pits. The distal articular surfaces of the intermediate phalanges mimic that of the proximal phalanges and demonstrate the same saddle shape.

The first intermediate phalanx of the fourth digit is nearly identical to the intermediate phalanges of the second and third digits. The single notable difference is the shape of the base and proximal articular surface. This element does not possess the interlocking saddle shape



which complements the distal surface of the proximal phalanx. The proximally oriented projections on the dorsal and plantar edges remain, as do the distally receding medial and lateral edges; however, the smooth saddle shape is lost and is replaced instead by a cranio-caudally oriented ridge bisecting the proximal articular surface. The result is a phalanx which deviates from the roughly quadrangular shape of the other phalanges and is somewhat more reminiscent of a chevron. The first intermediate phalanx of the fourth digit retains the dorsal process and lateral pits seen on the intermediate phalanges of the second and third digits. The remaining two intermediate phalanges of the fourth digit continue the trend toward chevron shaped elements (figure 13). The phalanges become progressively shorter as they progress distally and these elements lack the dorsal process of their immediate, more proximal, predecessor.

### Unguals

The unguals are the terminal phalanges of each digit, and are easily differentiated by their unique shape. When viewed from the dorsal aspect, each ungual has a mushroom shaped outline with a narrow base and a broad, spatulate distal end.

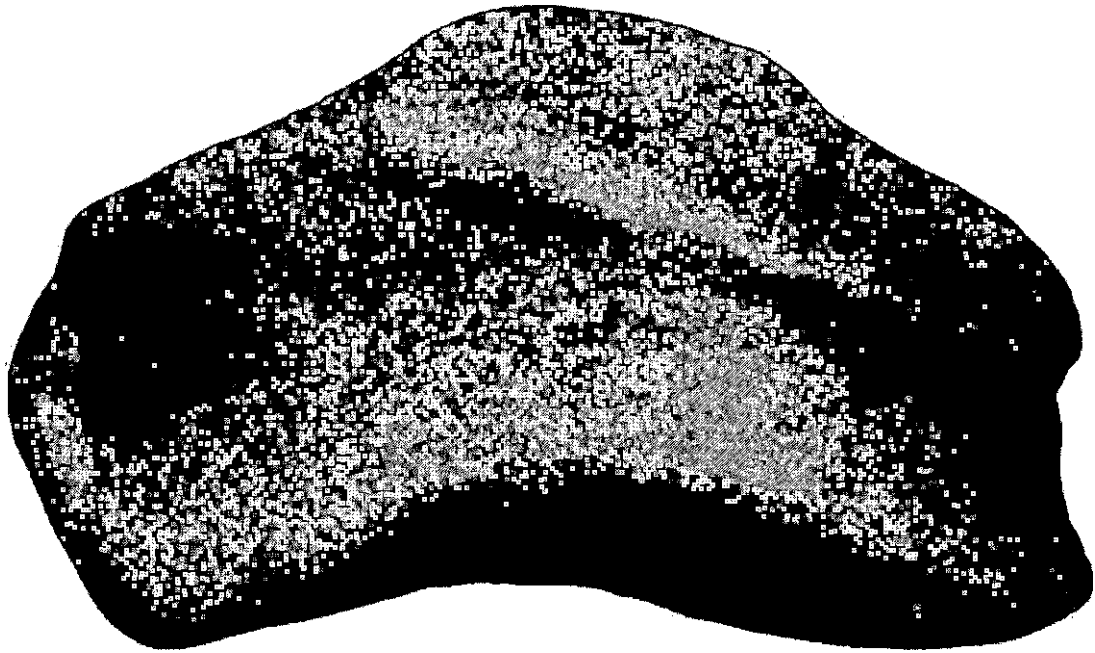


Figure 13. Chevron Shape of an Intermediate Phalanx. This is the Characteristic Shape of an Intermediate Phalanx. Dorsal is Facing the Viewer, Distal is to the Bottom.

In lateral view the unguals are cuneiform, beginning with a broad proximal end and tapering to a narrow distal tip. The unguals of the first and fourth digits are the smallest and are approximately equal in size. Those of the second and third digits are larger with the third being the absolute largest. The fifth digit, having no phalanges, lacks an ungual. The proximal articular surfaces of the unguals vary in shape from flat to slightly concave.

Smaller unguals, particularly those of the first and fourth digits, exhibit the flatter base while larger unguals tend toward the concave base. In contrast to the intermediate phalanges which immediately precede them, the unguals have rugose articular surfaces. A short distance distal to the articular surface, the ungual widens drastically in the lateral and medial directions. Curving in the proximal direction from the now widened body of the ungual are symmetrical processes (figure 14). The dorsal and ventral surfaces of the unguals are rough near the base and become increasingly more so with various foramina and small processes marking the surface as the element tapers toward the narrow, distal edge of the phalanx. The most prominent of these foramina are located near the base of the proximally directed processes that extend from the medial and lateral edges of the ungual. These foramina are more visible on the larger unguals, namely those of the second and third digits. The smaller foramina are more plentiful along the perimeter of the ungual and as they approach the edge they ultimately result in a crenellated and uneven border. This pattern of surface morphology, when observed in fossil materials, is frequently associated with the presence of a horny sheath or hoof-like covering.



Figure 14. Ungual Demonstrating the Proximally Directed Processes.

The association of the foramina with a hoof is likely due to examination of the unguals of extant ungulates like horses and ruminants. The unguals of horses have been exhaustively studied and described (Getty, 1975; Dyce et al., 1996) and are similar to those of the ceratopsids in

one particular aspect: the unguals of horses are riddled with foramina. The purpose of these foramina is to supply vasculature to the corium (dermis) of the hoof (Getty, 1975; Dyce et al., 1996) and it is probable that a similar purpose can be ascribed to the foramina of the ceratopsid unguals.

CHAPTER THREE  
RESULTS II: FUNCTIONAL HYPOTHESES AND  
INTERPRETATIONS

As mentioned above, ceratopsian dinosaurs are an attractive focus for locomotor studies, as testable questions remain about their locomotor capabilities. Significantly, their postcranial skeletal structure remains conservative enough that careful analysis of one taxon can provide significant insights about other closely related taxa. As large herbivores with a vertebral column that acts as a stiff, weight-supporting strut, questions of ceratopsian posture and locomotion are limited largely to limb orientation and movement. The phylogeny of ceratopsians, particularly that of neoceratopsians is fairly well resolved (Dodson and Currie, 1990; Dodson, 1996) thus addressing the importance of a phylogenetic context for functional analyses (e.g. Sumida and Modesto, 2001).

A Biological Problem

Both the paleobiological inquiry into lifestyles of extinct archosaurs, and the public's interest in all things

dinosaurian have encouraged the understanding and dissemination of information regarding dinosaur locomotion. A variety of recent studies have begun to unravel the details of locomotor behavior in major groups of dinosaurs such as hadrosaurs (Dilkes, 1999, 2001), sauropodomorphs (Wilson and Carrano, 1999; Carrano, 2001), large terrestrial theropods (Hutchinson and Garcia, 2002), and feathered theropod dinosaurs (Xu, et al., 2002), as well as the evolution of individual elements of the locomotor apparatus across clades (Carrano, 2000). However, in the case of ceratopsian dinosaurs, there exists a polarized debate in which limb structure and orientation have been restored in fundamentally different ways. This range of potential postural differences of course then affects significantly any interpretation of locomotor capabilities.

Reconstruction of the limb posture in ceratopsians spans a range of disagreement. Most of the controversy has centered on the structure and posture of the forelimb. However the same limitations of analysis that have caused so much debate about the forelimb must be noted for the hindlimb as well.

- (1) In one manner, the forelimbs have been reconstructed with a "sprawling" orientation in

which the elbow joint is flexed to a significant degree and directed laterally. This would then imply that ceratopsians were unable to run at high speeds (e.g. Johnson and Ostrom, 1995; Dodson, 1996). Furthermore, it then requires the pes to be directed in one of two ways: laterally, a position in which the toes are frequently reconstructed as splayed; or cranially, a position that then requires significant rotation at the knee and/or ankle.

- (2) In a marked departure from previous interpretations, Bakker (1987) suggested that most nonavian dinosaurs, ceratopsids amongst them were extremely agile; and capable of locomotor speeds rivaling those of mammals of similar size. To adopt such a mammalian set of locomotor capabilities, Bakker restored ceratopsians with a parasagittal limb posture, i.e. limbs tucked directly underneath the body. Support of the large, barrel-shaped herbivores' body further suggested to him that the limbs were carried in an essentially columnar, or graviportal fashion, much like that of extant elephants. Bakker's



three-dimensional hypothesis of body structure and subsequent locomotor capability was based on his own two-dimensional drawings. Though compelling, it remained a functional hypothesis that was "tested" only by analysis of his own illustrations. In this case, the pes is directed cranially, with no significant rotation necessary at the ankle. This hypothesis demands neither a splayed or nonsplayed foot posture, though Bakker generally illustrates the foot as similar to that of a rhino with no explanation based on actual elements of the pes.

- (3) Both of the previous studies contrast with the view of Paul and Christiansen (2000). They restored ceratopsids as rhinoceros-like organisms with parasagittal locomotor kinematics and an ability to run faster than extant elephants (see also Garstka and Burnham (1997) in an earlier though less detailed study). Their view differed from that of Bakker (1987) in that although postural support is by parasagittal limbs, they retain significant flex at both the elbow and knee joints, even when not at motion. Despite

that they differ in certain of the postural details from the interpretation of Bakker (1987), their study suffers from a similar dependence on interpretation their own two-dimensional drawings for support of their three-dimensional locomotor hypotheses. The range of potential pedal postures for this hypothesis is essentially similar to that of Bakker's model.

Thus, there currently exist three hypotheses for the range of postural and linked locomotor ability in ceratopsians offering a wide range of potential orientations of pedal skeletal elements and related postures. Although all of these studies have as their basis actual skeletal elements, only that of Johnson and Ostrom (1995) actually generated a working three-dimensional model of a ceratopsian limb. That being said, the model produced was necessarily limited to being a single hypothetical example. The more recent study of Paul and Christiansen (2000) criticized that of Johnson and Ostrom (1995) but suffered in its own right as it was a three-dimensional functional interpretation based on strictly lateral and frontal view two-dimensional drawings.

Thus, the question of ceratopsian posture and (consequently) locomotion remain uncertain.

This study proposes to serve as (1) a first step towards solving this dilemma; and (2) a model for future steps. To do so requires two significant philosophical differences from those studies that have preceded it. First, no one particular hypothesis of ceratopsian limb posture and locomotory ability is advocated here as a first principle. Such a priori reasoning would simply place artificial limitations on the study. Rather, the limb elements themselves (not two-dimensional drawings of them) should provide the three-dimensional data, and therefore, potential posture and range of movement. More properly, a range of potential limb structures and joint morphologies must be considered a continuum of potential hypotheses of limb orientation and potential function. The second difference in this study then suggests that the only way to do this is to develop multiple three-dimensional models that span the range of potential joint morphologies. Those potential joint morphologies must take into account the necessary contribution of soft tissue structures that are not normally preserved in the fossil record and were not included in the above three classes of studies. Addressing

the range of potential element and joint morphologies remains difficult in execution given the size of ceratopsian dinosaurs; thus, it is important that there be availability of reliably well preserved materials needed to generate those hypotheses.

It must be noted in passing that, although significant publicity has been generated by the digital *Triceratops* project (Andersen et al., 1999; Chapman et al., 2001; Walters et al., 2001), that project was limited by a number of conditions: (1) the manus and pes were presumed to be noncompliant blocks instead of as a mosaic of interacting elements; (2) reconstruction of joint surfaces did not take into account potentially differing thicknesses of cartilage and related joint congruence; (3) postural assumptions did not consider data from internal trabecular structure (e.g. see Swartz et al., 1998) or gross morphological curvature of the skeletal elements (e.g. as prescribed and demonstrated by Bertram and Biewener, 1988) ; and (4) the software package utilized was of minimal versatility for biomechanical analysis and dissemination.

The problem of determining biologically realistic locomotor behaviors for ceratopsians dinosaurs can be addressed, but only if certain criteria can be met:

- Representative skeletal material must be from one (or preferably more) well-preserved individual(s), or if disarticulated materials are to be used, there must be confidence that they are all from similar ontogenetic stages of the same taxon.
- Skeletal preservation must be excellent, and distortion must be either minimal, or easily correctable.

As demonstrated in the materials and methods in Chapter One and the morphological description in Chapter Two, the study specimens utilized here satisfy these criteria.

#### A Multidisciplinary Approach and Solution

Ultimately, the strategies utilized to address the questions of ceratopsian structure, posture, and limb mechanics must combine biological, geological, computer, and digital modeling and animation. I have developed a digital model that can be further used to develop an interactive, animatable model of the pes of the centrosaurine ceratopsian dinosaur *Centrosaurus*. Given the conservative nature of the ceratopsian postcranial skeleton (Dodson, 1996), this model could then be easily modified

for use with other ceratopsians, other quadrupedal dinosaurs, and other tetrapods in general.

Placement of individual elements of the limb in the three-dimensional digital volume allows an assessment of each joint individually, and all joints as a linked series. The first step of joint analysis will be to consider the potential articular surfaces. Extinct archosaurs have variably ossified limb bones, so the cartilaginous contribution to joint morphology is generally under appreciated or excluded in functional analyses (Holliday et al., 2001). Additionally, testable hypotheses are often rare or completely absent from so-called functional analyses of fossil vertebrate. The extant phylogenetic bracket criterion demands that the range of variability of structures in extinct taxa must be determined by those that can be observed in bracketing extant taxa (Witmer, 1995). Holliday et al. (2001) have demonstrated that the thickness of articular cartilages may change joint shape and element length by as much as 6% in long bones to 20% in the scapula and pelvic girdle of alligators, crocodiles, and birds. Thus, it is reasonable to presume that a similar range of cartilaginous thickness must be considered for extinct archosaurs, including centrosaurine ceratopsian dinosaurs.

The strength of Maya together with ZBrush as modeling programs is that it allows modification of the base structure as defined by the bony structure derived from the 3-D laser scans. Guided by the extant phylogenetic bracket taxa defined by Witmer (1995) and Holliday et al. (2001), a series of thickness of cartilage caps may be developed as individually testable models. Those thicknesses and shapes that define a joint morphology that are not completely congruent will suffer from the digital condition of "interpenetration"—the condition in which volumes attempt to pass through one another in three-dimensional digital space (Bruderlin, 2001; Lewis et al., 2001). In essence, a series of testable joint morphologies can be generated.

Once the three-dimensional limitations of individual joints are determined by the elimination of impossible morphologies, each joint can be linked to the others within the modeling program. The program can construct three-dimensional moving volumes with a series of ever-increasing numbers. The raw polygonal structures that determine surface structure (and thus movements) are commonly referred to as wireframes. The greater the number of polygons that determine a wireframe's surface, the more closely it mirrors an actual biological structure.

Although expensive in terms of computing memory and necessary processor speed, Sumida (2000, 2001) has shown that the most efficient wireframe for modeling animal locomotion is the skeleton itself. These strategies in concert with these tools have been used only sparingly in paleobiological investigations (Gatesy et al., 1999; Evans and Fortelius, 2008; Polly and MacLeod, 2008; Rybczynski et al., 2008), but are the common standard of the animation and digital special effects industry. Thus, the generation of high fidelity, complete skeletal animations is not new—any current movie with digitally modeled characters attests to that. However, skeletal imaging and animation of this quality has rarely been achieved for publication or similar dissemination in the paleobiological sciences.

#### Postural Interpretations and Implications of the Reconstructed Pes

Although this study does not presume to provide an answer to all questions regarding the structure and function of the ceratopsid pes, it does offer some clarity and direction in: (1) it complements studies that are otherwise biased toward the skull or more proximal elements; (2) it provides a tentative reconstruction



allowing the most reasonable comparison to date with extant models; and (3) it provides the necessary distal element for future inverse kinetic hypotheses of locomotor function.

The debate over limb posture and orientation is far from resolved and even the manner in which to approach this problem is debatable. One thing however is clear: the distal most element of the appendage, manus or pes, is an essential component of any hypothesis and must absolutely be accounted for. In the case of the hind limb, the foot is the element which contacts the ground. This point of contact with the substrate should provide the starting point for any analyses of limb posture. Traditional descriptions of the ceratopsid limb focus on the head, the most variable of ceratopsian traits and the one used to differentiate species (Hatcher et al., 1907; Brown, 1917; Gilmore, 1917; Lull, 1933), but the level of detail falls off dramatically for the more distal skeletal elements. This is also true for functional analyses, which focus on the large bones of the limb and their orientation to the exclusion of the ground contact element (Bakker, 1987; Johnson and Ostrom, 1995; Dodson, 1996; Garstka and Burnham, 1997; Paul and Christiansen, 2000). Paul and

Christiansen (2000) extend their analyses to the ground by attempting to match their hypothesis with trackways attributed to ceratopsians, but do so only after establishing limb posture based on the orientation of the larger, more proximal limb elements. Future studies should take care not to underestimate the importance of the ground contact element of the limb and properly account for its posture and orientation.

#### Revisiting the Ceratopsian Pes

Ceratopsid tarsals are exceptionally rare and are even more rarely described. It is believed that there were two rows of tarsals (Brown, 1917; Gilmore, 1917; Lull, 1933), but their exact number and proportions are not known. The tarsals are widely believed to have been poorly ossified leading to their rarity in the fossil record (Lull, 1933; Dodson and Currie, 1990; Dodson, 1996). Descriptions of the known tarsals make it apparent that they were not particularly robust elements (Brown, 1917; Gilmore, 1917; Lull, 1933; Dodson and Currie, 1990; Dodson, 1996). In ceratopsians, the metatarsals and digits are the dominant elements and the tarsals are relegated to secondary status. This is in contrast with the large tarsals of elephants that coincidentally have similarly robust metatarsals.

Elephant tarsals are stout and the entire tarsal apparatus rivals that of the metatarsals in volume occupied within the foot (Starck, 1979).

Ceratopsid metatarsals are closely applied to each other along their length. This is especially true of metatarsals II and III, which likely served as the principal axis of the foot. This is similar to the foot of the rhinoceros, but contrasting with the foot of the elephant. Whereas elephant feet have large tarsals and metatarsals that are short, broad and tend to splay away from each other to accommodate a large, central fat pad; rhinoceros tarsals are smaller and less robust than those of elephants, and the metatarsals are relatively longer and more closely applied to each other (Starck, 1979).

The ceratopsid pes likely had small tarsals, and definitely has elongate metatarsals that fit closely along their length. Although there are obvious size and proportional differences, the external morphology is reminiscent of that of the extant ungulates. In ungulates, horses and ruminants particularly, the distal elements of the limb are reduced and this results in a closely packed metatarsus serving as a single functional unit (Getty, 1975; Dyce et al., 1996).

In Chapter Two it was noted that ceratopsid unguals are broad and spatulate. This is similar to the unguals of hadrosaurs, and ceratopsid phalanges can be confused with those of hadrosaurs when encountered together (Ryan, 1992; Ryan et al. 2001). In addition, ceratopsid unguals are porous, with the dorsal and distal surfaces displaying numerous foramina. This is again reminiscent of the condition in extant ungulates. In them the distal phalanx has an extensive network of foramina to house the vasculature supplying and draining the dermis of the hoof (Getty, 1975; Dyce et al., 1996). This is in direct contrast with the elephant, in which the distal phalanges are small, rounded and lack significant numbers of foramina (figure 18); the rhinoceros is intermediate, with distal phalanges that are broad and flattened with large foramina on the proximal end but lacking the extensive network of foramina on the dorsal and distal surfaces (Starck, 1979).

#### Life Reconstructions

Comparisons with extant large mammals, ungulates and extinct hadrosaurs lead to several hypotheses regarding the form of the pes in a live ceratopsid. The lack of ossification and probable insignificant size of the ceratopsid tarsals coupled with the elongate, closely

associated metatarsals and the large, spatulate unguals indicate that the metatarsals and digits were likely the primary weight bearing elements of the foot. In elephants, the tarsals sit upon a large fat pad with the metatarsals and digits splayed and arrayed around the pad (Stark, 1979). The unguals of the elephant are small and rounded, unlike those of the rhinoceros, ceratopsids and hadrosaurs. Hadrosaurs are facultative bipeds and it is well known that their unguals were weight-bearing elements (Weishampel and Horner, 1990). The close association of the metatarsals and the spatulate unguals indicate that the ceratopsid pes bore weight on the digits, particularly the unguals, and not on a large fat pad as in the elephant. The most extreme example of tightly packed metatarsals and weight-bearing unguals can be seen in extant ungulates that have long metatarsals and broad porous unguals (Getty, 1975; Dyce et al., 1996).

The porous nature of ceratopsid unguals highlights another similarity with extant ungulates: the likely presence of a hoof, or a horny covering of the distal phalanx. In horses and ruminants, the presence of a network of foramina throughout the ungual is necessary to allow the vasculature which supplies and drains the corium

(dermis) of the hoof to pass through the bone and reach the dermis, which it is unable to do superficially due to the presence of the hoof (Getty, 1975; Dyce et al., 1996). A similar association between a porous ungual and the presence of a hoof, or at the very least a tough covering of keratinized tissue, can be reasonably postulated for the ceratopsids. This contrasts sharply with the distal phalanges of the elephant. Elephants are large mammals with columnar limbs and comparison can be made between the limbs of elephants and those of ceratopsids. In the elephant, the distal phalanges are small and rounded and lack an extensive network of foramina (Starck, 1979).

Taken together, these traits indicate the morphology of the ceratopsid pes is likely a hybrid of features seen in extant taxa: (1) The small, variably ossified tarsals, close-packed metatarsals and spatulate unguals indicate a pes with the metatarsals and digits as the primary weight-bearing element. (2) The close-packing and broad unguals are incompatible with the idea of a widely splayed foot with the digits arrayed around a large centrally located fat pad. (3) The network of foramina of the unguals are indicative of a hoof or horny covering on the distal phalanges. Digits II and III would be the primary weight-

bearing elements, closely followed by digit IV and digit I relegated to a minor role. This conclusion can be inferred by comparing the relative sizes of not only the metatarsals but the unguals of those digits. Although there are obvious size and proportional differences, the morphology of the ceratopsid pes calls to mind that of suids in which all digits bear a hoof and "full complement of bones" and the accessory digits are located caudal to the principal weight-bearing digits (Dyce et al., 1996). In the pig, the accessory digits are smaller than the principal ones and only bear weight on soft ground (Dyce et al., 1996). A similar condition, with a slight modification in which the accessory digits are located more lateral than caudal is proposed here for the ceratopsid pes.

APPENDIX A  
SPECIMENS UTILIZED IN THIS STUDY



		Accessioned Specimens in Tyrell Collections						Field Numbers from DPP Field Station Specimens (Unaccessioned)
Disarticulated Unassociated Elements	Metapodial	81.16.225	85.36.216	88.36.32	66.32.14	81.18.34	BB 91-267	
		80.18.43	81.19.297	93.666.20	81.26.181	79.11.152		
		89.18.92	79.14.304	81.23.168	80.18.266	82.18.255		
		79.11.72	65.23.51	67.8.62	80.18.95	80.18.43		
		82.18.183	80.16.1289	79.14.434	96.12.314	87.18.34		
	Phalanges	66.14.13	82.16.217	96.12.138	91.36.618	82.16.109	None	
		65.23.54	80.16.729	92.36.971	92.36.758	79.14.362		
		66.10.54	80.18.207	81.18.26	82.18.182	67.9.78		
		81.41.36	80.8.276	66.36.5	79.11.176	66.11.21		
		79.14.361	82.19.265	66.31.69	86.36.285	79.14.355		
		81.41.40	80.29.12	92.36.160	67.19.99	90.36.44		
		79.14.349	64.5.40	93.110.11	66.36.2	67.9.85		
		91.36.352	66.14.21	81.19.132	88.36.34	67.20.82		
		92.50.89	82.21.11	92.36.759	81.18.32	91.50.57		
		80.29.8	67.20.171	67.19.103	80.16.875	99.55.80		
		79.14.350	79.14.821	81.16.472	79.14.364	96.12.279		
		66.31.52	92.36.599	81.18.9	91.36.543	80.30.12		
		80.16.1413	92.36.285	67.9.86	91.36.755	94.44.13		
		81.19.242	67.17.87	92.36.399	66.10.56	94.12.344		
		67.9.91	85.56.240	92.36.771	67.8.65	96.12.25		
67.16.19	85.56.107	80.18.134	80.16.288	90.57.1				
79.14.430	94.44.5	92.36.764	91.36.348	90.5.56				
65.23.55	92.36.163	88.18.14	67.17.17	95.12.111				
81.16.394	80.16.147	92.36.265	66.36.4	94.12.861				
66.36.3	79.14.1060	89.36.280	82.19.246	98.93.18				
	82.16.271	82.16.267	81.16.393					

		Accessioned Specimens in Tyrell Collections					Field Numbers from DPP Field Station Specimens (Unaccessioned)	
Articulated Elements	Tyrell Museum	Pes (Composite of unassociated elements.)	79.14.818	79.14.352	66.32.10	80.16.52	79.14.358	None
			84.37.116	80.16.1655	82.18.103	66.33.2	82.18.77	
			82.18.159	82.18.129	65.23.58	67.9.73	80.16.1224	
			81.18.80	80.16.1376	67.8.41	80.16.1615		
	DPP Field Station	Manus (Complete & articulated, not a composite.)	89.97.01					None

APPENDIX B  
MEASUREMENTS OF TMP 89.97.01, BEFORE  
RECONSTRUCTION

Metatarsal Measurements

Metatarsal I	
Plantar surface of proximal portion of Metatarsal I obscured. All measurements taken from dorsal surface.	mm
Maximum medial length (condylar surface to condylar surface)	80.75
Maximum medial length (epicondyle to epicondyle)	48.66
Center proximal to center distal length (condylar surface to condylar surface)	90.16
Center proximal to center distal length (epicondyle to epicondyle)	52.29
Maximum lateral length (epicondyle to epicondyle)	60.20
Maximum proximal width	55.97
Maximum distal width	50.29
Medial height of distal articular surface	42.74
Lateral height of distal articular surface	29.52

Metatarsal II	
Dorsal surface of proximal portion of Metatarsal II obscured. Unable to measure from dorsal surface. All measurements taken from plantar surface.	mm
Maximum medial length (condylar surface to condylar surface)	174.00
Maximum medial length (epicondyle to epicondyle)	135.00
Maximum lateral length (condylar surface to condylar surface)	165.00
Maximum lateral length (epicondyle to epicondyle)	127.00
Maximum dorsal width of distal articular surface	64.25
Maximum plantar width of distal articular surface	62.24
Width of medial condyle of distal articular surface	26.71
Width of lateral condyle of distal articular surface	20.65
Medial height at distal articular surface	57.92
Lateral height at distal articular surface	52.80

Metatarsal III	
Tarsal attached to proximal end of plantar surface. Dorsal surface of proximal portion of Metatarsal III obscured. Tarsal attached to plantar surface. Unable to measure proximal end.	mm
Medial length (condylar surface to condylar surface, including Tarsal & matrix)	210.00
Lateral length (condylar surface to condylar surface)	197.00
Maximum dorsal width of distal articular surface	62.10
Maximum plantar width of distal articular surface	64.75
Maximum medial height of distal articular surface	57.95
Maximum lateral height of distal articular surface	48.59
Width of medial condyle of distal articular surface	26.86
Width of lateral condyle of distal articular surface	25.55

Metatarsal IV.		
Metatarsal V attached to proximal end of plantar surface. Most of head missing. Measurements taken to end of available specimen.		mm
Dorsal surface	Maximum medial length (condylar surface to condylar surface)	149.70
	Maximum medial length (epicondyle to epicondyle)	106.80
	Maximum center length (condylar surface to condylar surface)	150.60
	Maximum lateral length (condylar surface to condylar surface)	150.00
	Maximum width of proximal articular end	68.89
	Maximum width of distal articular surface	46.36
Plantar surface	Maximum medial length	130.10
	Maximum center length	145.30
	Maximum lateral length	144.90
	Maximum width of proximal articular end	70.70
	Maximum width of distal articular surface	46.25
Proximal articular end	Medial height	43.39
	Center height	41.80
	Lateral height	20.21
Distal articular surface	Medial height	36.50
	Center height	49.94
	Lateral height	50.26

Metatarsal V		
	Metatarsal V broken mid-shaft and fused to proximal end of Metatarsal IV	mm
Dorsal surface	Maximum medial length	38.73
	Maximum lateral length	37.84
	Maximum width of proximal end	21.72
Plantar surface	Maximum width of distal end	19.04

Phalangeal Measurements

Phalanges - All measurements in mm												
		Digit I	Digit II		Digit III			Digit IV				Digit V
		Phalanx 1	Phalanx 1	Phalanx 2	Phalanx 1	Phalanx 2	Phalanx 3	Phalanx 1	Phalanx 2	Phalanx 3	Phalanx 4	No Phalanges
	Medial length	73.36	53.59	26.86	49.50	25.50	25.83	36.48	22.32	20.49	15.96	N/A
	Center length	84.82	58.28	39.70	44.59	33.79	29.06	40.27	31.27	24.52	19.64	N/A
	Lateral length	60.12	58.73	33.30	47.66	21.54	26.24	54.28	26.46	14.99	15.84	N/A
Proximal articular surface	Maximum width	62.04	71.32	60.83	70.80	54.66	47.87	65.29	53.17	50.92	40.76	N/A
	Maximum height	43.70	42.88	39.85	50.02	39.94	33.33	46.73	43.40	39.02	30.91	N/A
Distal articular surface	Maximum width	43.84	63.14	56.24	58.81	55.11	50.82	55.15	53.54	48.39	39.08	N/A
	Maximum height	29.30	40.68	35.16	37.23	37.05	31.44	41.43	39.00	36.76	29.29	N/A

74

Ungual Measurements

Unguals (terminal phalanges) - All measurements in mm					
	Digit I	Digit II	Digit III	Digit IV	Digit V
Center length	55.48	82.86	73.88	61.07	N/A
Maximum articular surface width	47.45	61.51	52.99	38.89	N/A
Maximum articular surface height	32.38	35.00	30.50	25.99	N/A
Maximum width of spatulate portion of ungual	59.22	87.26	73.05	59.37	N/A

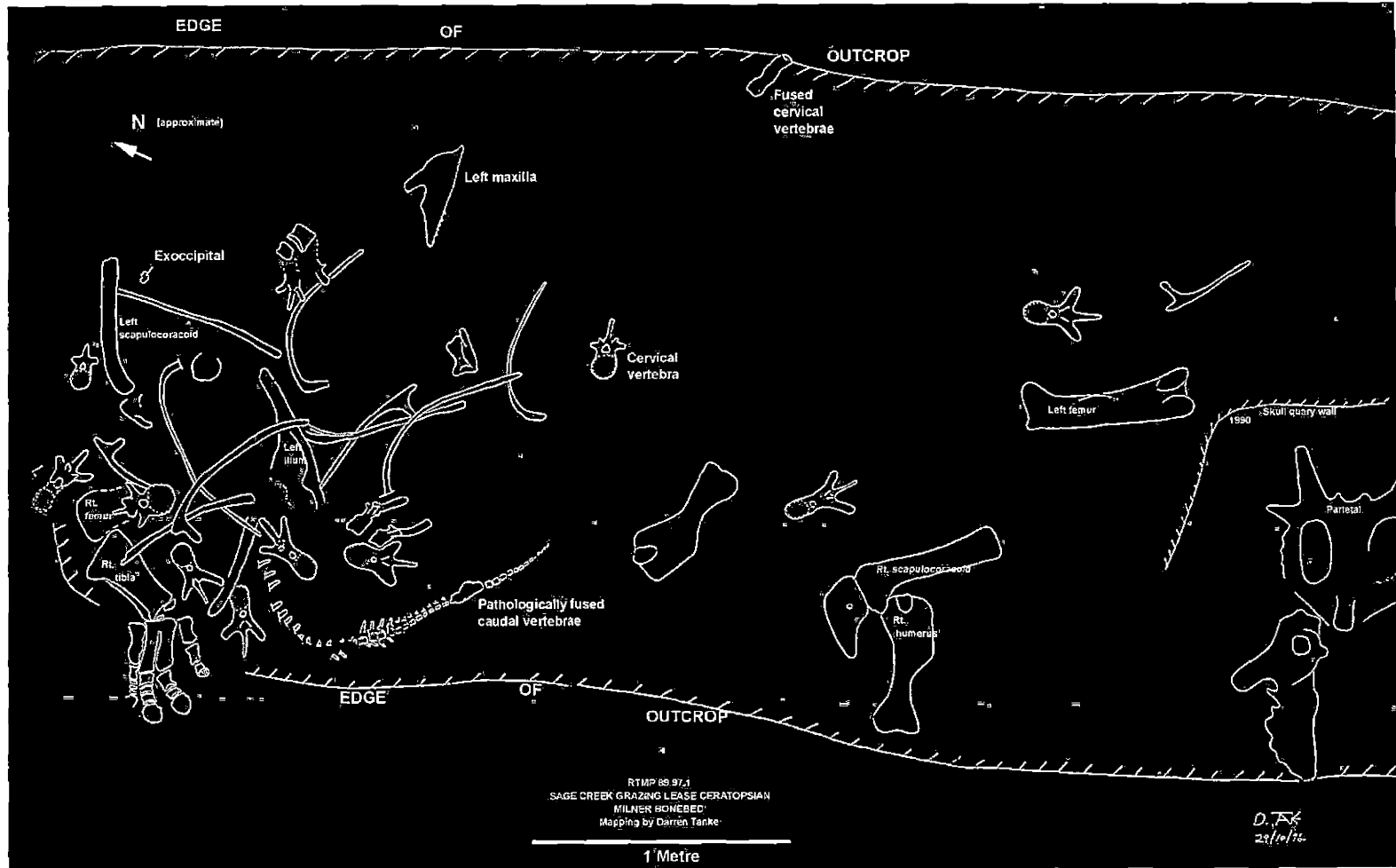
### Tarsal Measurements

Tarsal Bone	
Fused to proximal end of plantar surface of Metatarsal III.	mm
Maximum dorsal width	27.81
Maximum center width	53.11
Maximum plantar width	22.95
Maximum medial height	19.52
Maximum center height	45.93
Maximum lateral height	27.74
Maximum medial depth	22.49
Maximum center depth	18.95
Maximum lateral depth	14.02

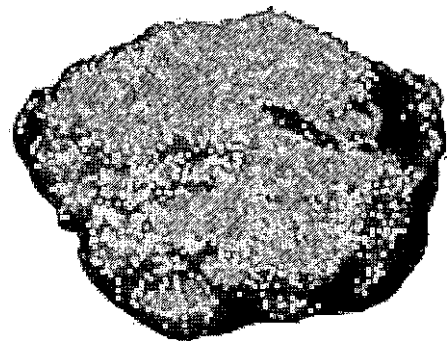
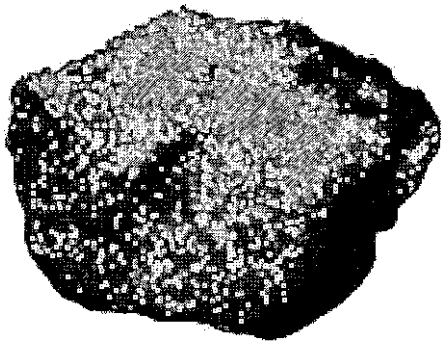
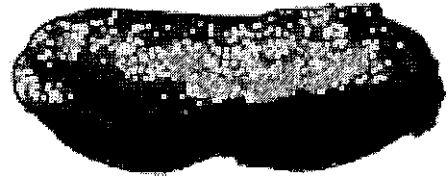
APPENDIX C

QUARRY MAP OF SITE FROM WHICH TMP 89.97.01 WAS  
RECOVERED

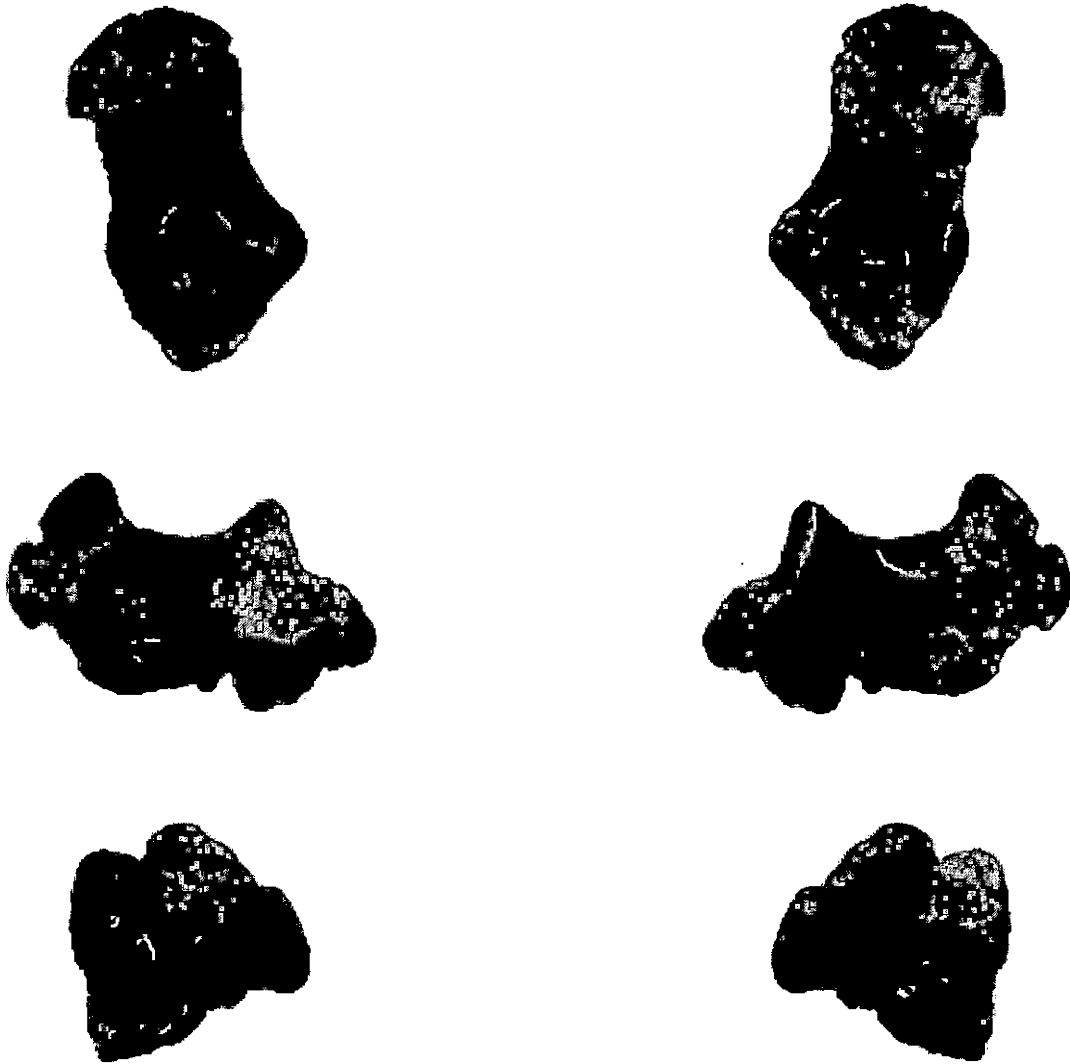




APPENDIX D  
ILLUSTRATIONS OF TMP 89.97.01 INDIVIDUAL ELEMENTS,  
BEFORE RECONSTRUCTION



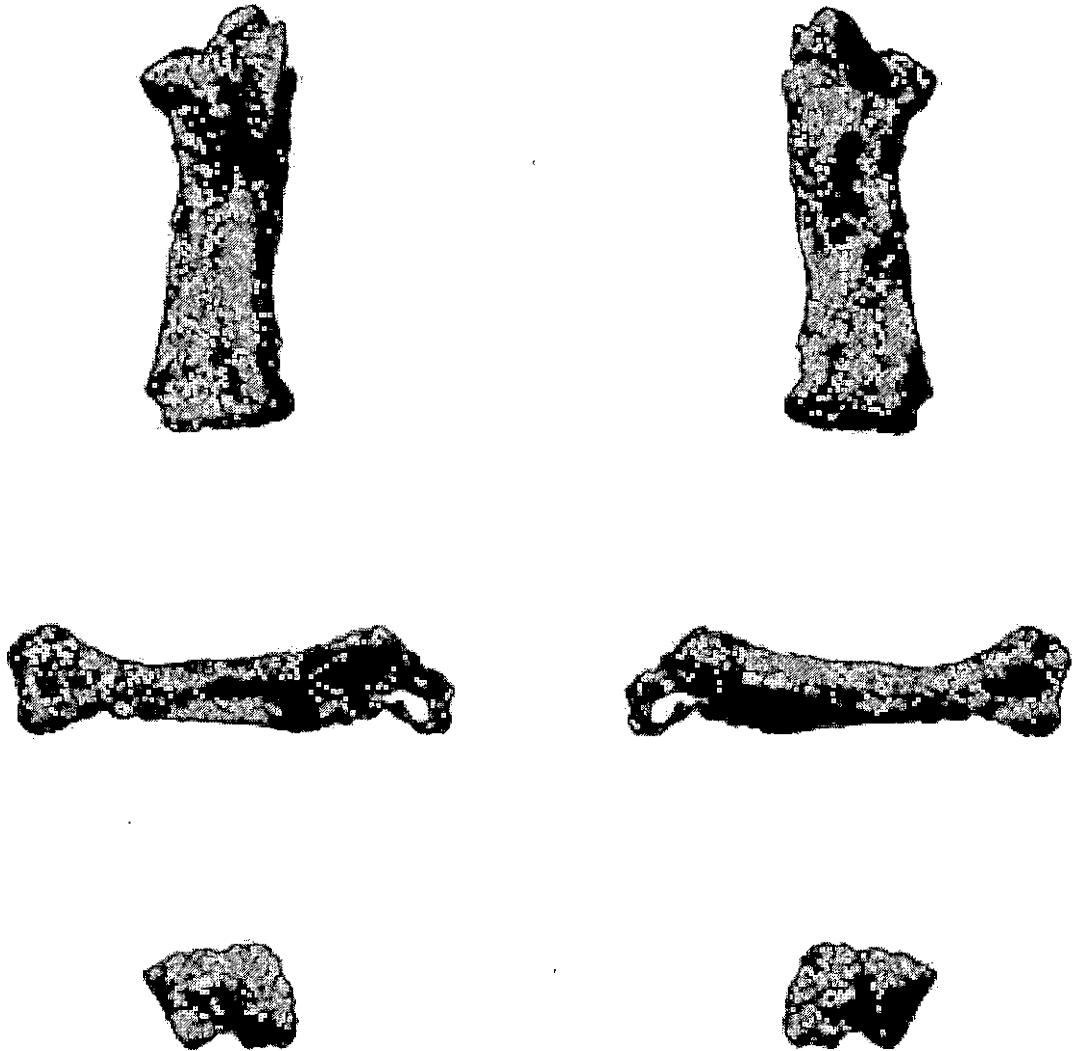
Tarsal of TMP 89.97.01.  
Dorsal View is Upper Left; Plantar is Upper Right;  
Medial is Middle Left; Lateral is Middle Right;  
Distal is Lower Left; Proximal is Lower Right.



Metatarsal I of TMP 89.97.01.  
Dorsal View is Upper Left; Plantar is Upper Right;  
Medial is Middle Left; Lateral is Middle Right;  
Distal is Lower Left; Proximal is Lower Right.



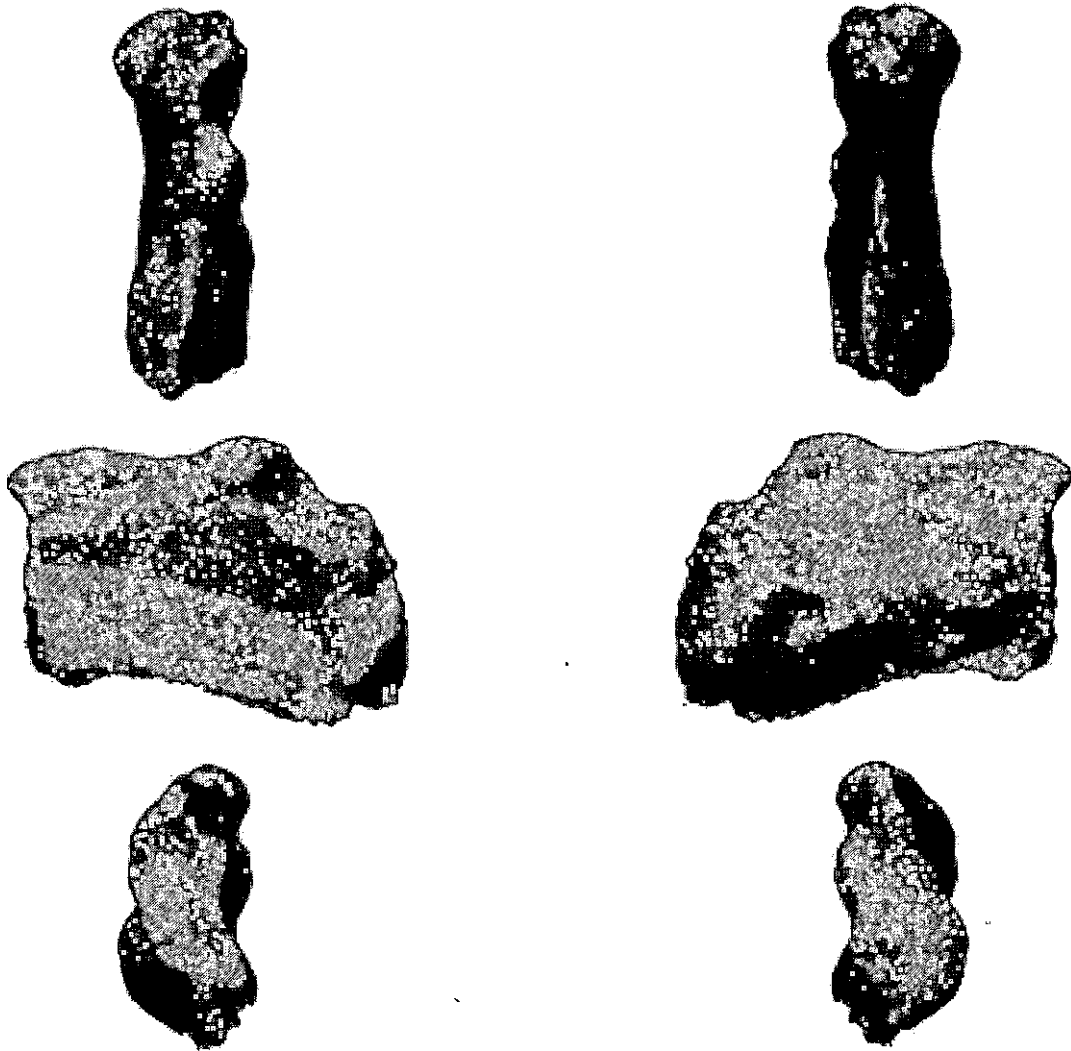
Metatarsal II of TMP 89.97.01.  
Dorsal View is Upper Left; Plantar is Upper Right;  
Medial is Middle Left; Lateral is Middle Right;  
Distal is Lower Left; Proximal is Lower Right.



Metatarsal III of TMP 89.97.01.  
Dorsal View is Upper Left; Plantar is Upper Right;  
Medial is Middle Left; Lateral is Middle Right;  
Distal is Lower Left; Proximal is Lower Right.

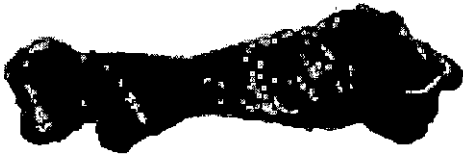
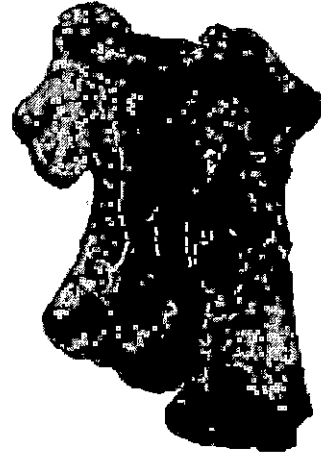
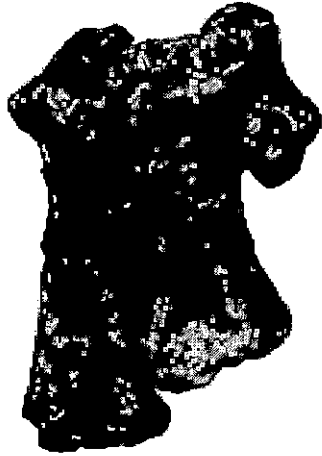


Metatarsal IV of TMP 89.97.01.  
Dorsal View is Upper Left; Plantar is Upper Right;  
Medial is Middle Left; Lateral is Middle Right;  
Distal is Lower Left; Proximal is Lower Right.

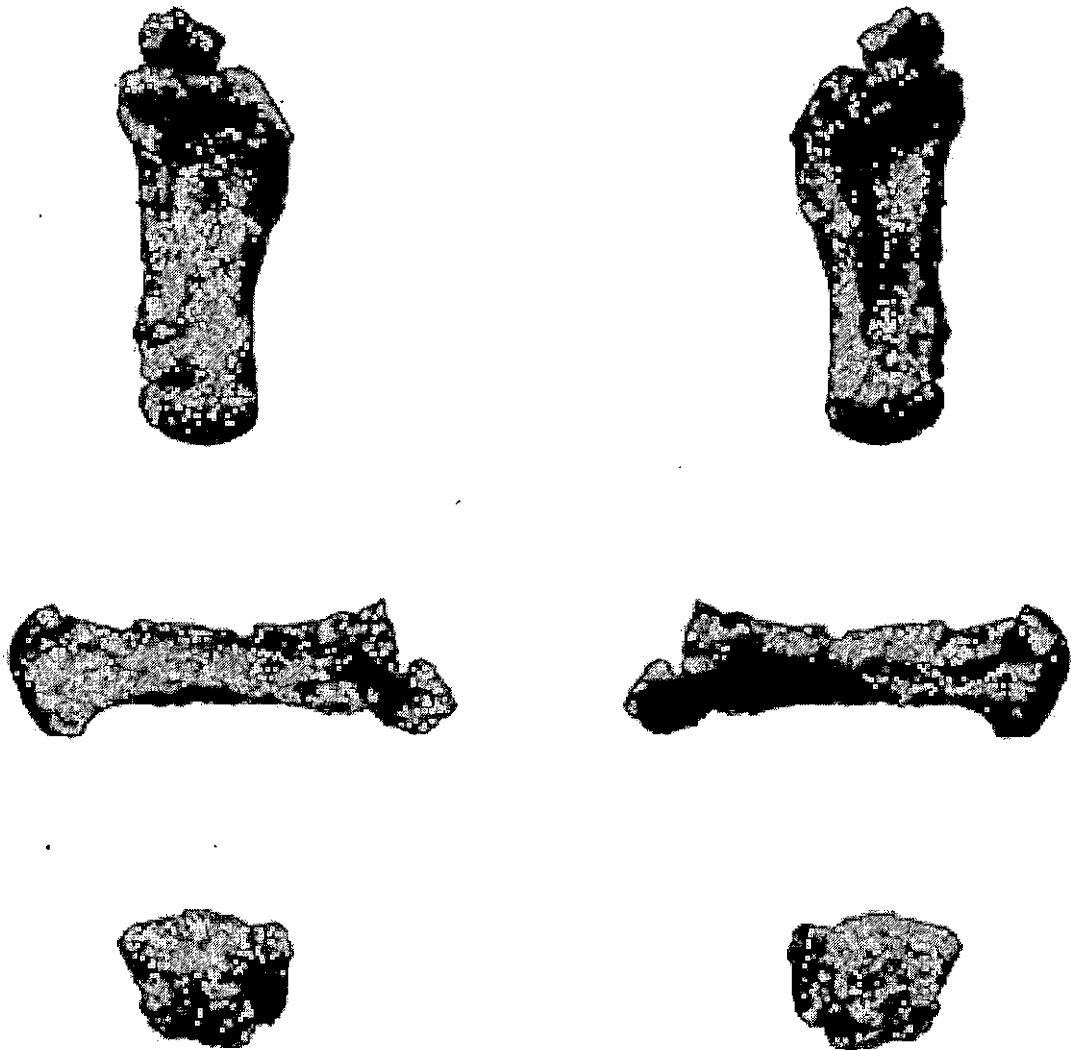


Metatarsal V of TMP 89.97.01.  
Dorsal View is Upper Left; Plantar is Upper Right;  
Medial is Middle Left; Lateral is Middle Right;  
Distal is Lower Left; Proximal is Lower Right.

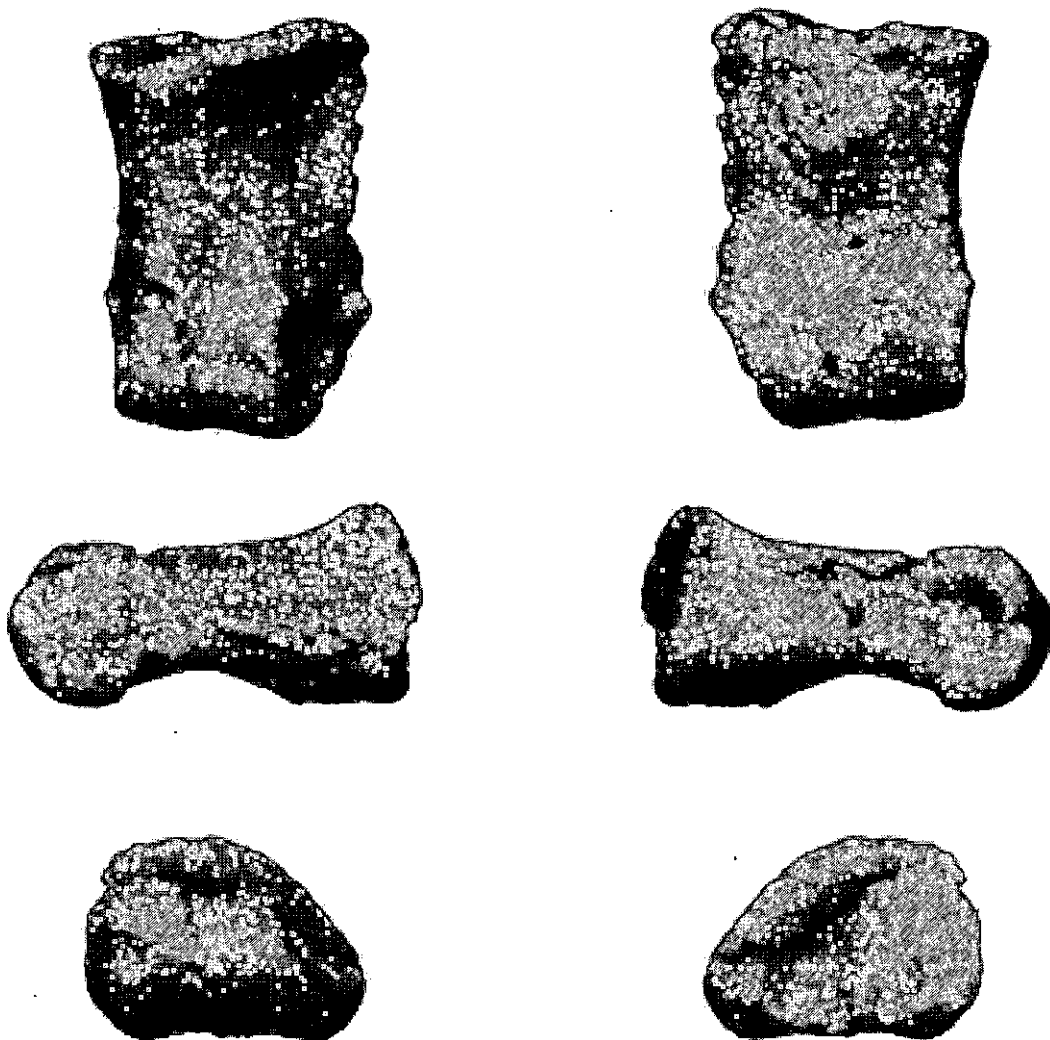




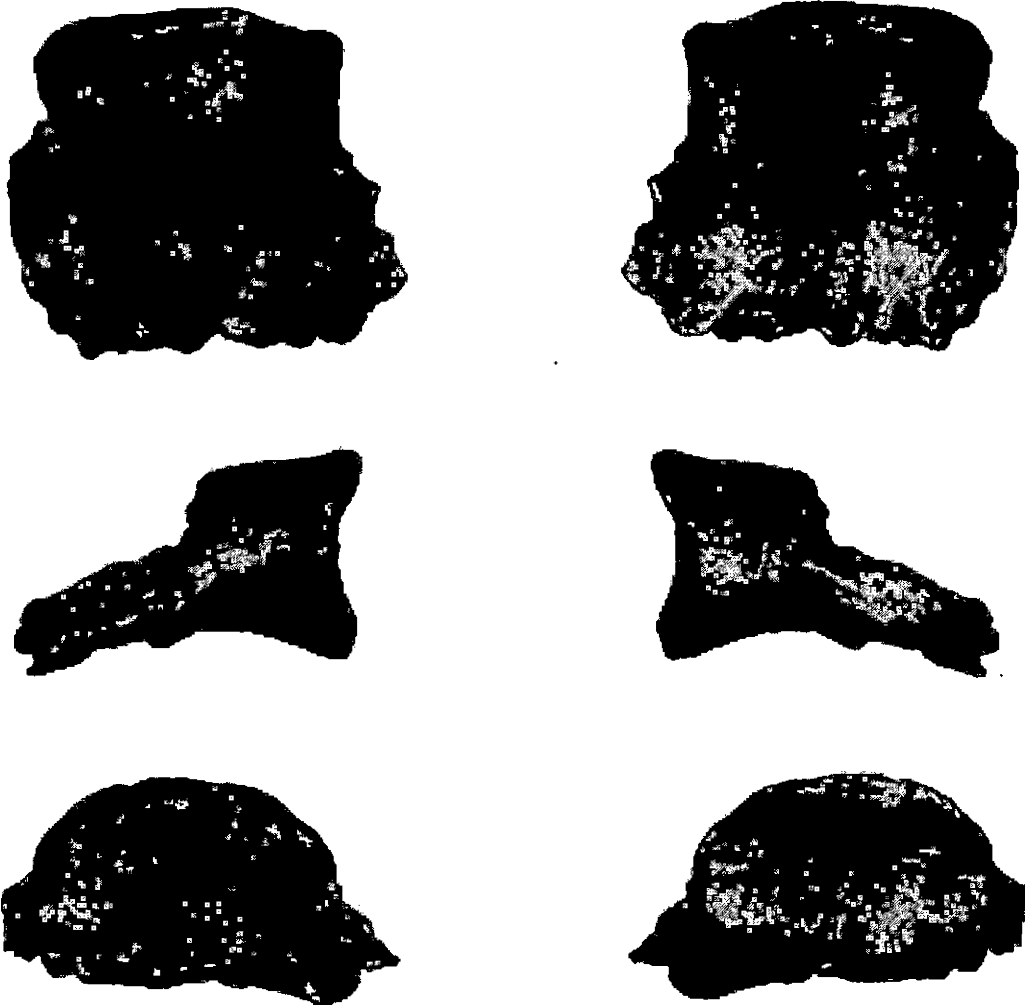
Metatarsal I to III of TMP 89.97.01.  
Dorsal View is Upper Left; Plantar is Upper Right;  
Medial is Middle Left; Lateral is Middle Right;  
Distal is Lower Left; Proximal is Lower Right.



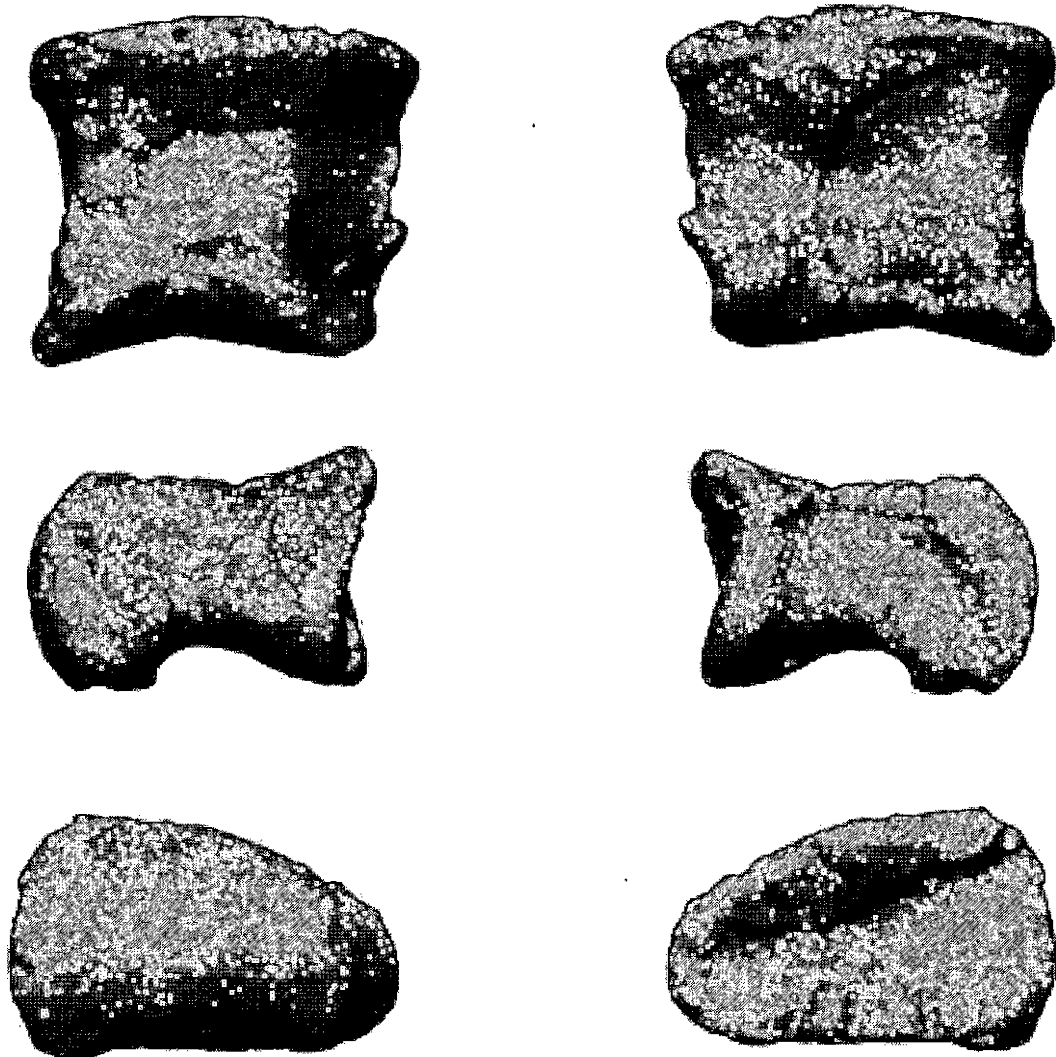
Metatarsal IV to V of TMP 89.97.01.  
Dorsal View is Upper Left; Plantar is Upper Right;  
Medial is Middle Left; Lateral is Middle Right;  
Distal is Lower Left; Proximal is Lower Right.



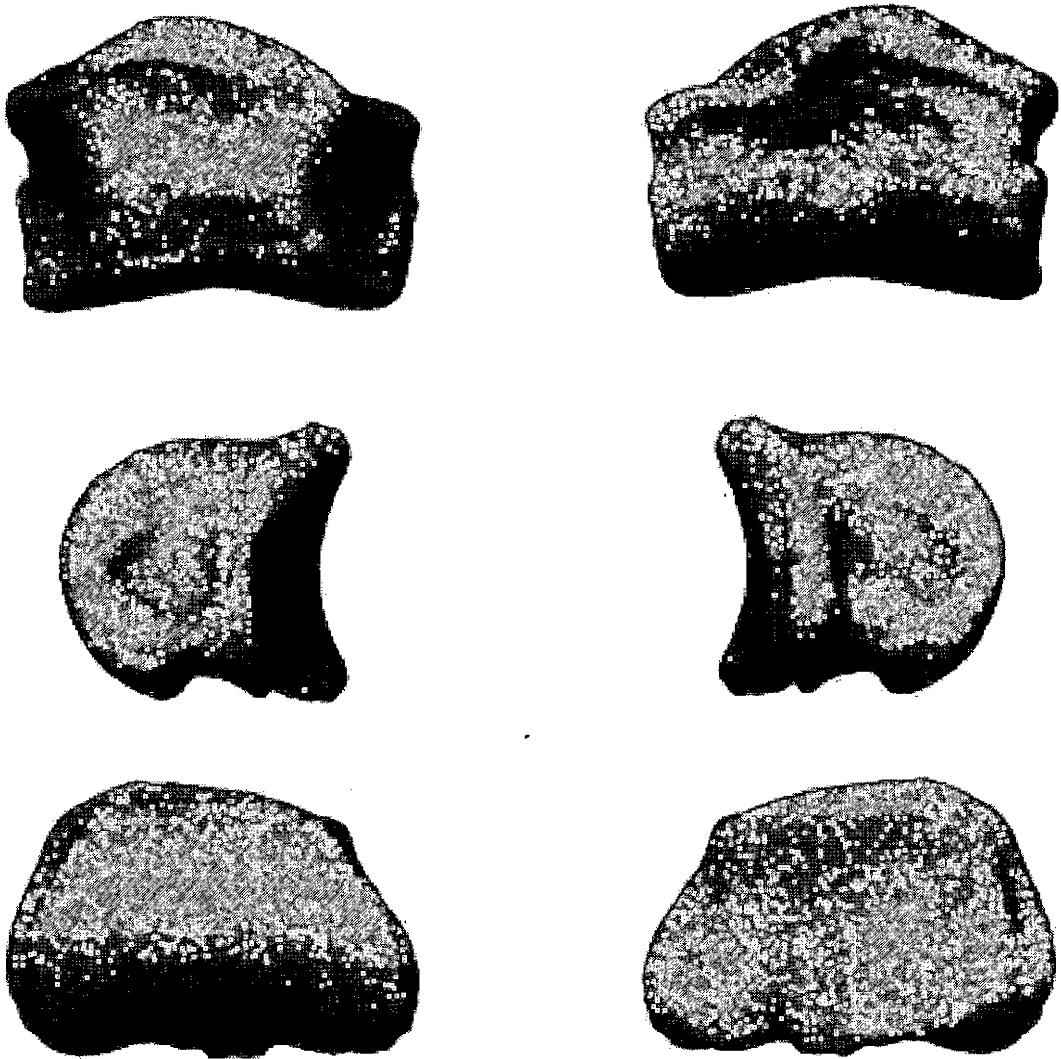
Digit I, Phalanx 1 of TMP 89.97.01.  
Dorsal View is Upper Left; Plantar is Upper Right;  
Medial is Middle Left; Lateral is Middle Right;  
Distal is Lower Left; Proximal is Lower Right.



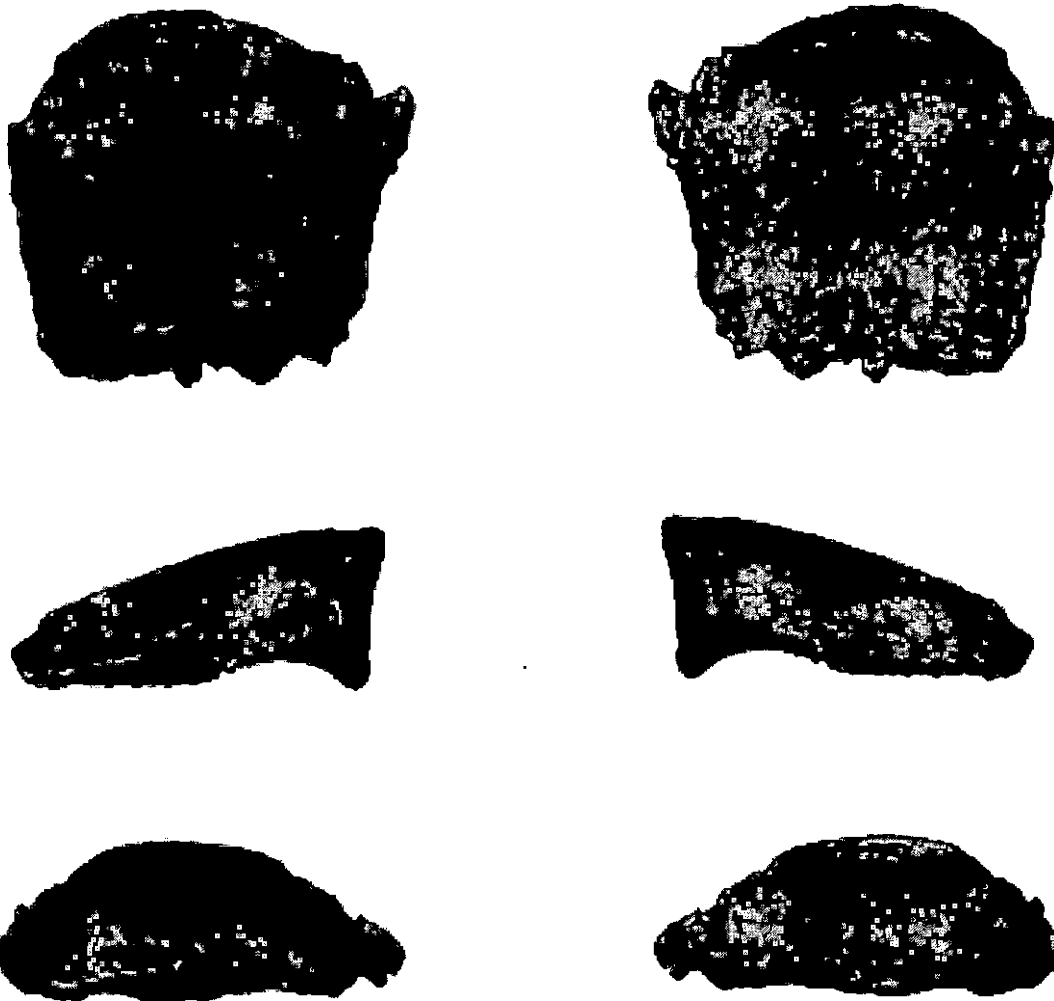
Digit I, Phalanx 2 of TMP 89.97.01.  
Dorsal View is Upper Left; Plantar is Upper Right;  
Medial is Middle Left; Lateral is Middle Right;  
Distal is Lower Left; Proximal is Lower Right.



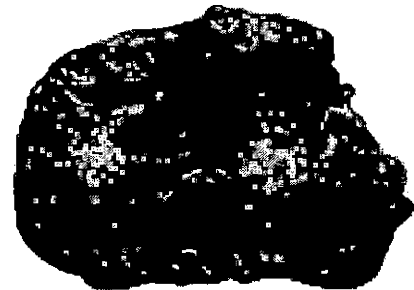
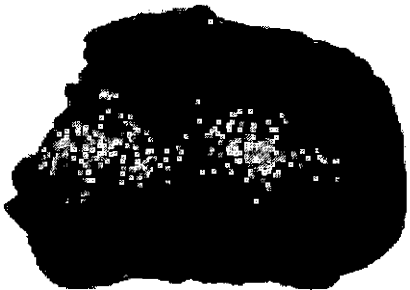
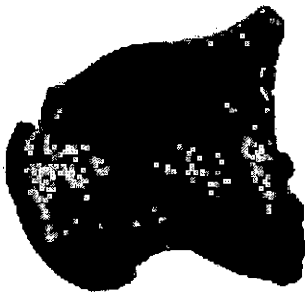
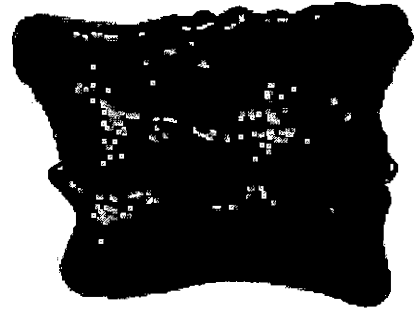
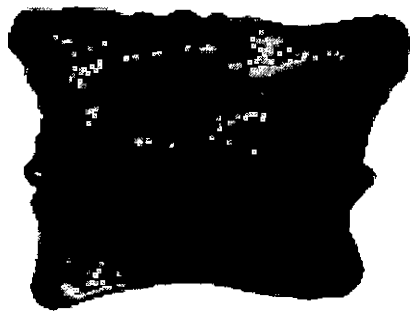
Digit II, Phalanx 1 of TMP 89.97.01.  
Dorsal View is Upper Left; Plantar is Upper Right;  
Medial is Middle Left; Lateral is Middle Right;  
Distal is Lower Left; Proximal is Lower Right.



Digit II, Phalanx 2 of TMP 89.97.01.  
Dorsal View is Upper Left; Plantar is Upper Right;  
Medial is Middle Left; Lateral is Middle Right;  
Distal is Lower Left; Proximal is Lower Right.

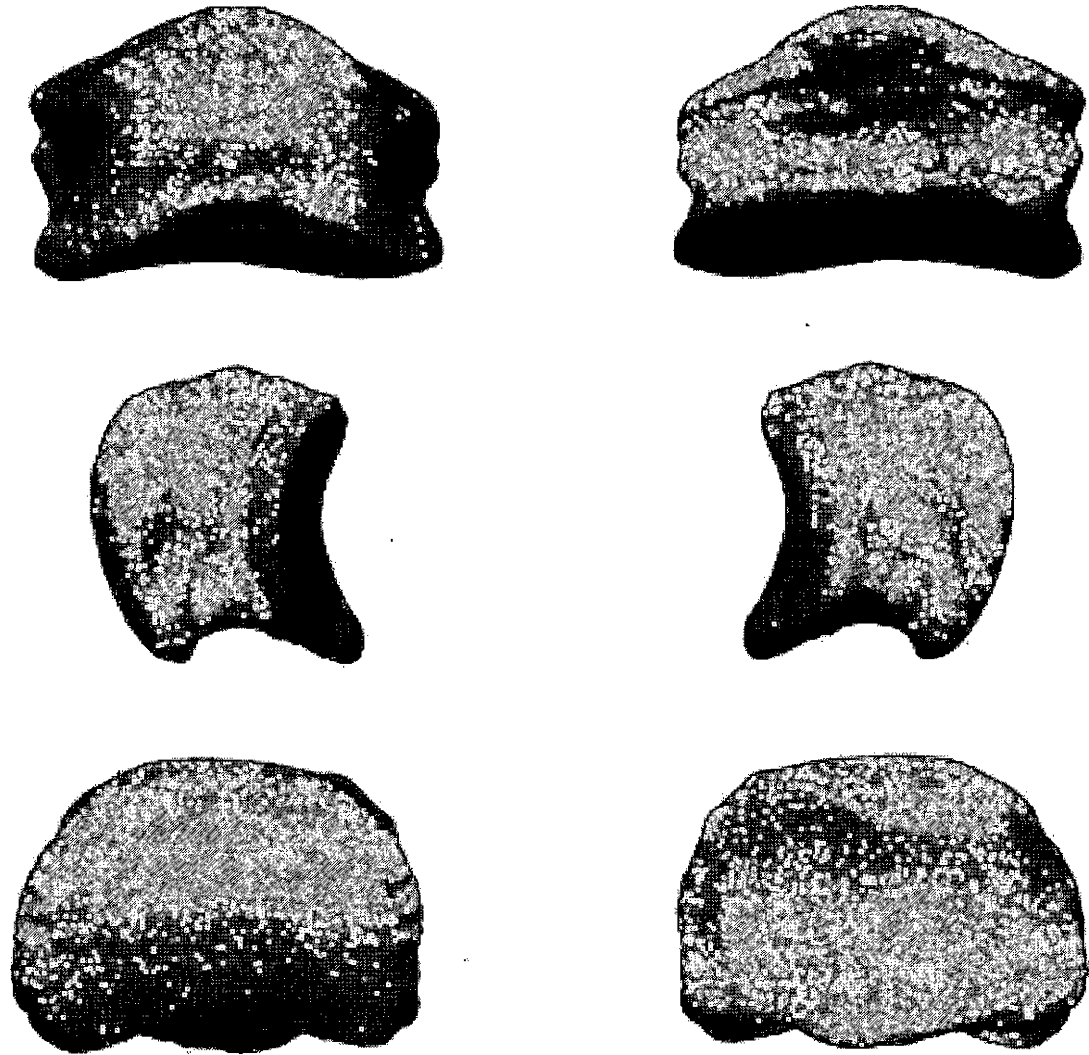


Digit II, Phalanx 3 of TMP 89.97.01.  
Dorsal View is Upper Left; Plantar is Upper Right;  
Medial is Middle Left; Lateral is Middle Right;  
Distal is Lower Left; Proximal is Lower Right.

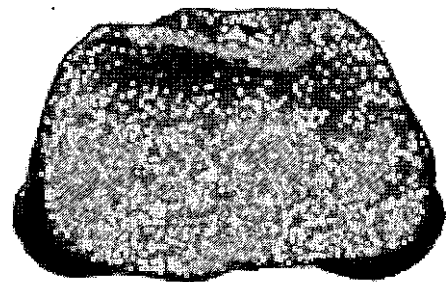
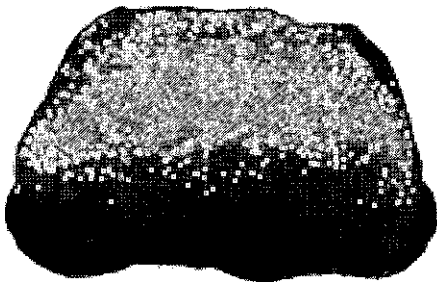
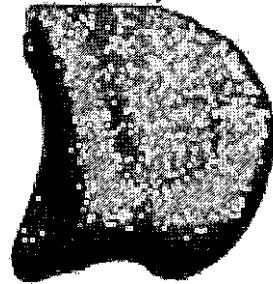
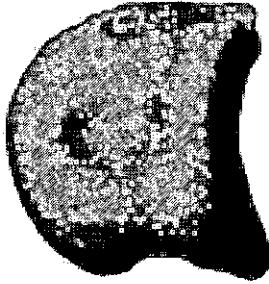
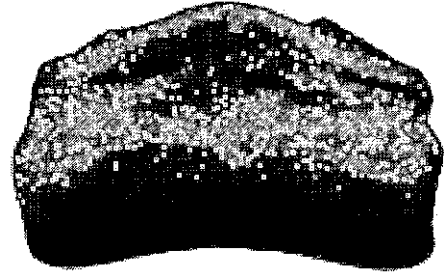
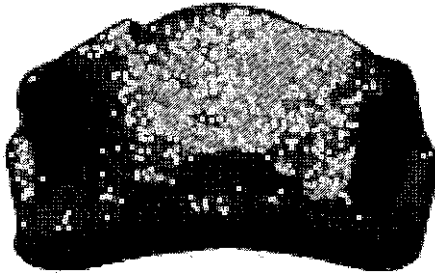


Digit III, Phalanx 1 of TMP 89.97.01.  
Dorsal View is Upper Left; Plantar is Upper Right;  
Medial is Middle Left; Lateral is Middle Right;  
Distal is Lower Left; Proximal is Lower Right.

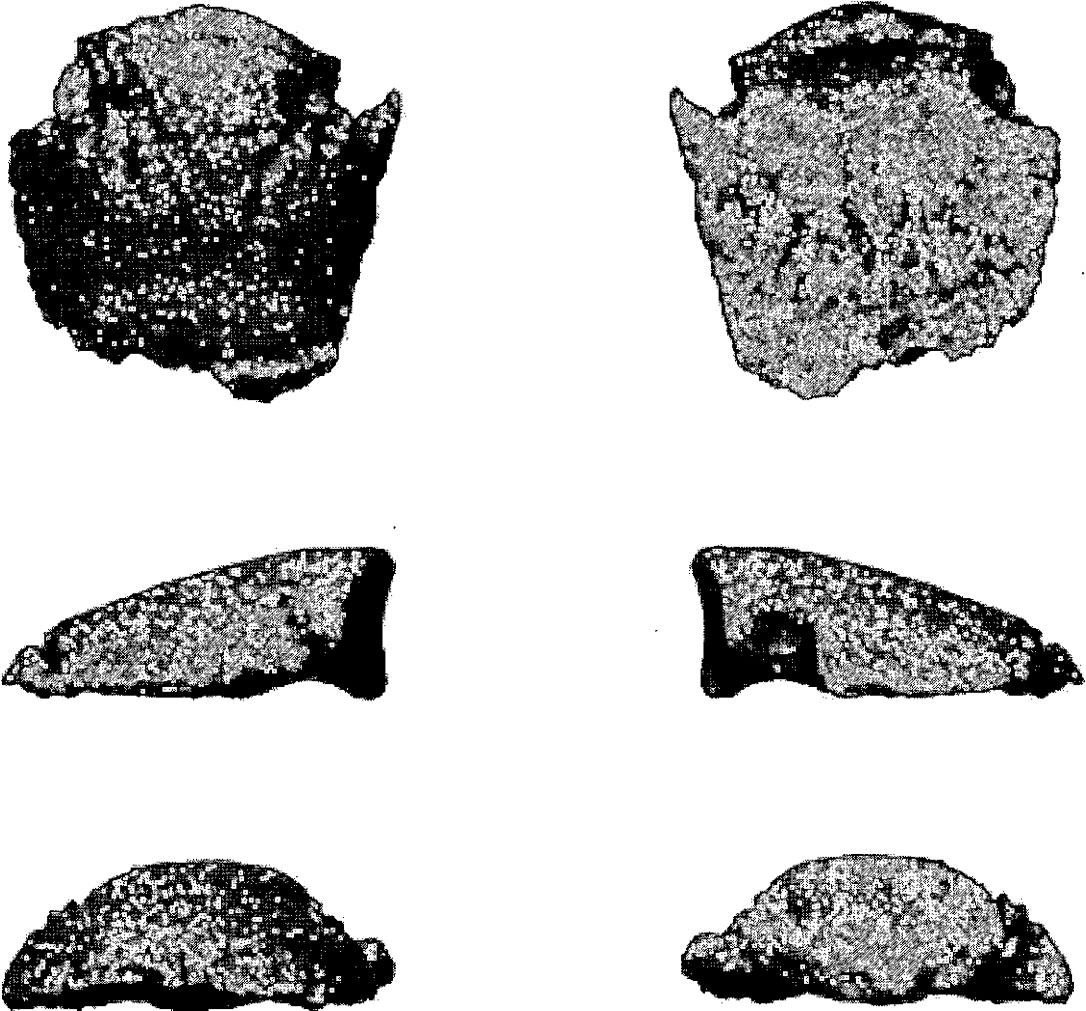




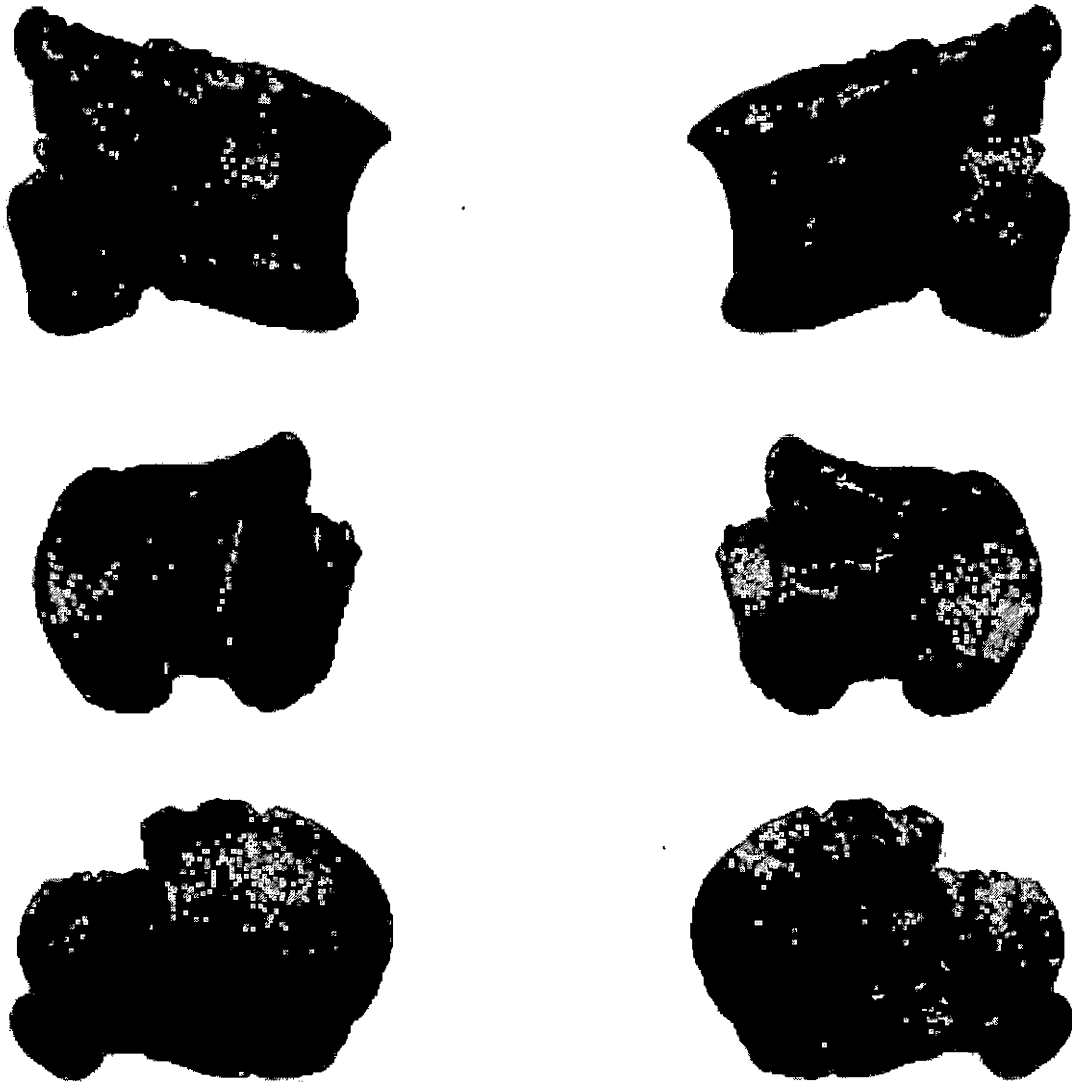
Digit III, Phalanx 2 of TMP 89.97.01.  
Dorsal View is Upper Left; Plantar is Upper Right;  
Medial is Middle Left; Lateral is Middle Right;  
Distal is Lower Left; Proximal is Lower Right.



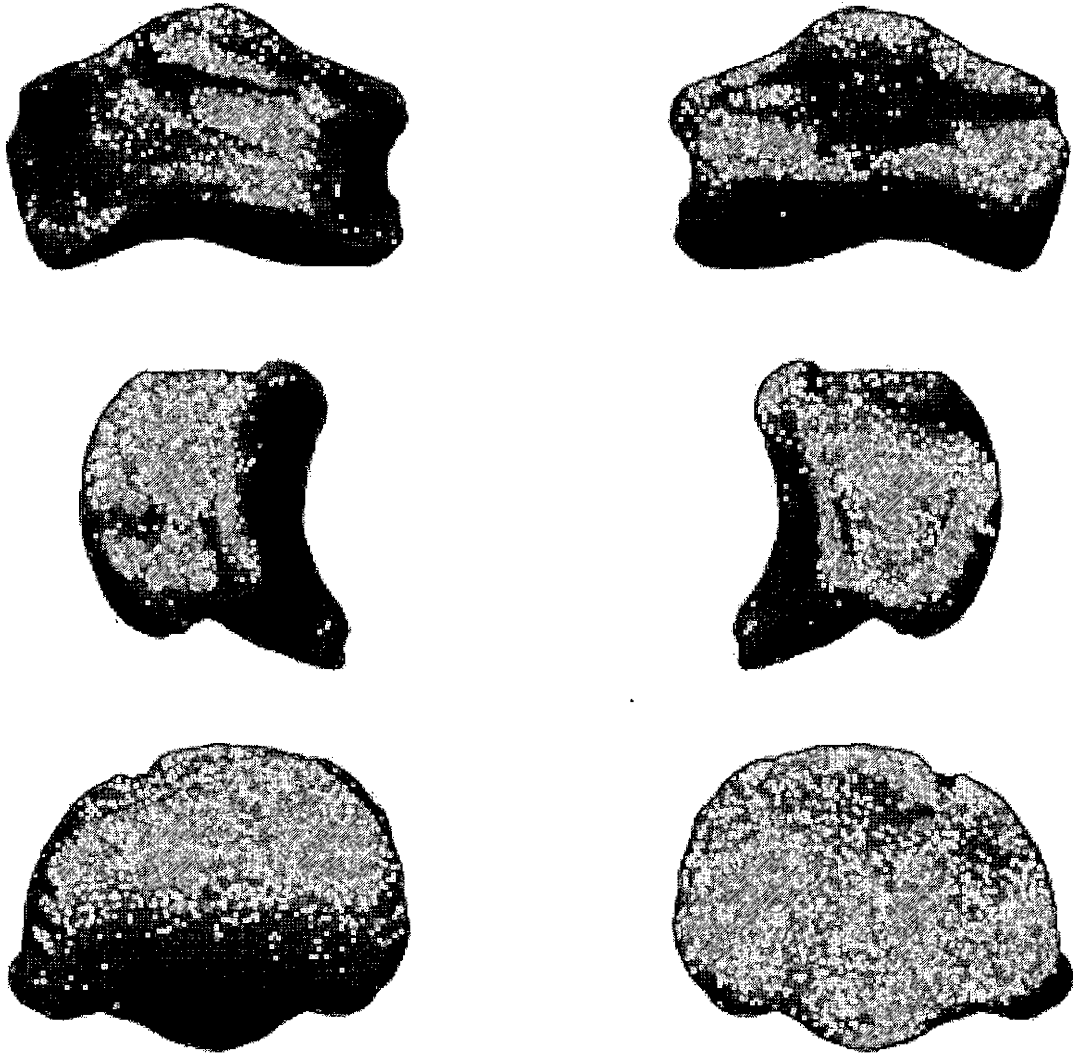
Digit III, Phalanx 3 of TMP 89.97.01.  
Dorsal View is Upper Left; Plantar is Upper Right;  
Medial is Middle Left; Lateral is Middle Right;  
Distal is Lower Left; Proximal is Lower Right.



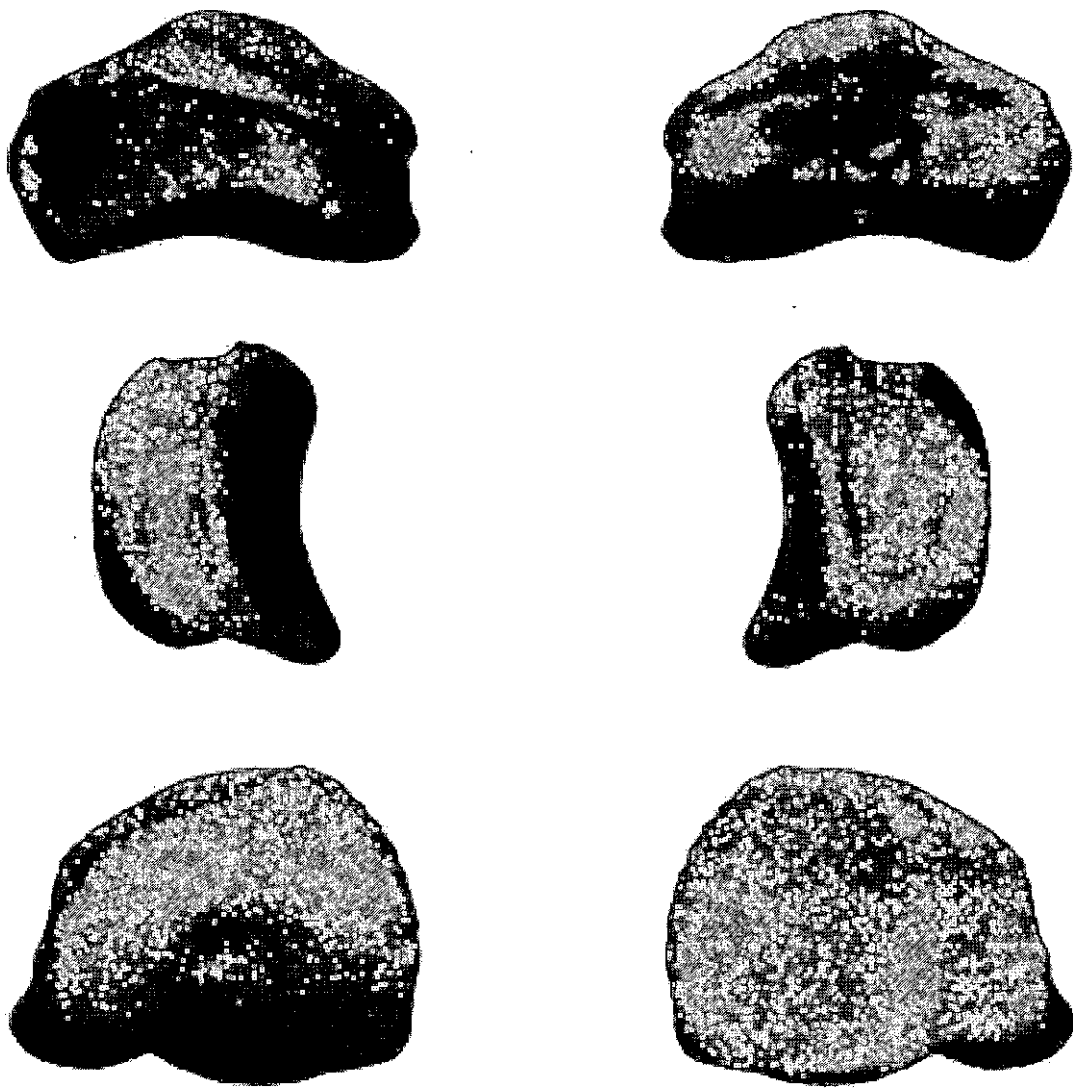
Digit III, Phalanx 4 of TMP 89.97.01.  
Dorsal View is Upper Left; Plantar is Upper Right;  
Medial is Middle Left; Lateral is Middle Right;  
Distal is Lower Left; Proximal is Lower Right.



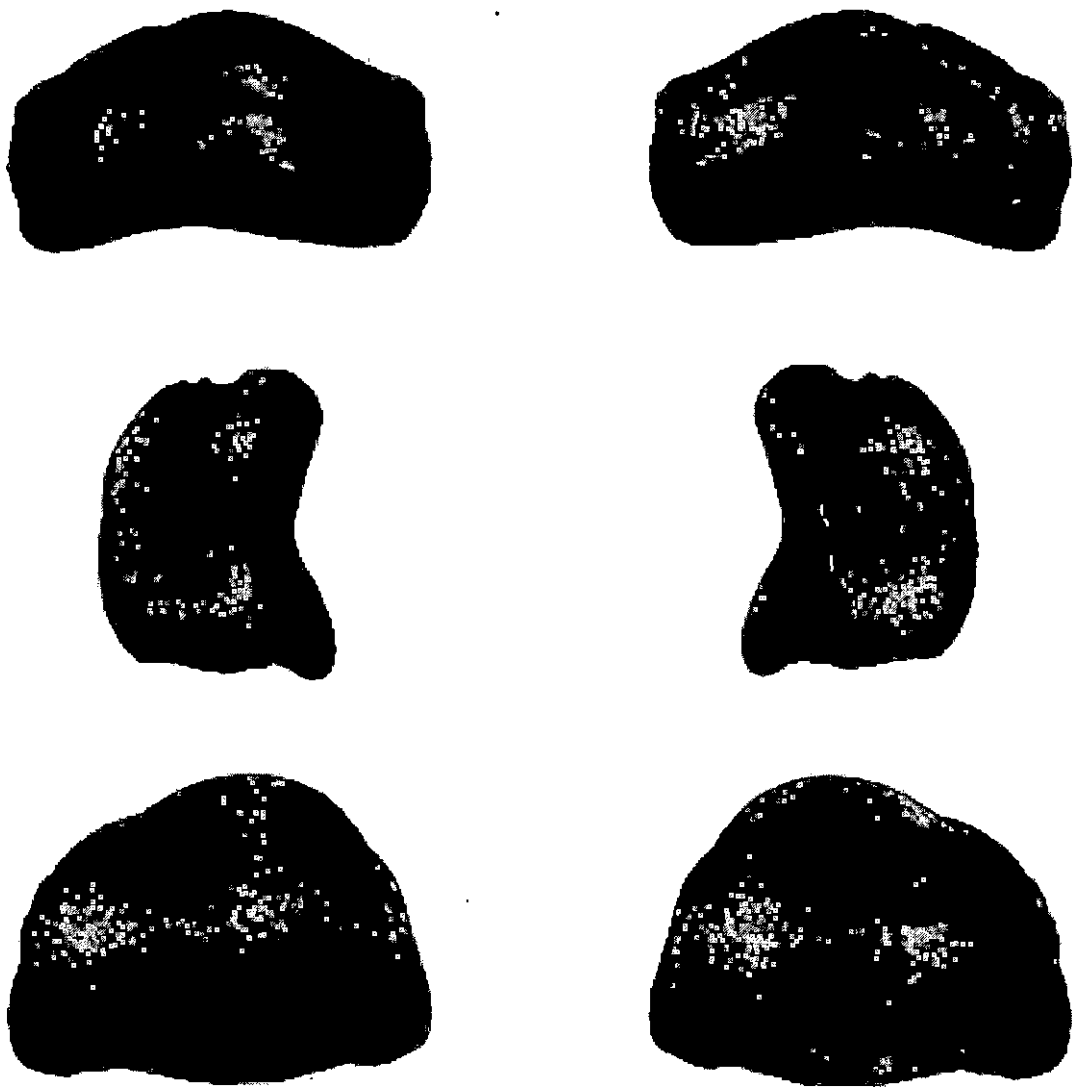
Digit IV, Phalanx 1 of TMP 89.97.01.  
Dorsal View is Upper Left; Plantar is Upper Right;  
Medial is Middle Left; Lateral is Middle Right;  
Distal is Lower Left; Proximal is Lower Right.



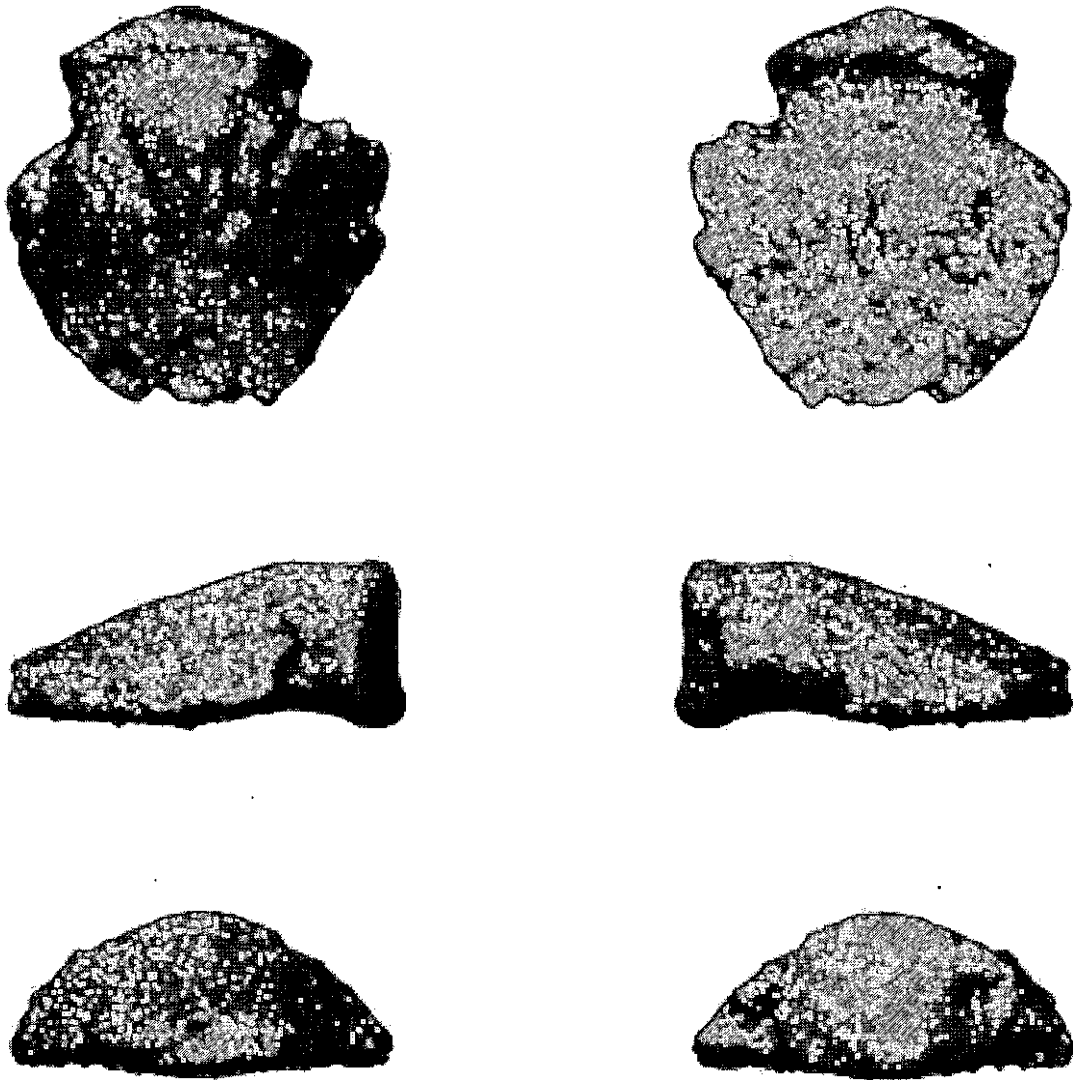
Digit IV, Phalanx 2 of TMP 89.97.01.  
Dorsal View is Upper Left; Plantar is Upper Right;  
Medial is Middle Left; Lateral is Middle Right;  
Distal is Lower Left; Proximal is Lower Right.



Digit IV, Phalanx 3 of TMP 89.97.01.  
Dorsal View is Upper Left; Plantar is Upper Right;  
Medial is Middle Left; Lateral is Middle Right;  
Distal is Lower Left; Proximal is Lower Right.

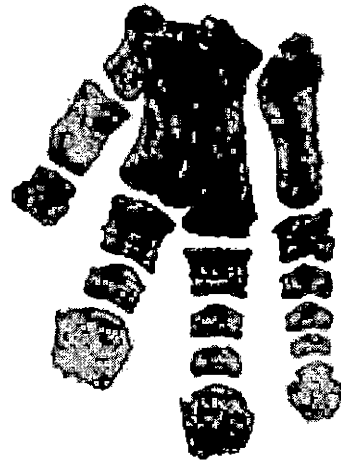
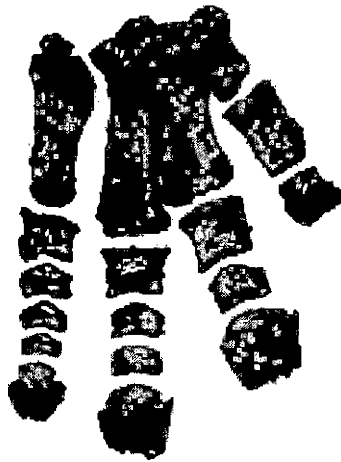


Digit IV, Phalanx 4 of TMP 89.97.01.  
Dorsal View is Upper Left; Plantar is Upper Right;  
Medial is Middle Left; Lateral is Middle Right;  
Distal is Lower Left; Proximal is Lower Right.



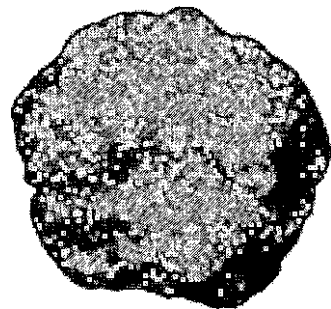
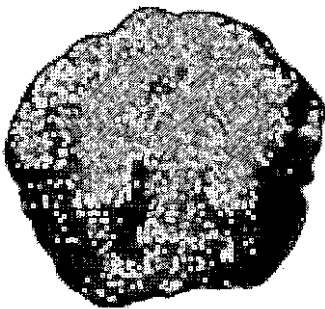
Digit IV, Phalanx 5 of TMP 89.97.01.  
Dorsal View is Upper Left; Plantar is Upper Right;  
Medial is Middle Left; Lateral is Middle Right;  
Distal is Lower Left; Proximal is Lower Right.



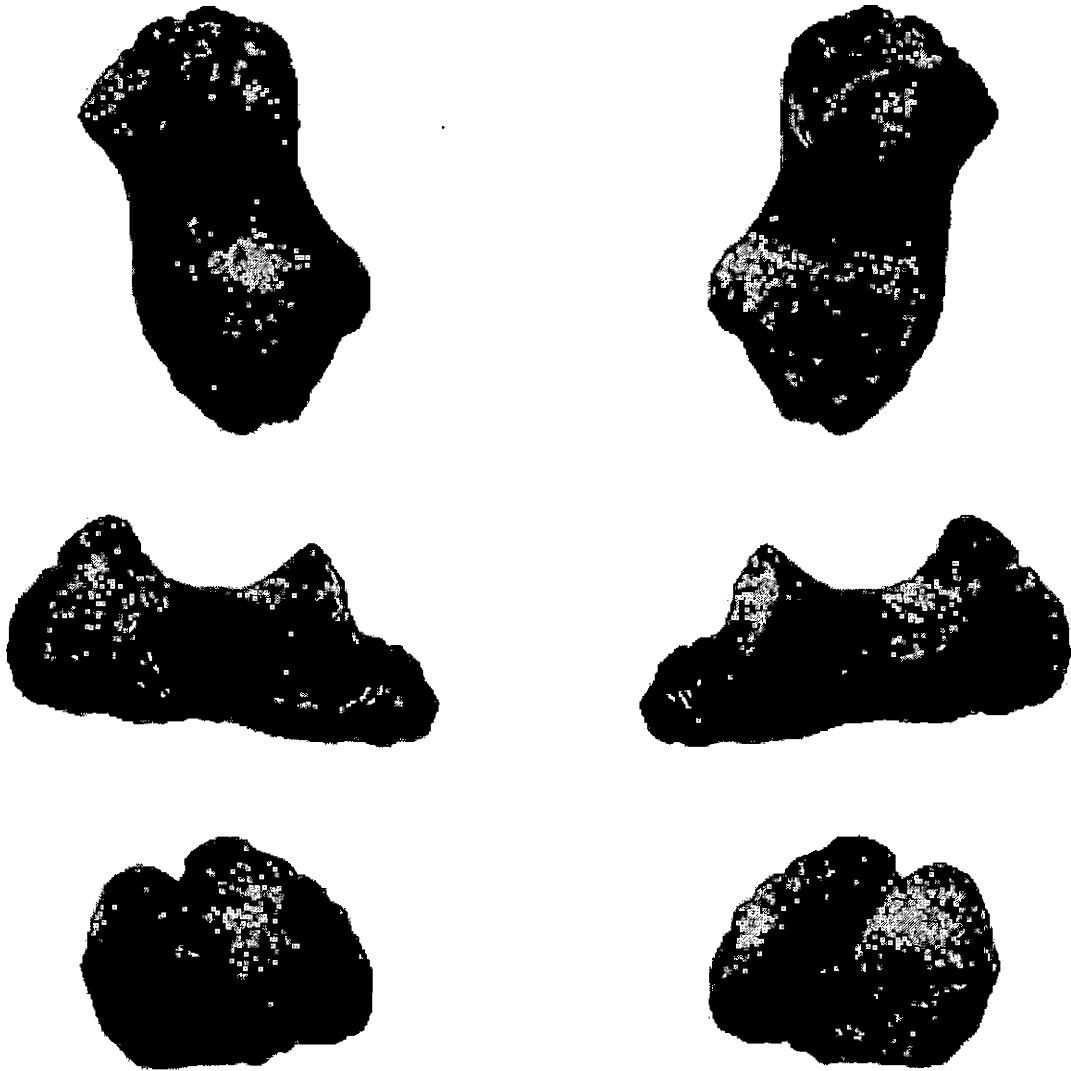


Entire Specimen of TMP 89.97.01.  
Dorsal View is Upper Left; Plantar is Upper Right;  
Medial is Middle Left; Lateral is Middle Right;  
Distal is Lower Left; Proximal is Lower Right.

APPENDIX E  
ILLUSTRATIONS OF TMP 89.97.01, INDIVIDUAL ELEMENTS,  
AFTER RECONSTRUCTION



Tarsal of TMP 89.97.01.  
Dorsal View is Upper Left; Plantar is Upper Right;  
Medial is Middle Left; Lateral is Middle Right;  
Distal is Lower Left; Proximal is Lower Right.



Metatarsal I of TMP 89.97.01.

Dorsal View is Upper Left; Plantar is Upper Right;  
Medial is Middle Left; Lateral is Middle Right;  
Distal is Lower Left; Proximal is Lower Right.



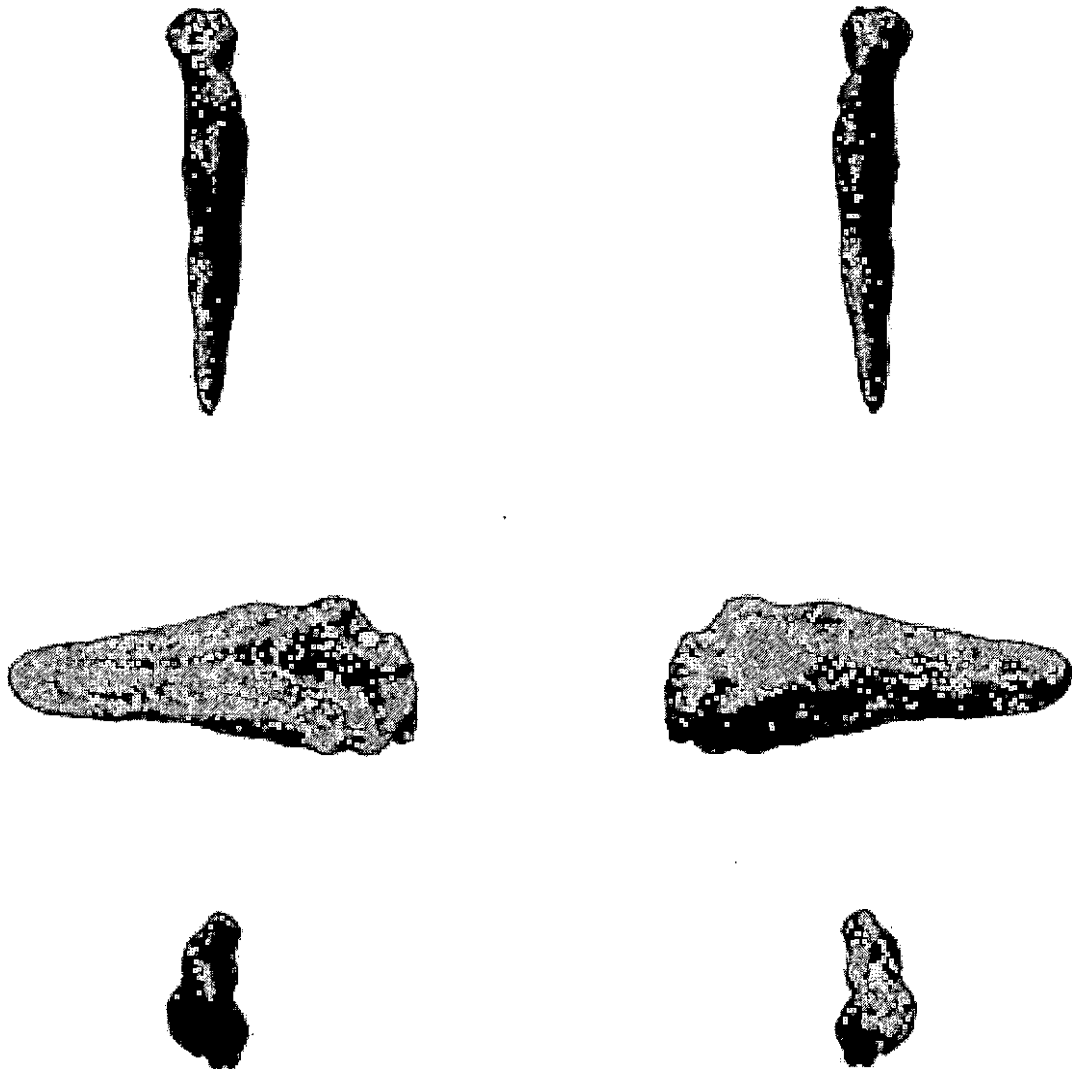
Metatarsal II of TMP 89.97.01.  
Dorsal View is Upper Left; Plantar is Upper Right;  
Medial is Middle Left; Lateral is Middle Right;  
Distal is Lower Left; Proximal is Lower Right.



Metatarsal III of TMP 89.97.01.  
Dorsal View is Upper Left; Plantar is Upper Right;  
Medial is Middle Left; Lateral is Middle Right;  
Distal is Lower Left; Proximal is Lower Right.



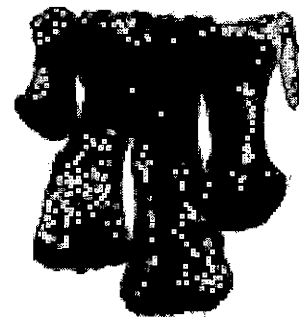
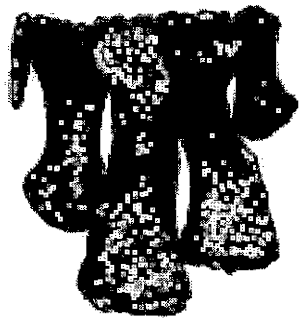
Metatarsal IV of TMP 89.97.01.  
Dorsal View is Upper Left; Plantar is Upper Right;  
Medial is Middle Left; Lateral is Middle Right;  
Distal is Lower Left; Proximal is Lower Right.



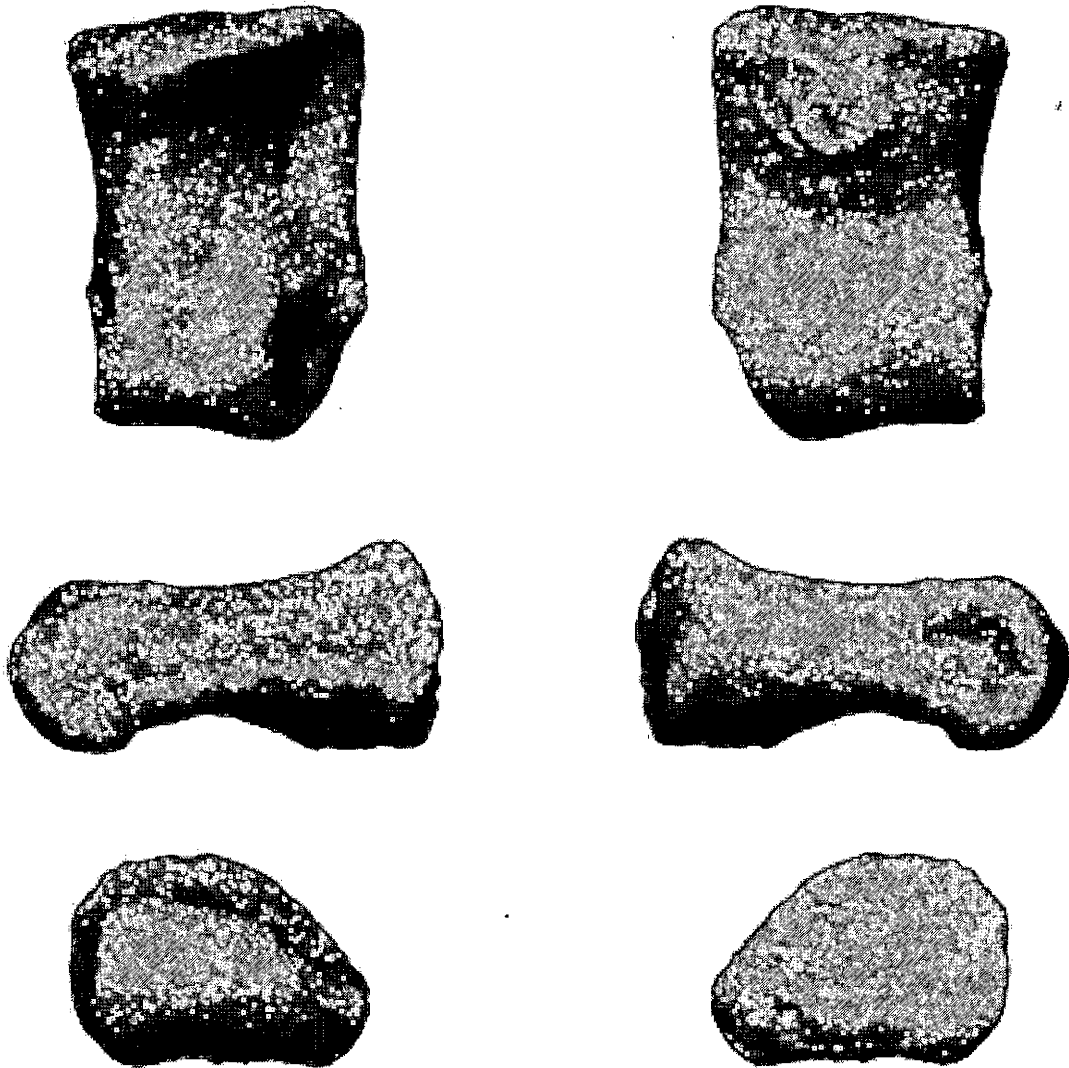
Metatarsal V of TMP 89.97.01.

Dorsal View is Upper Left; Plantar is Upper Right;  
Medial is Middle Left; Lateral is Middle Right;  
Distal is Lower Left; Proximal is Lower Right.

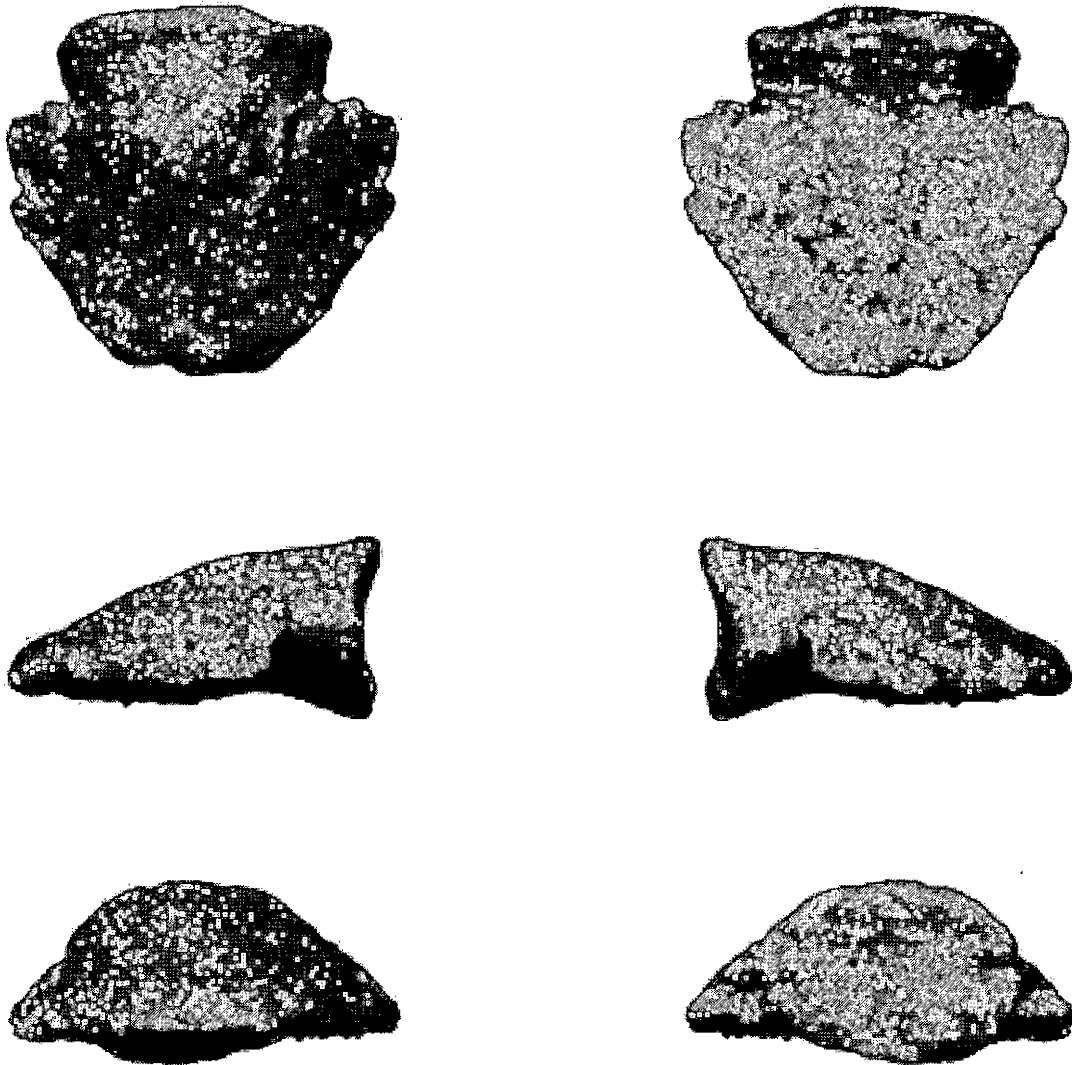




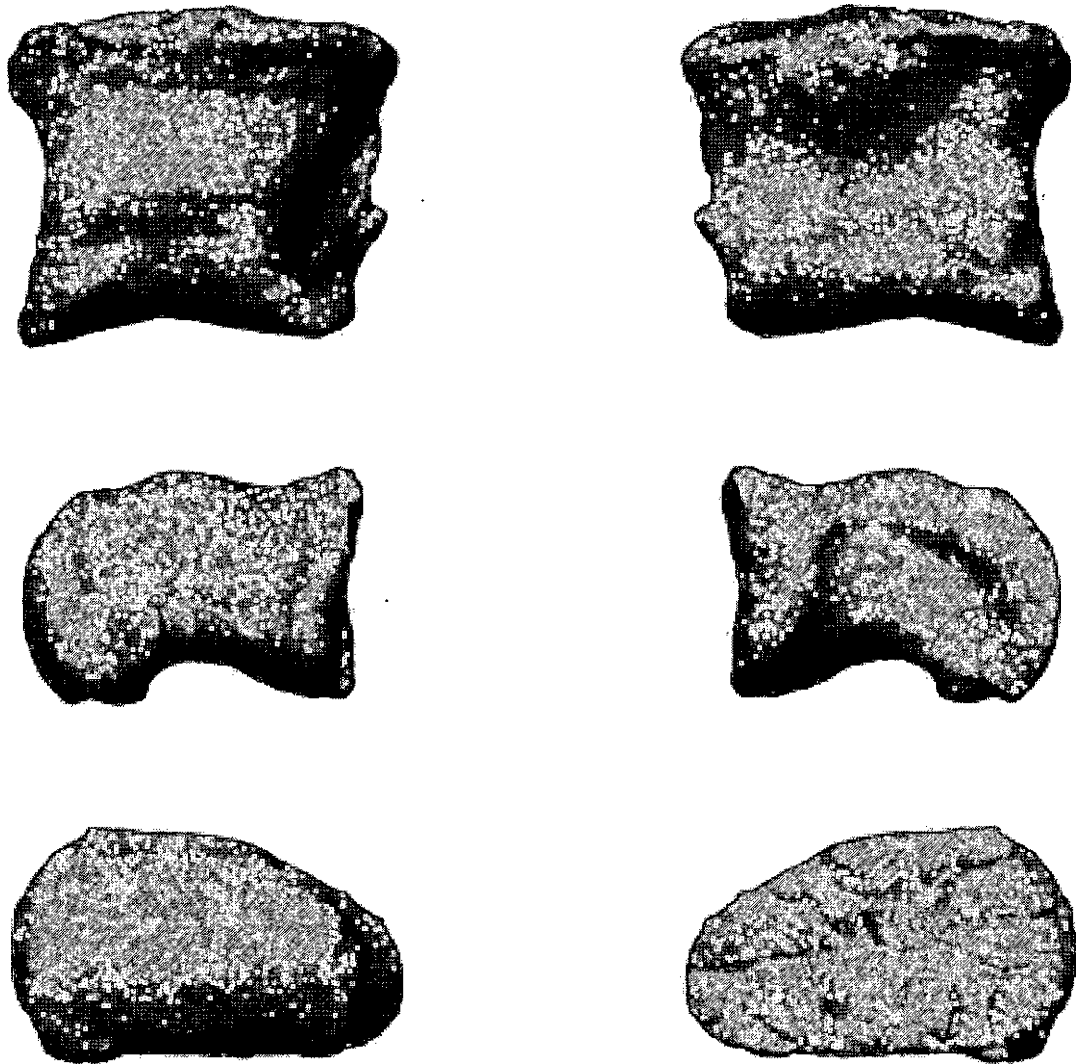
All Metatarsals of TMP 89.97.01.  
Dorsal View is Upper Left; Plantar is Upper Right;  
Medial is Middle Left; Lateral is Middle Right;  
Distal is Lower Left; Proximal is Lower Right.



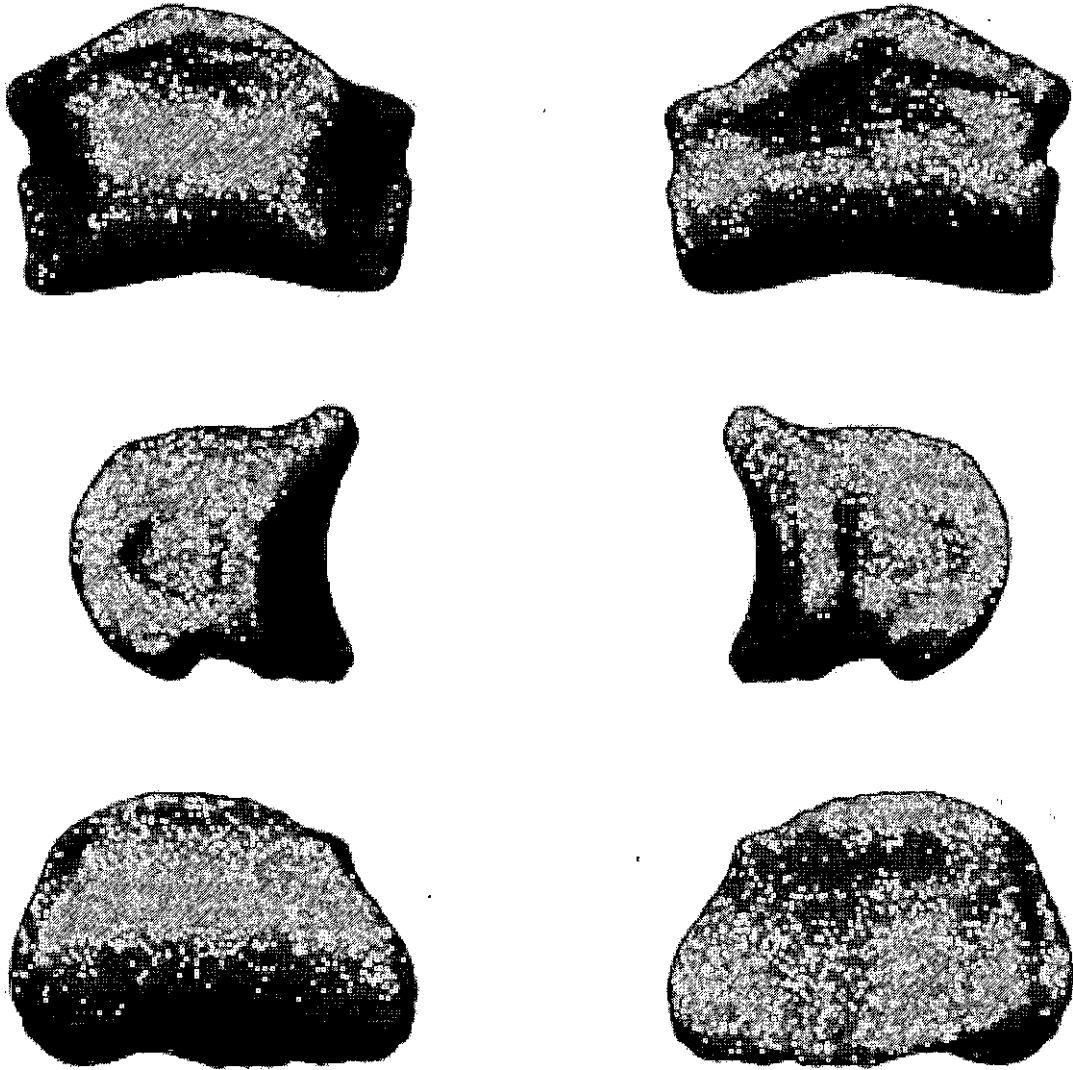
Digit I, Phalanx 1 of TMP 89.97.01.  
Dorsal View is Upper Left; Plantar is Upper Right;  
Medial is Middle Left; Lateral is Middle Right;  
Distal is Lower Left; Proximal is Lower Right.



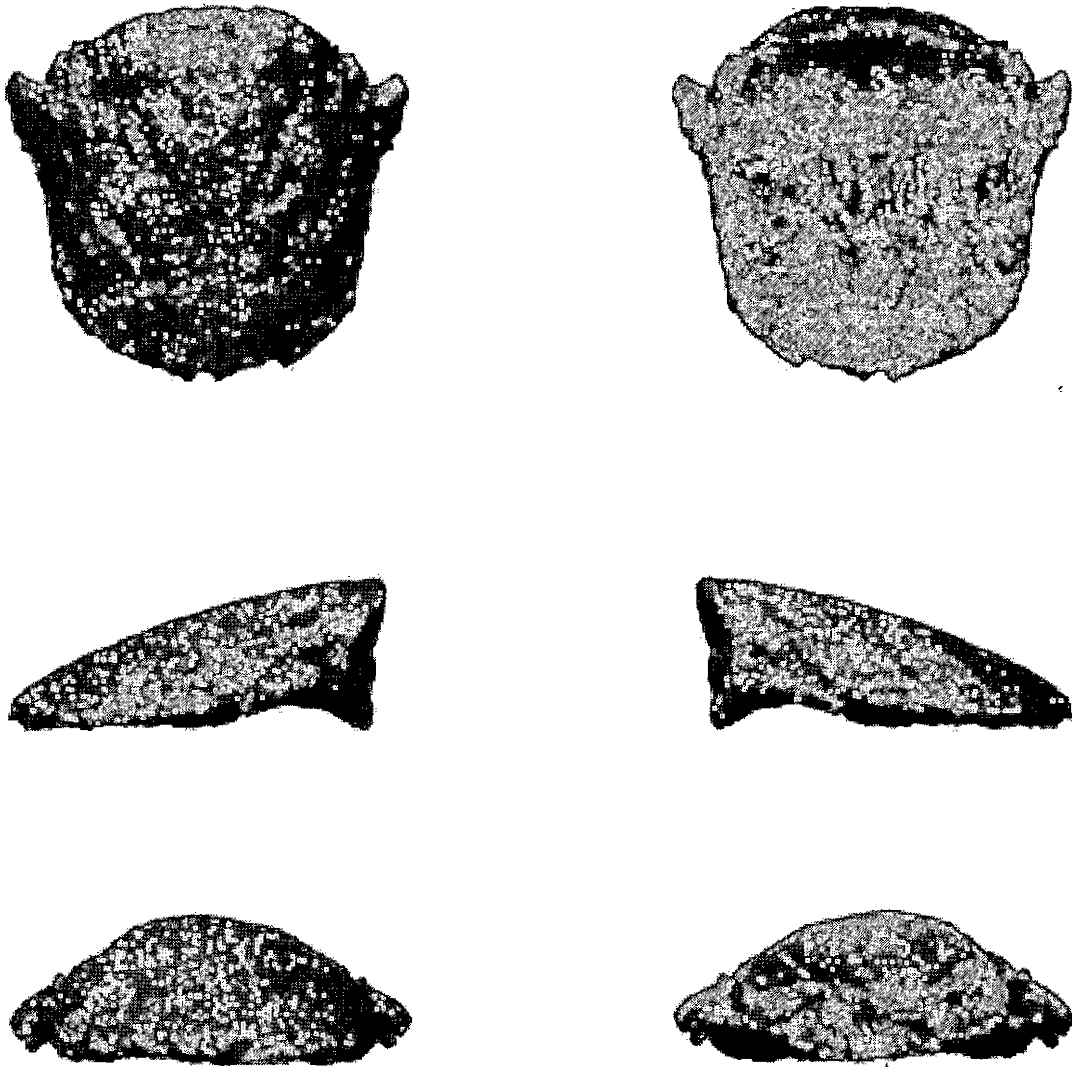
Digit I, Phalanx 2 of TMP 89.97.01.  
Dorsal View is Upper Left; Plantar is Upper Right;  
Medial is Middle Left; Lateral is Middle Right;  
Distal is Lower Left; Proximal is Lower Right.



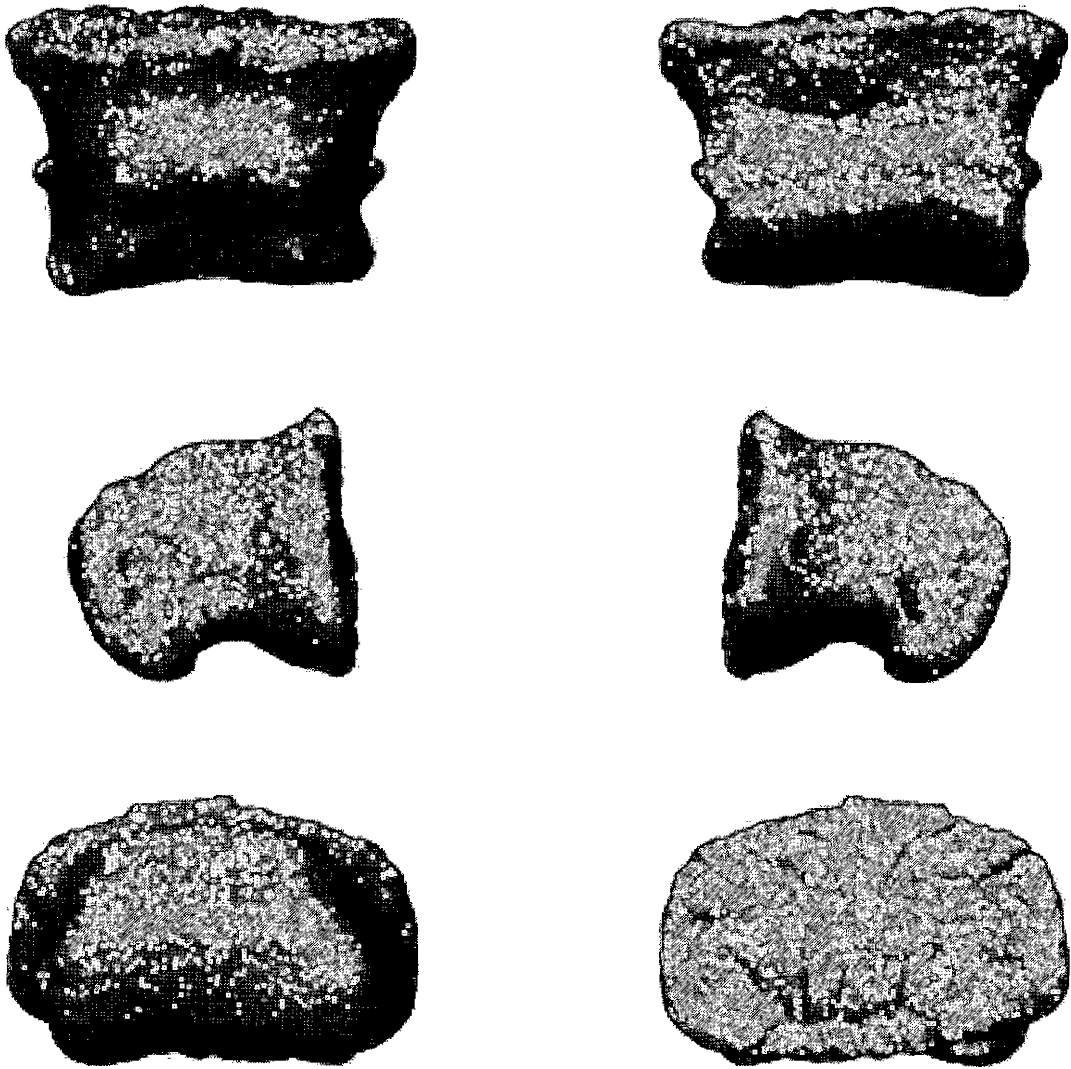
Digit II, Phalanx 1 of TMP 89.97.01.  
Dorsal View is Upper Left; Plantar is Upper Right;  
Medial is Middle Left; Lateral is Middle Right;  
Distal is Lower Left; Proximal is Lower Right.



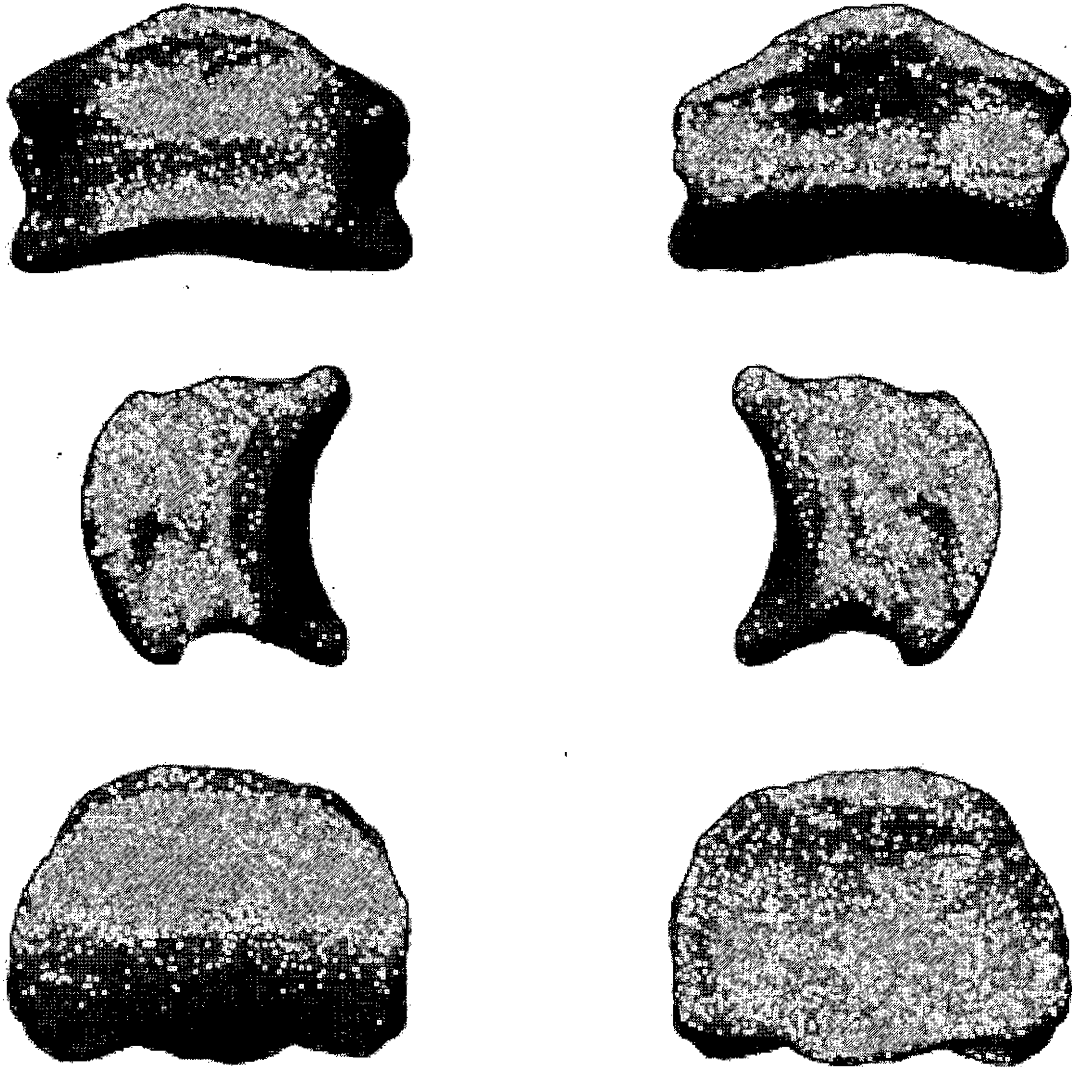
Digit II, Phalanx 2 of TMP '89.97.01.  
Dorsal View is Upper Left; Plantar is Upper Right;  
Medial is Middle Left; Lateral is Middle Right;  
Distal is Lower Left; Proximal is Lower Right.



Digit II, Phalanx 3 of TMP 89.97.01.  
Dorsal View is Upper Left; Plantar is Upper Right;  
Medial is Middle Left; Lateral is Middle Right;  
Distal is Lower Left; Proximal is Lower Right.

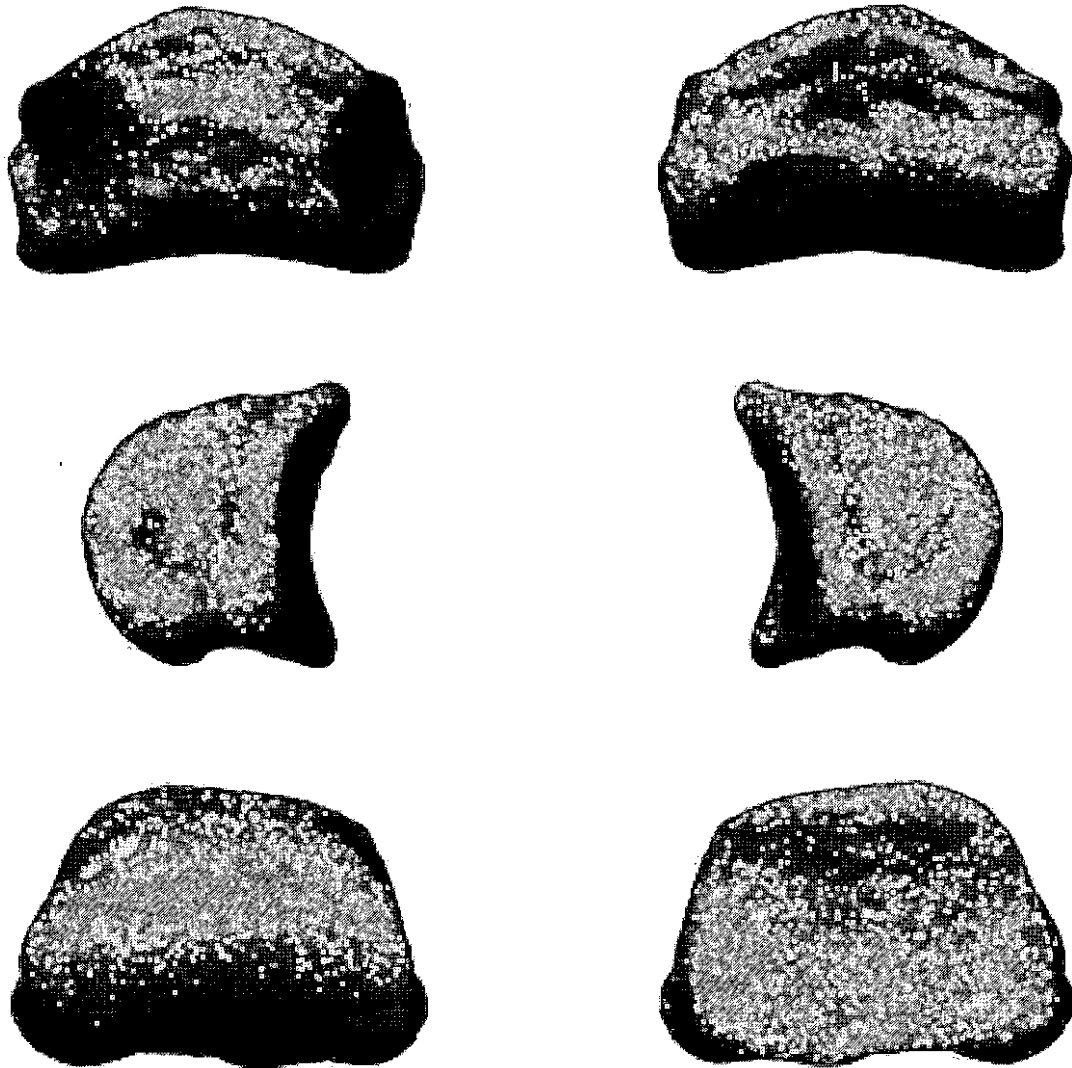


Digit III, Phalanx 1 of TMP 89.97.01.  
Dorsal View is Upper Left; Plantar is Upper Right;  
Medial is Middle Left; Lateral is Middle Right;  
Distal is Lower Left; Proximal is Lower Right.

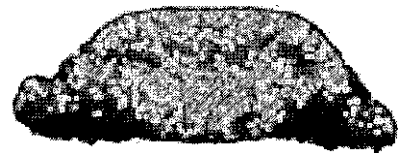
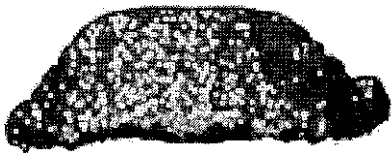
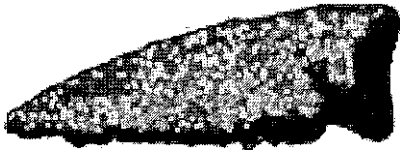
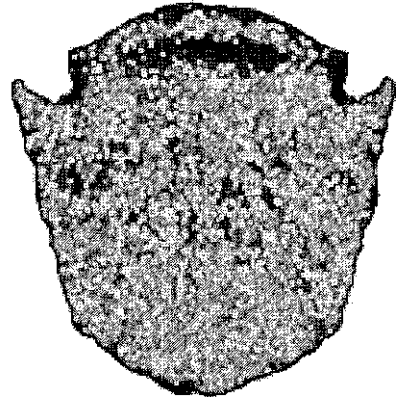
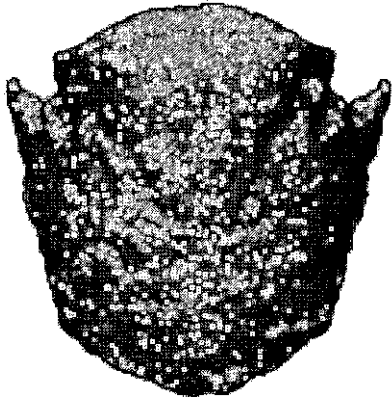


Digit III, Phalanx 2 of TMP 89.97.01.  
Dorsal View is Upper Left; Plantar is Upper Right;  
Medial is Middle Left; Lateral is Middle Right;  
Distal is Lower Left; Proximal is Lower Right.

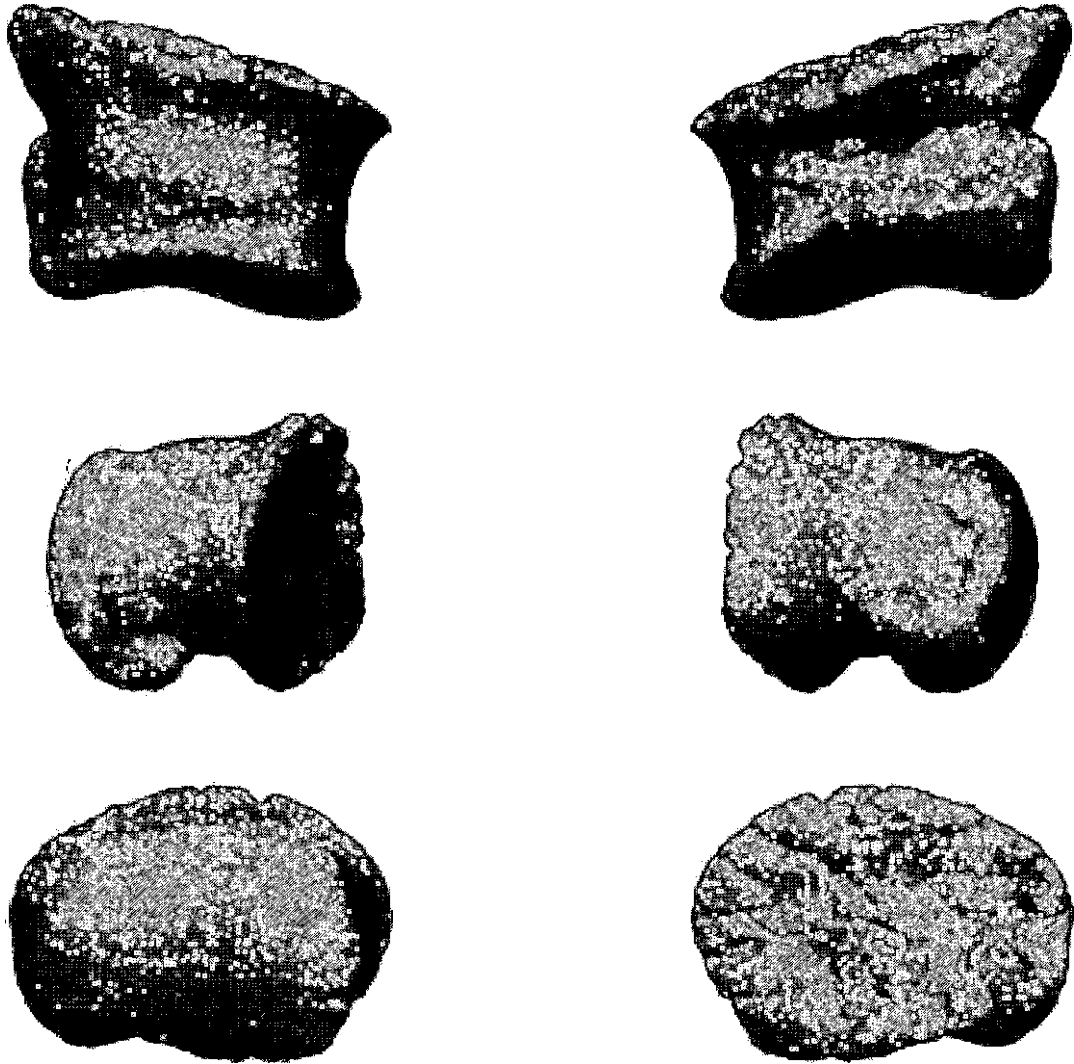




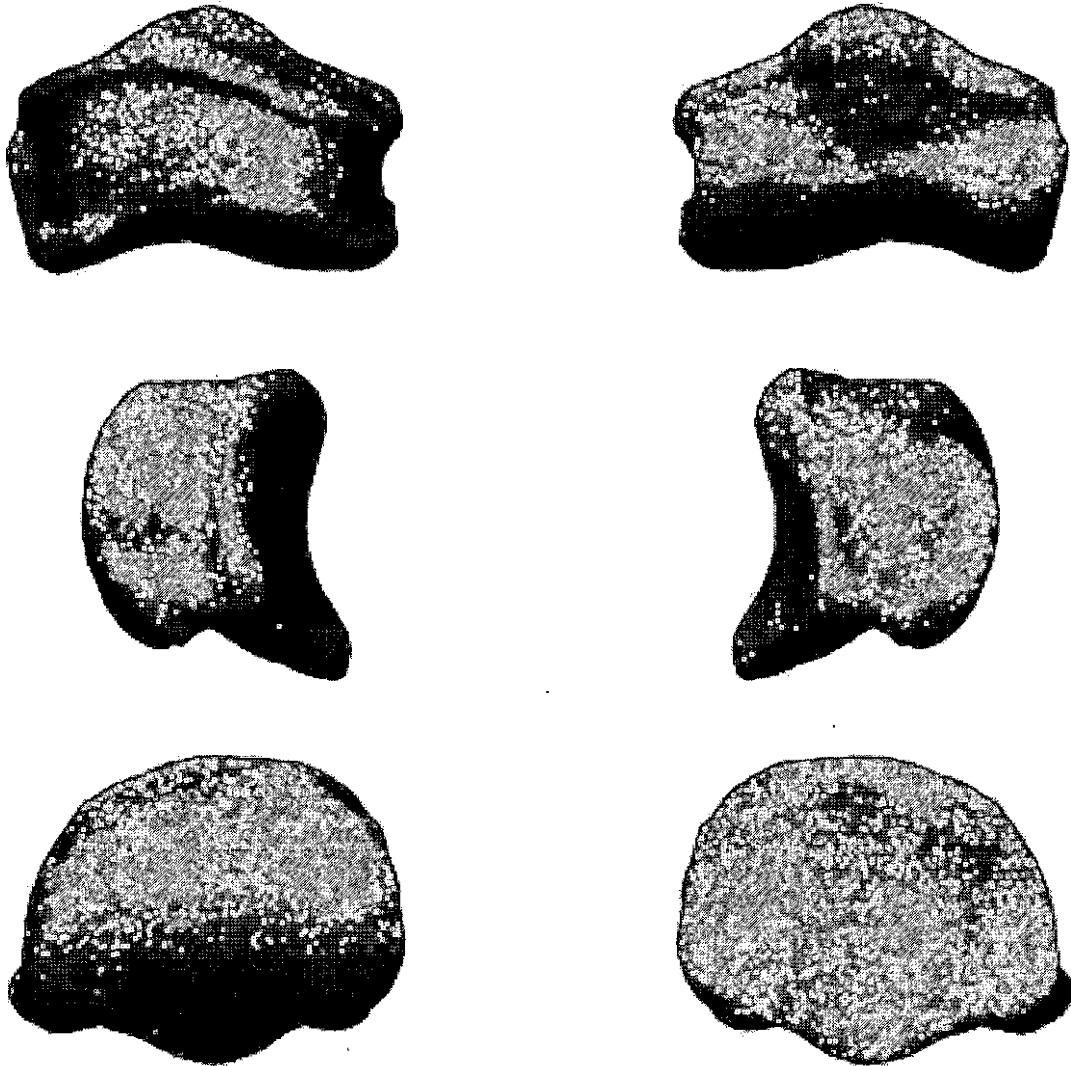
Digit III, Phalanx 3 of TMP 89.97.01.  
Dorsal View is Upper Left; Plantar is Upper Right;  
Medial is Middle Left; Lateral is Middle Right;  
Distal is Lower Left; Proximal is Lower Right.



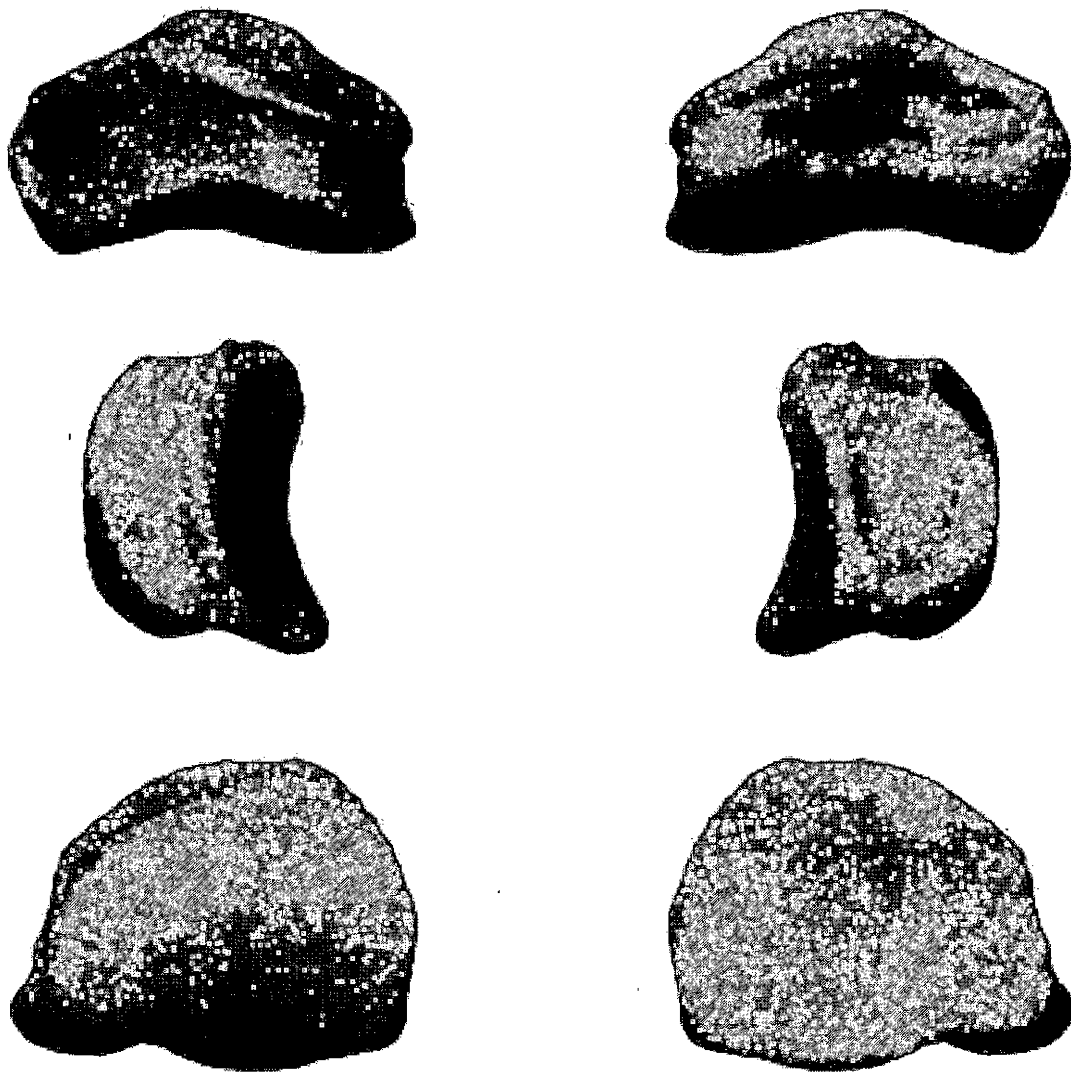
Digit III, Phalanx 4 of TMP 89.97.01.  
Dorsal View is Upper Left; Plantar is Upper Right;  
Medial is Middle Left; Lateral is Middle Right;  
Distal is Lower Left; Proximal is Lower Right.



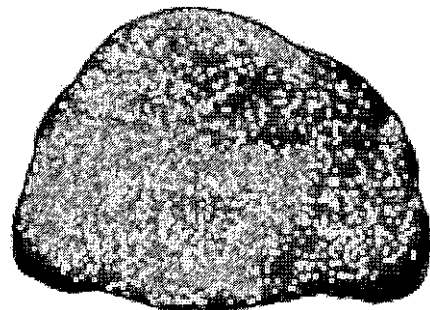
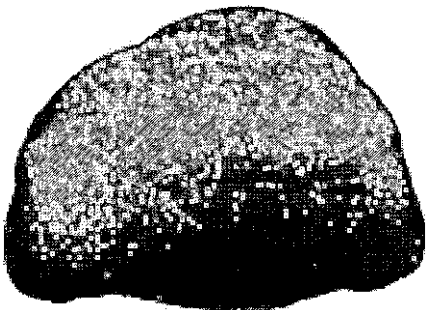
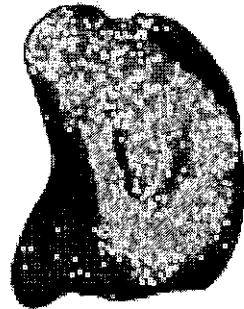
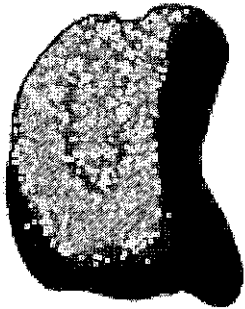
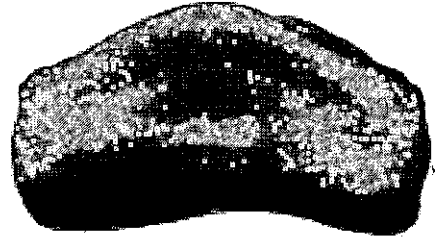
Digit IV, Phalanx 1 of TMP 89.97.01.  
Dorsal View is Upper Left; Plantar is Upper Right;  
Medial is Middle Left; Lateral is Middle Right;  
Distal is Lower Left; Proximal is Lower Right.



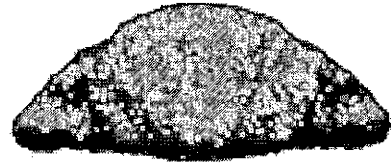
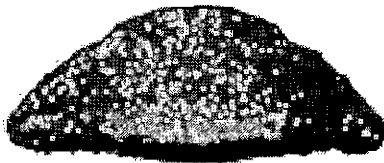
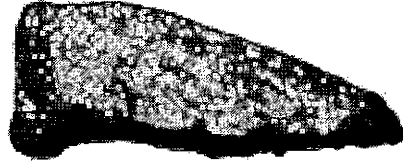
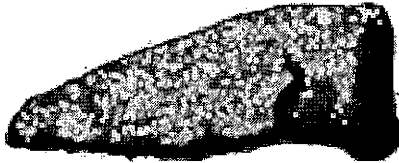
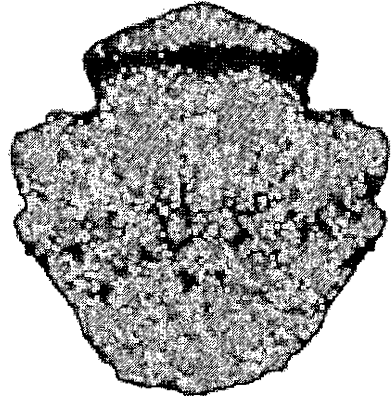
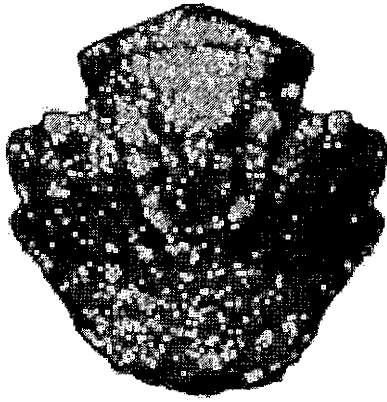
Digit IV, Phalanx 2 of TMP 89.97.01.  
Dorsal View is Upper Left; Plantar is Upper Right;  
Medial is Middle Left; Lateral is Middle Right;  
Distal is Lower Left; Proximal is Lower Right.



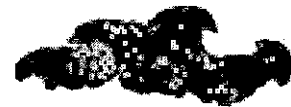
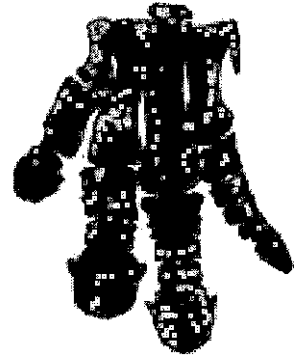
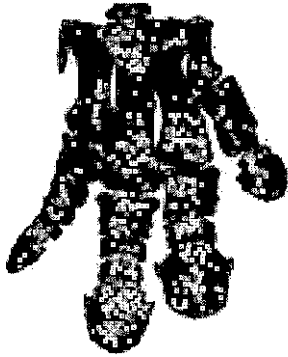
Digit IV, Phalanx 3 of TMP 89.97.01.  
Dorsal View is Upper Left; Plantar is Upper Right;  
Medial is Middle Left; Lateral is Middle Right;  
Distal is Lower Left; Proximal is Lower Right.



Digit IV, Phalanx 4 of TMP 89.97.01.  
Dorsal View is Upper Left; Plantar is Upper Right;  
Medial is Middle Left; Lateral is Middle Right;  
Distal is Lower Left; Proximal is Lower Right.



Digit IV, Phalanx 5 of TMP 89.97.01.  
Dorsal View is Upper Left; Plantar is Upper Right;  
Medial is Middle Left; Lateral is Middle Right;  
Distal is Lower Left; Proximal is Lower Right.



Entire Specimen of TMP 89.97.01.  
Dorsal View is Upper Left; Plantar is Upper Right;  
Medial is Middle Left; Lateral is Middle Right;  
Distal is Lower Left; Proximal is Lower Right.

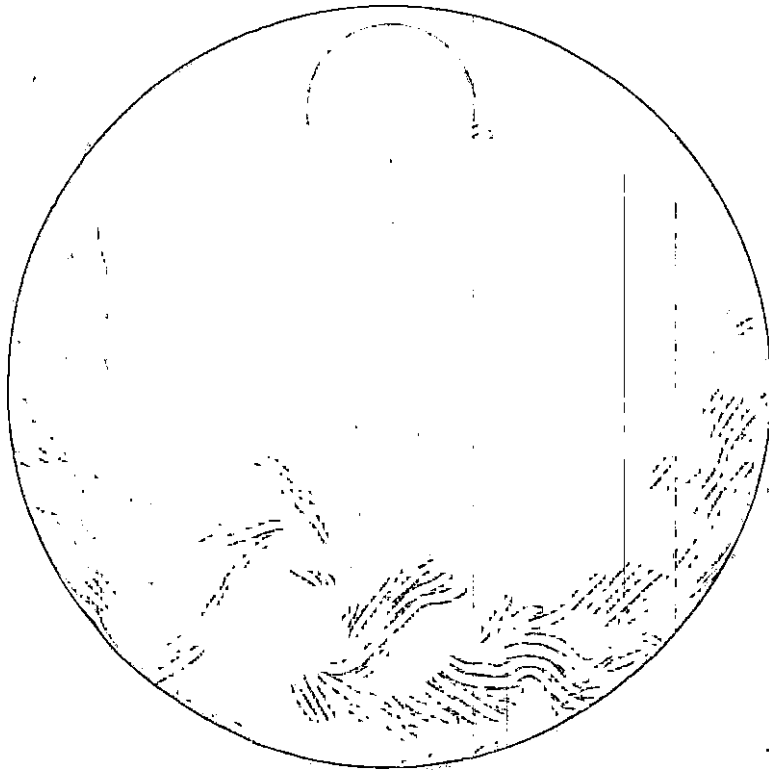


APPENDIX F

DVD OF QUICKTIME FILES AND IMAGES OF TMP 89.97.01

CD MOVED TO BACK OF BOOK

---



## LITERATURE CITED

- Andersen, A. F., R. E. Chapman, K. Kenny, and H. C. Larsson. 1999. Animation of 3-D digital data; the walking *Triceratops*. *Journal of Vertebrate Paleontology*, 19:29A.
- Autodesk Maya Press. 2006. *Learning Autodesk Maya 8: Foundation*. Sybex, San Francisco, California.
- Bakker, R. T. 1987. The return of the dancing dinosaurs. Pp. 38-69 in: S. J. Czerkas and E. C. Olson (eds.), *Dinosaurs Past and Present, Volume I*. University of Washington Press, Seattle.
- Bertram, J. E. A. and A. A. Biewener. 1988. Bone curvature: sacrificing strength for load predictability? *Journal of Theoretical Biology*, 131:75-92.
- Boyd, A. A., and R. Motani. 2008. Three-dimensional re-evaluation of the deformation removal technique based on "jigsaw puzzling". *Palaeontologia Electronica* Vol. 11, Issue 2; 7A:7p; <[http://palaeo-electronica.org/2008\\_2/131/index.html](http://palaeo-electronica.org/2008_2/131/index.html)> Accessed 2008 Jul 12.
- Brown, B. 1917. A complete skeleton of the horned dinosaur *Monoclonius* and description of a second skeleton showing skin impressions. *Bulletin of the American Museum of Natural History*, 37:281-306.

- Bruderlin, A. 2001. Feather software design issues. Pp. 22-24 in: J. Smolin (ed.), *From Ivory Tower to Silver Screen: Visual Effects Companies Reveal how Research and Development Finds its Way into Production*. Siggraph 2001 Course Notes 36, The Visual Effects Society.
- Carrano, M. T. 2000. Homoplasy and the evolution of dinosaur locomotion, *Paleobiology*, 26:489-512.
- Carrano, M. T. 2001. The evolution of sauropod locomotion; morphological diversity of a secondarily quadrupedal radiation. *Journal of Vertebrate Paleontology*, 21:38A.
- Chapman, R. E., R. A. Snyder, S. Jabo, and A. Andersen. 2001. On a new posture for the horned dinosaur Triceratops. *Journal of Vertebrate Paleontology*, 21:39A-40A.
- Derakhshani, D. 2004. *Introducing Maya 6: 3D for Beginners*. Sybex, San Francisco, California.
- Dilkes, D. W. 1999. Appendicular myology of the hadrosaurian dinosaur *Maiasaura peeblesorum* from the Late Cretaceous (Campanian) of Montana. *Transactions of the Royal Society of Edinburgh—Earth Sciences*, 90:87-126.

- Dilkes, D. W. 2001. An ontogenetic perspective on locomotion in the Late Cretaceous dinosaur *Maiasaura peeblesorum* (Ornithischia: Hadrosauridae). *Canadian Journal of Earth Sciences*, 38:1205-1227.
- Dodson, P. 1996. *The Horned Dinosaurs: A Natural History*. Princeton University Press, Princeton, New Jersey.
- Dodson, P. and P. Currie. 1990. Neoceratopsia. Pp. 593-681 in: D. B. Weishampel, P. Dodson, and H. Osmolska (eds.), *The Dinosauria*. University of California Press, Berkeley, California.
- Dyce, K. M., W. O. Sack, and C. J. G. Wensing (eds). 1996. *Textbook of Veterinary Anatomy*. 2<sup>nd</sup> Ed. W.B. Saunders, Philadelphia, Pennsylvania.
- Eberth, D. A. 2005. The Geology. Pp. 54-82 in: P. J. Currie and E. B. Koppelhus (eds.), *Dinosaur Provincial Park: A Spectacular Ecosystem Revealed*. Indiana University Press, Bloomington and Indianapolis, Indiana.
- Evans, R. A. and M. Fortelius. 2008. Three-dimensional reconstruction of tooth relationships during carnivoran chewing. *Palaeontologia Electronica* Vol. 11, Issue 2; 10A:11p; <[http://palaeo-electronica.org/2008\\_2/133/index.html](http://palaeo-electronica.org/2008_2/133/index.html)> Accessed 2008 Jul 12.

- Garstka, W. R. and D. A. Burnham. 1997. Posture and stance in *Triceratops*: Evidence of digitigrade manus and cantilever vertebral column. Pp. 385-391 in: D. L. Wolberg, E. Stump, and G. D. Rosenberg (eds.), *DINOfest International: Proceedings of a Symposium Held at Arizona State University*. Academy of Natural Sciences, Philadelphia.
- Gatesy, S. M., K. M. Middleton, F. A. Jenkins, and N. H. Shubin. 1999. Three-dimensional preservation of foot movements in Triassic theropod dinosaurs. *Nature*, 399:141-144.
- Gatesy, S. M., M. Bäker, and J. R. Hutchinson. Constraint-based exclusion of limb poses for reconstructing theropod dinosaur locomotion. In Press at *Journal of Vertebrate Paleontology*.
- Getty, R. (ed.). 1975. *Sisson and Grossman's: The Anatomy of the Domestic Animals*. 5<sup>th</sup> Ed. W. B. Saunders, Philadelphia, Pennsylvania.
- Gilmore, C. W. 1917. *Brachyceratops*, A ceratopsian dinosaur from the Two Medicine formation of Montana. *U.S. Geological Survey Professional Paper* 103:1-45.
- Hatcher, J. B., Marsh, O. C., and Lull, R. S. 1907. *The Ceratopsia*. U.S. Geological Survey Monograph, 49:1-300.

- Holliday, C. M., R. C. Ridgely, J. C. Sedlmayr, and L. M. Witmer. 2001. The articular cartilage of extant archosaur limb bones: implications for dinosaur functional morphology and allometry. *Journal of Vertebrate Paleontology*, 21:62A.
- Hutchinson, J. R. and M. Garcia, 2002. *Tyrannosaurus* was not a fast runner, *Nature*, 415:1018-1021.
- Hutchinson, J. R., and S. M. Gatesy. 2006. Dinosaur locomotion: beyond the bones. *Nature* 440:292 -294.
- Johnson, R. E. and J. H. Ostrom. 1995. The forelimb of *Torosaurus* and an analysis of the posture and gait of ceratopsians. Pp. 205-218 in: J. Thomasson (ed.), *Functional Morphology in Vertebrate Paleontology*. Cambridge University Press, New York.
- Lewis, J. P., M. Cordner, and N. Fong. 2001. Pose-space deformation: a unified approach to shape interpolation and skeleton-driven deformation. Pp. 38-45 in: J. Smolin (ed.), *From Ivory Tower to Silver Screen: Visual Effects Companies Reveal how Research and Development Finds its Way into Production*. Siggraph 2001 Course Notes 36, The Visual Effects Society.

- Lombard, R. E. and S. S. Sumida. 1992. Recent progress in understanding early tetrapods. *American Zoologist*, 32:609- 622.
- Lull, R. S. 1933. A revision of the Ceratopsia, or horned dinosaurs. *Memoirs of the Peabody Museum of Natural History*, 3:1-175.
- Lutz, M. 2007. *ZBrush3 Offline Reference.pdf*.  
<<http://www.marcus-lutz.de/downloads/ZBrush3-Offline-Reference.pdf>> Downloaded 2007 Jul 14.
- Paul G. S. and P. Christiansen. 2000. Forelimb posture in neoceratopsian dinosaurs: implications for gait and locomotion. *Paleobiology*, 26:450-465.
- Pixologic. 2007. *ZBrush 3 Practical Manual 070307.pdf*.  
<<http://www.zbrush.info/docs/index.php/Downloads>>  
Downloaded 2007 Jul 14.
- Polly, P. D. and N. MacLeod. 2008. Locomotion in fossil Carnivora: an application of eigensurface analysis for morphometric comparison of 3D surface. *Palaeontologia Electronica* Vol. 11, Issue 2; 10A:13p; <[http://palaeo-electronica.org/2008\\_2/135/index.html](http://palaeo-electronica.org/2008_2/135/index.html)> Accessed 2008 Jul 12.
- Ryan, M. J. 1992. The taphonomy of a *Centrosaurus* (Ornithischia: Ceratopsidae) bonebed from the Dinosaur



Park Formation (Campanian), Alberta, Canada.

Unpublished M. S. Thesis, University of Calgary,  
Alberta, Canada, 526 pp.

Ryan, M. J., A. P. Russell, D. A. Eberth, and P. J. Currie.

2001. The taphonomy of a *Centrosaurus* (Ornithischia: Ceratopsidae) bonebed from the Dinosaur Park Formation (Upper Campanian), Alberta, Canada, with comments on cranial ontogeny. *Palaios*, 16:482-506.

Rybczynski, N., A. Tirabasso, P. Bloskie, R. Cuthbertson,

and C. Holliday. 2008. A three-dimensional animation model of *Edmontosaurus* (Hadrosauridae) for testing chewing hypotheses. *Palaeontologia Electronica* Vol. 11, Issue 2; 9A:14p; <[http://palaeo-electronica.org/2008\\_2/132/index.html](http://palaeo-electronica.org/2008_2/132/index.html)> Accessed 2008 Jul 12.

Smith, N. E. and S. G. Strait. 2008. PaleoView3D: from

specimen to online digital model. *Palaeontologia Electronica* Vol. 11, Issue 2; 11A:17p; <[http://palaeo-electronica.org/2008\\_2/134/index.html](http://palaeo-electronica.org/2008_2/134/index.html)> Accessed 2008 Jul 12.

Starck, D. 1979. *Vergleichende Anatomie der Wirbeltiere*

*auf evolutionsbiologischer Grundlage, Band 2: Das Skeletsystem, Allgemeines, Skeletsubstanzen, Skelet der*

- Wirbeltiere einschließlich Lokomotionsstypen.*  
Springer-Verlag, Berlin, Heidelberg, and New York.
- Sumida, S. S. 2000. Biological Principles that drive digital effects and strategies of animation: trading lessons between vertebrate mechanics and commercial entertainment. *American Zoologist*, 41:1225.
- Sumida, S. S. 2001. Digital representation of the domestic cat: cooperative utilization of technology from the film industry and the academic community. *Journal of Morphology*, 248(3):289.
- Sumida, S. S. and S. P. Modesto. 2001. A phylogenetic perspective on locomotory strategies in early amniotes. *American Zoologist*, 41:586-597.
- Swartz, S. M., A. Parker, and C. Huo. 1998. Theoretical and empirical scaling patterns and topological homology in bone trabeculae. *Journal of Experimental Biology* 201:573-590.
- Walters, R., R. E. Chapman, and R. A. Snyder. 2001. Fleshing-out *Triceratops*; adding muscle and skin to the virtual *Triceratops*. *Journal of Vertebrate Paleontology*, 21:111A.
- Weishampel, D. B. and J. R. Horner. 1990. Hadrosauridae. Pp. 534-561 in: D. B. Weishampel, P. Dodson, and H.

Osmolska (eds.), *The Dinosauria*. University of California Press, Berkeley, California.

Wilson, J. A. and M. T. Carrano. 1999. Titanosaurs and the origin of "wide-gauge" trackways; a biomechanical and systematic perspective on sauropod locomotion, *Paleobiology*, 25:252-267.

Witmer, L. M. 1995. The extant phylogenetic bracket and the importance of reconstructing soft tissues in fossils. pp. 19-33 in: J. J. Thomason (ed.), *Functional Morphology in Vertebrate Paleontology*, Cambridge University Press, New York.

Xu, A., Z. Zhou, X. Wang, X. Kuang, F. Zhang, and X. Du. 2002. Four-winged dinosaurs from China. *Nature*, 421:335-340.